Analysis and modelling of respiratory metabolism in *Neisseria meningitidis*

Andrew Schofield

PhD

The University of York

Biology

April 2012

Abstract

N. meningitidis is capable of respiration in both aerobic and microaerobic environments by reduction of oxygen and nitrite respectively. The respiratory chain and genetic regulation of this system are already well understood, but there are complex interactions between components which make predicting which respiratory path will be used difficult. To predict the respiratory behaviour of *N. meningitidis* I have built a mathematical model using a novel combination of experiments and Bayesian fitting.

Contents

1 Introduction **9**
- 1.1 Biology of *Neisseria meningitidis* . . . 9
- 1.2 Pathogenicity of *N. meningitidis* . . . 10
- 1.3 Growth of *N. meningitidis* . . . 12
- 1.4 Organisation of the Respiratory Chain of *N. meningitidis* . . . 12
- 1.5 Respiratory Enzymes in *N. meningitidis* . . . 17
  - 1.5.1 Cytochrome cbb_3 oxidase . . . 17
  - 1.5.2 NorB Nitric Oxide Reductase . . . 19
  - 1.5.3 AniA Nitrite Reductase . . . 20
- 1.6 Respiratory Electron Transporters in *N. meningitidis* . . . 21
  - 1.6.1 NADH Dehydrogenase . . . 21
  - 1.6.2 Cytochrome bc_1 Complex . . . 21
  - 1.6.3 Cytochromes c_4, c_x and c_5 . . . 22
  - 1.6.4 Quinone Pool . . . 24
- 1.7 Respiration Regulatory Proteins in *N. meningitidis* . . . 25
  - 1.7.1 NsrR - Nitrite Sensing Repressor Protein . . . 25
  - 1.7.2 FNR - Fumarate and Nitrate Reductase Regulator . . . 25
  - 1.7.3 NarQ/NarP - Nitrite Response Sensor/Regulator . . . 26
- 1.8 Organisation of Respiratory Chains in Other Bacteria . . . 26
  - 1.8.1 The Respiratory Chain of *Paracoccus denitrificans* . . . 27
  - 1.8.2 The Respiratory Chain of *Escherichia coli* . . . 28
- 1.9 Systems Biology . . . 30
- 1.10 Modelling . . . 33
  - 1.10.1 Modelling Respiratory Systems . . . 33
  - 1.10.2 Modelling Tools . . . 34
- 1.11 Aims . . . 35

2 Materials and Methods **36**
- 2.1 *Neisseria meningitidis* Strains Used in This Work . . . 36
- 2.2 Culturing *Neisseria meningitidis* . . . 37
  - 2.2.1 Growth of *Neisseria meningitidis* . . . 37
  - 2.2.2 Preparation of Antibiotic Selective Media . . . 37
  - 2.2.3 Preparation of Frozen Bacterial Stocks . . . 37
  - 2.2.4 Streaking Plates for OD to CFU Ratio Calculation . . . 38
- 2.3 Measuring Oxygen Concentration . . . 38
  - 2.3.1 Calibration of Oxygen Electrode . . . 38
- 2.4 Measuring Nitric Oxide Concentration . . . 39
  - 2.4.1 Calibration of Nitric Oxide Electrode . . . 40

2.5 Measuring Nitrite Concentration (Griess Assay) 41
2.6 Nitric Oxide Production 41

3 Model - Construction and Parameters **44**
3.1 Construction 44
3.1.1 Converting Biological Reactions into Differential Equations 45
3.1.2 Assumptions and their Justifications 50
3.2 Parameters and their Prior Distributions 51
3.3 Implementation of the model 58
3.4 Solving Ordinary Differential Equations 58
3.5 Parameter Estimation 59

4 Parameter Estimation Methodologies **60**
4.1 Simulated Annealing 61
4.2 Approximate Bayesian Computation by Sequential Monte Carlo . . 65
4.3 Metropolis Hastings Monte Carlo 69
4.4 Implementation 71
4.5 Integrative Scheme 73

5 Oxygen Reduction in *N. meningitidis* **74**
5.1 Aerobic Reduction of Oxygen 74
5.1.1 Introduction 74
5.1.2 Experimental Results 75
5.1.3 Rate of oxygen diffusion 88
5.1.4 Discussion 88

6 Nitric Oxide Reduction in *N. meningitidis* **90**
6.1 Aerobic Nitric Oxide Reduction 93
6.1.1 Introduction 93
6.1.2 Results 93
6.1.3 Discussion 93
6.2 Microaerobic Nitric Oxide Reduction 93
6.2.1 Introduction 93
6.2.2 Results 93
6.2.3 Discussion 93
6.3 Aerobic Nitric Oxide Reduction in *nsrR*$^-$ mutant 93
6.3.1 Introduction 93
6.3.2 Results 93
6.3.3 Discussion 93

7 Nitrite Reduction in *N. meningitidis* **94**
7.1 Microerobic Nitrite Reduction 97
7.1.1 Introduction 97
7.1.2 Results 97
7.1.3 Discussion 97
7.2 Microaerobic Nitrite Reduction in *norB*$^-$ mutant 97
7.2.1 Introduction 97
7.2.2 Results 97
7.2.3 Discussion 97

7.3 Aerobic Nitrite Reduction in *nsrR*$^-$ mutant 97
7.3.1 Introduction 97
7.3.2 Results 97
7.3.3 Discussion 97
7.4 Aerobic Nitrite Reduction in *nsrR*$^-$-*norB*$^-$ mutanterobic Nitrite Reduction in nsrR- - norB- mutant 97
7.4.1 Introduction 97
7.4.2 Results 97
7.4.3 Discussion 97

8 AniA and NorB Expression in *N. meningitidis* 98
8.1 Aerobic and Microaerobic Expression 98
8.1.1 Introduction 98
8.1.2 Results 98
8.1.3 Discussion 98

9 The Completed Model 99
9.1 Amalgamation of cytochromes 99

A Appendix 100

List of Abbreviations 102

References 103

List of Figures

1.1 Complete denitrification. 13
1.2 Layout of the components of the respiratory system in *Neisseria meningitidis*. 15
1.3 Regulation of respiratory components in *Neisseria meningitidis*. . . . 17
1.4 The cbb_3 oxidase. 18
1.5 The modified Q-cycle used by the bacterial bc_1 complex. 23
1.6 Structure of the ubiquinone molecule. 24
1.7 Branched electron transport chains of *N. meningitidis*. 27
1.8 Branched electron transport chains of *Paracoccus* species. 28
1.9 Branched electron transport chains of *E. coli*. 29
1.10 Systems biology cycle. 31
1.11 System complexity. 32

2.1 Exploded view of the oxygen electrode 39
2.2 Oxygen electrode chamber with nitric oxide probe inserted 40
2.3 NO making apparatus. 42

4.1 Pseudo-code showing how the simplest annealing algorithm works. 62
4.2 Example simulated annealing temperature schedule 63
4.3 Schematic diagram showing the technique used to generate a spread of parameters using a synthetic chromosome. 64
4.4 Simulation results of the Lotka-Volterra validation run. 71
4.5 MHMC results of the Lotka-Volterra validation run. 72

5.1 Oxygen reducing electron transport chain of *N. meningitidis* 75
5.2 Highly repeatable oxygen reduction 76
5.3 Aerating oxygen reducing cultures with significant delay 77
5.4 Prior probability distributions for oxygen reduction 79
5.5 Oxygen Reduction in *Neisseria meningitidis*. 80
5.6 Simulation fitness value improves as parameter estimation progresses 81
5.7 Individual parameter trajectories for multiple runs on the same experimental dataset 82
5.8 Posterior probability distributions for oxygen reduction 84

6.1 Nitric oxide reducing electron transport chain of *N. meningitidis* . . 91
6.2 Nitric Oxide Reduction in *Neisseria meningitidis*. 92

7.1 Nitrite reducing electron transport chain of *N. meningitidis* 95
7.2 Nitrite Reduction in *Neisseria meningitidis*. 96

List of Tables

1.1 The reductions catalysed by the respiratory enzymes in *N. meningitidis* 14

2.1 Bacterial strains and sources 36
2.2 Final antibiotic concentrations 37
2.3 Sodium Nitrite concentrations used to calibrate ISO-NOP Nitric Oxide sensor. 41
2.4 Chemicals needed for preparation of Nitric Oxide solution. 43

3.1 Model parameters 52

5.1 Regression Analysis of Oxygen Reduction Parameters 87

A.1 Model Variables 101
A.2 Model Parameters 101

Acknowledgements

Chapter 1

Introduction

1.1 Biology of *Neisseria meningitidis*

Neisseria meningitidis is a Gram-negative, bean-shaped diplococcal bacterium[1], surrounded by a lipid membrane containing outer membrane proteins and lipopolysaccharides[1]. When pathogenic, the bacteria also has a polysaccharide capsule attached to the membrane[1]. It is non-spore forming, non-motile but piliated, and lives as an obligate human pathogen (humans being its only host)[2]. *N. meningitidis* inhabits the mucosal membranes primarily in the respiratory tract, and it is estimated that up to 20-25% of the population have this bacteria in their nasopharynx while being asymptomatic[2–4].

The *Neisseria* genus contains a number of non-pathogenic species which are part of the normal human flora including *N. subflava*, *N. flavescens*, *N. lactamica* and *N. sicca*[5]. Two species of *Neisseria* are the causative agents of human diseases, *N. meningitidis*, which causes bacterial meningitis and *N. gonorrhoea* which causes gonorrhoea. Being β-proteobacteria[2], the *Neisseria* genus is also related to a number of other pathogenic bacteria including *Bordetella*, *Burkholderia* and *Spirillum*. This taxa also includes ammonia-oxidising bacteria such as *Nitrosomonas*[6], .

N. meningitidis is classified into 13 different serogroups based on the differences in lipopolysaccharides, capsules, outer membrane proteins and adhesion

molecules[1,2,7]. 3 of these 13 serogroups are the main cause of meningococcal meningitis, with serogroups B and C being the most prevalent[1]. Vaccines for serogroup C are available, but serogroup B currently has no effective vaccine, as it mimics human antigens[2] and it is a poor immunogen[8]. In addition to being the causative agent for meningococcal meningitis, *N. meningitidis* also causes septicaemia and the combination has a mortality rate of 10% even with therapy[1,2].

N. meningitidis is dependent on a source of iron, and must source this from its environment[9]. It does this by directly capturing iron from the host via human transferrins[9–11] and lactoferrin[9]. This capture is brought about by membrane surface receptors that can bind the transferrins which then go on to internalise the iron into the bacterium for growth[12].

1.2 Pathogenicity of *N. meningitidis*

Meningitis is caused by *N. meningitidis* entering the bloodstream and travelling to the meninges, a set of membranes that envelope the central nervous system, where the bacteria goes on to cause inflammation. Once it has entered the bloodstream, *N. meningitidis* is capable of switching its capsule by phase-variation to avoid host-immune detection[13,14]. After colonisation by the bacterium, in order to enter the bloodstream, it must first adhere to the mucosal tissue. This is facilitated by adhesion molecules on the outer membrane and by pili, with the latter being the primary source of adhesion[1,7]. Once the bacteria are adhered to the mucosal cells, additional contacts are made with the outer membrane proteins. Interestingly, the presence of the polysaccharide capsule, which is required for survival in the bloodstream, interferes with these additional contacts[2]. *N. meningitidis* invades the bloodstream by being endocytosed by the mucosal epithelial cells, a process which is triggered by the pili and outer membrane proteins on the bacteria.

N. meningitidis is able to survive in the bloodstream (typically an antimicrobial environment) mainly by virtue of its polysaccharide capsule as this is able

to protect the bacteria against various immune responses by the host including complement-mediated bacteriolysis and phagocytosis by neutrophils[1]. Despite these protective features, specific antibodies *do* provide full protection against the bacteria, but the time taken for these antibodies to be produced means that the host has a period of at least 1 week in which it must rely on innate immune response[1]. Evidence suggests that systemic infection by *N. meningitidis* can only occur in hosts which are immunocompromised in some way, specifically if they do not have the serum bactericidal antibodies against capsular or non-capsular antigens, or they are missing certain complement components[4]. A number of factors can increase the likelihood of contracting bacterial meningitis including smoking and travelling to epidemic regions[2]. In developed countries, the highest rates of invasive meningococcal meningitis are seen in infants and children less than 4 years-old, adolescents, military recruits and groups where crowding and new exposures occur such as college students living in dormitories, however the disease is capable of affecting all age groups[2].

There is evidence to suggest that much of the damage done to the host during a meningococcal infection is actually caused by the host in an attempt to rid itself of the bacteria[15]. A systemic infection causes a massive inflammatory response and the resulting quantities of cytokines produced eventually lead to organ dysfunction and the proteases produced by neutrophil activation also lead to endothelial injury[15].

Once *N. meningitidis* has entered the bloodstream, it goes on to invade the cerebro-spinal fluid (CSF), which serves as an excellent culture medium for the bacteria[4]. The host response to this infection is inflammation of the meninges, the membranes surrounding the central nervous system. This leads to a build-up of serous fluid in the brain causing cerebral swelling. Once the bacteria have entered the CSF, antimicrobial treatment is required otherwise the effects are almost invariably fatal[4].

Initially a meningococcal infection presents as a slight fever and chills, which

may improve after 4-6 hours. Haemorrhagic skins lesions may appears between 8 and 18 hours, however roughly 20% of suffers never present with lesions. These skin lesions are possibly the most well known symptom of bacterial meningitis as they are characterised by a non-blanching (does not turn white under mild pressure) rash. The clearest evidence for meningococcal infection is a fever, stiff neck, aversion to bright light, vomiting, skin lesions and headaches. Unfortunately not all these symptoms may be present in all cases[4].

When meningococcal septicaemia occurs, renal function may be impaired as a direct consequence of cardiac impairment. Septicaemia causes "capillary leak" which reduces cardiac output and increases the effort required to breathe normally. Reduced cardiac output can also affect the gastrointestinal tract leading to reduced function. Once treated these symptoms will usually subside as cardiac output improves[15].

In most cases the treatment for meningococcal meningitis is with antibiotics, where the primary aim is to achieve a rapid bactericidal effect in the CSF[1]. This treatment is suggested prior to positive identification of cultures of the bacteria obtained from the CSF as any delay is potentially life-threatening if the bacteria have indeed invaded the CSF[4].

1.3 Growth of *N. meningitidis*

Bacteria require carbon and energy sources in order to grow, and these are often sourced from sugars present in the environment. *N. meningitidis* can only use the sugars glucose and maltose as carbon sources[16,17], however they can use peptides as carbon sources. The bacteria are usually grown on Müller-Hinton broth and Columbia agar which are peptide-based formulations.

1.4 Organisation of the Respiratory Chain of *N. meningitidis*

N. meningitidis is classified as an aerobe and as such has an oxidase pathway for reducing oxygen (O_2), but given that the environment in the nasopharynx is

$$NO_3^- \rightarrow NO_2^- \rightarrow NO \rightarrow N_2O \rightarrow N_2$$

Figure 1.1: **Complete denitrification.** The process of reducing nitrite to nitrogen gas. In *N. meningitidis* the first and final steps highlighted in blue do not occur.

poor in oxygen, the bacteria must also be capable of respiring in a microaerobic environment. This is evidenced by the fact that bacterial isolates from the nasopharynx routinely contain both strict aerobes and strict anaerobes[18]. Genomic analysis of 2 strains of *N. meningitidis* shows that there are 3 terminal oxidases; 1 of each for reducing oxygen, nitrite (NO_2^-) and nitric oxide (NO)[19]. This analysis may be expanded as there are now many more genomes published. Experiments showed that under oxygen limiting conditions, *N. meningitidis* was capable of growth when nitrite was present in the media (Müller-Hinton Broth), and that nitrate (NO_3^-), the probable source for nitrite, had no effect on growth[19]. Additionally the bacteria require carbon dioxide, as shown by Tuttle and Scherp[20] and have 2 enzymes which catalyse the reduction of CO_2[4].

In vivo, nitrite is obtained as a product of digesting nitrate in food. There are a number of facultative nitrate-reducing bacteria present in the mouth and pharynx responsible for this[18] which additionally have a proposed benefit of protecting the host against peridontal and cariogenic bacteria[21]. Nitrite is also created by oxidation of nitric oxide, which is produced as a host signalling molecule and as a toxin as part of the host immune response[18,21].

The respiratory pathway for reducing nitrite in *N. meningitidis* involves two steps; nitrite is reduced to nitric oxide, which is then further reduced to nitrous oxide. This represents incomplete reduction, as a further reduction step is possible (shown in Figure 1.1), reducing nitrous oxide to dinitrogen gas[18,22].

Reduction of oxygen is favourable over nitrite reduction due to the redox potential differences. The redox potential of O_2/H_2O is +820 mV, NO_2^-/NO is +348 mV, thus O_2 has a higher tendency to acquire electrons resulting in a electrochemically favourable reaction[23]. The electron flow towards the oxidase is also preferred physiologically as it liberates more energy by virtue of the translo-

Reduction			Enzyme
NO_2^-	$\rightarrow$	NO	AniA
NO	$\rightarrow$	N_2O	NorB
O_2	$\rightarrow$	H_2O	*cbb*$_3$

Table 1.1: The reductions catalysed by the respiratory enzymes in *N. meningitidis*

cation of more protons than the reduction of nitrite. The translocated protons are ultimately used in the synthesis of ATP molecules for energy. This results in reduction of oxygen in preference to nitrite when both are present (in most cases).

Reduction of oxygen in *N. meningitidis* is carried out by the oxygen reductase cytochrome *cbb*$_3$ oxidase, a membrane-bound heme-copper oxidase[24]. *cbb*$_3$ is capable of binding oxygen and nitric oxide, which means that during nitrite reduction (denitrification), the oxidase can be competitively inhibited (chemically) by the intermediate product of denitrification. *cbb*$_3$ can be permanently damaged at high concentrations of NO and O_2, as they can both bind at the *cbb*$_3$ active site and react together to form peroxynitrite[25–27].

Nitrite is reduced by the nitrite reductase AniA, which is a copper containing reductase. This reduction does not involve translocation of protons, and thus does not produce any usable energy. Nitrite is reduced to nitric oxide which can then be further reduced by a nitric oxide reductase NorB. Since *N. meningitidis* is capable of reducing nitric oxide, a host toxin, directly, this may help it defend itself against part of the host immune response[18,28] as has been shown in tissue culture by Anjum et al.[27].

The reduction processes carried out by these enzymes are shown in the table in Table 1.1.

The major source for electrons in both respiratory pathways is NADH, although electrons can also be obtained from pyruvate and lactate amongst others. These reduced substrates lead to reduction of ubiquinone to ubiquinol in the ubiquinone pool that exists within the bacteria. Ubiquinol is oxidised either by the cytochrome *bc*$_1$ complex or directly by the NorB enzyme whilst reducing NO

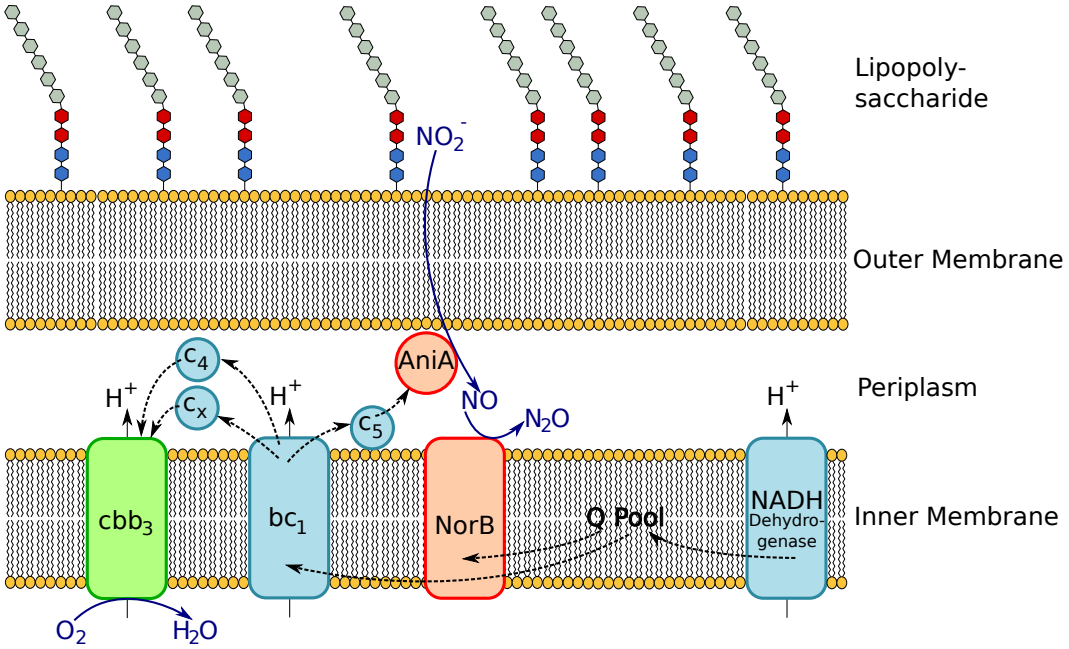

Figure 1.2: **Layout of the components of the respiratory system in *Neisseria meningitidis*.** Oxygen reducing components are shown in green, nitrogen reducing components in red. Components transporting electrons are coloured light blue, and their transport is indicated by dashed arrows. Respiratory substrates are shown in dark blue, with corresponding arrows linking them to their reducing enzymes. Components which produce membrane potential are also indicated.

to N_2O. Cytochrome bc_1 is oxidised by a number of intermediate cytochromes which act to transport electrons to the terminal oxidases; AniA and cbb_3. The c_5 cytochrome transports electrons from the bc_1 complex to AniA, and two cytochromes, $c_{2/x}$ and c_4, transport electrons to cbb_3. It is not understood why cbb_3 has 2 alternate cytochromes, and there is evidence to suggest that it can also be supplied, in a limited capacity, by the c_5 cytochrome as well[29]. The electron transport chain (ETC) is shown graphically in Figure 1.2.

In addition to the difference in favourability between the two respiratory pathways, there is also a great deal of regulation, both at the enzymatic and transcriptional level. Chemical inhibition also plays a part in regulation as briefly mentioned previously. Expression of AniA is regulated by two processes, the reduction of oxygen and the presence of nitrite. The presence of oxygen down-regulates the expression of an activator of AniA expression. This activator is FNR (fumarate and nitrate reduction regulator), and the presence of oxygen effectively

means that AniA expression is repressed by the reduced expression of FNR. In *N. meningitidis*, FNR appears to work slightly differently than in facultative anaerobes such as *E. coli*, in that FNR is still expressed at quite high concentrations of oxygen, and is itself down-regulated by a separate co-factor[30].

The presence of nitrite triggers the two component NarP/NarQ system which activates expression of AniA in response to increasing levels of nitrite[18]. The activity of AniA is also controlled by the competition for electrons by the other reductase enzymes in the respiratory chain. Both NorB and cbb_3 have a higher affinity for electrons than AniA, and as a result the presence of these enzymes (when active) has an inhibitory effect on AniA. The regulation of AniA is further complicated by the production of nitric oxide, and the presence of a protein, NsrR.

Nitric oxide has a direct inhibitory effect on the expression of AniA, as does the NsrR protein. Nitric oxide also inhibits the NsrR protein, leading to a de-represssion of AniA[28]. In the absence of nitric oxide, AniA is almost fully repressed by active NsrR. As NO concentrations increase, NsrR is inactivated allowing full activation of AniA. Once NO reaches a sufficiently high level it will begin to inhibit AniA[18,30].

NorB is less tightly regulated by respiratory components, as it is only acted upon by NsrR, however it is regulated by FNR and NrsR outside the respiratory chain[31]. This regulation by NsrR works in a similar way to how NsrR acts upon AniA. When there is no nitric oxide present, the NsrR acts to inhibit NorB since there is no substrate for it to reduce. In the presence of nitric oxide, NsrR is inhibited, leading to the activation of NorB which is now able to reduce NO to N_2O. In this case nitric oxide is acting as a de-repressor of NorB.

This complicated set of regulatory relationships between the different components of the respiratory pathways is shown in Figure 1.3.

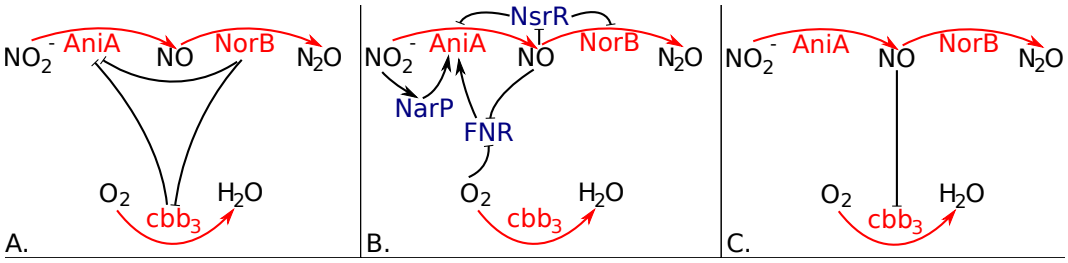

Figure 1.3: **Regulation of respiratory components in *Neisseria meningitidis*.** Enzymes and enzymatic reactions are shown in red. *A.* describes the regulation caused by competition for electrons between the respiratory enzymes. *B.* shows the genetic regulation, which also involves a number of additional components in dark blue. *C.* shows chemical inhibition of the respiratory components.

1.5 Respiratory Enzymes in *N. meningitidis*

1.5.1 Cytochrome *cbb*$_3$ oxidase

Cytochrome *cbb*$_3$ oxidase is a Haem Copper Oxidase (HCO) enzyme found commonly in proteobacteria. They have been characterised in at least *Pseudomonas denitrificans*, *Rhodobacter sphaeroides*, *Rhodobacter capsulatus* and *Bradyrhizobium japonicum*[32]. HCOs catalyse the reduction of Oxygen molecules to water whilst translocating protons across the inner membrane, from the cytoplasm to the periplasm, producing an electrochemical gradient.

HCOs can be separated into two categories by their electron donor type. Cytochrome *c* oxidases accept electrons from *c*-type cytochromes, and quinol oxidases accept electrons from ubiquinol. The major difference between these two categories is a missing Cu_A site in quinol oxidases[33]. HCOs can be further broken down to 3 type, the *aa*$_3$-type cytochrome *c* oxidase, the *bo*$_3$-type quinol oxidase and the *cbb*$_3$-type cytochrome *c* oxidase[34]. Alternatively 5 different HCO subclasses may be classified, the *aa*$_3$, *caa*$_3$ and *cbb*$_3$-type cytochrome *c* oxidases, and the *bo*$_3$ and *aa*$_3$-type quinol oxidases[35]. All of these different types of cytochrome *c* oxidases are found in bacteria, whereas those in mitochondria are limited to *aa*$_3$-type cytochrome *c* oxidases[36].

HCOs are themselves "defined by the primary sequence of their catalytic subunit, which is composed of twelve transmembrane helices with six invariant his-

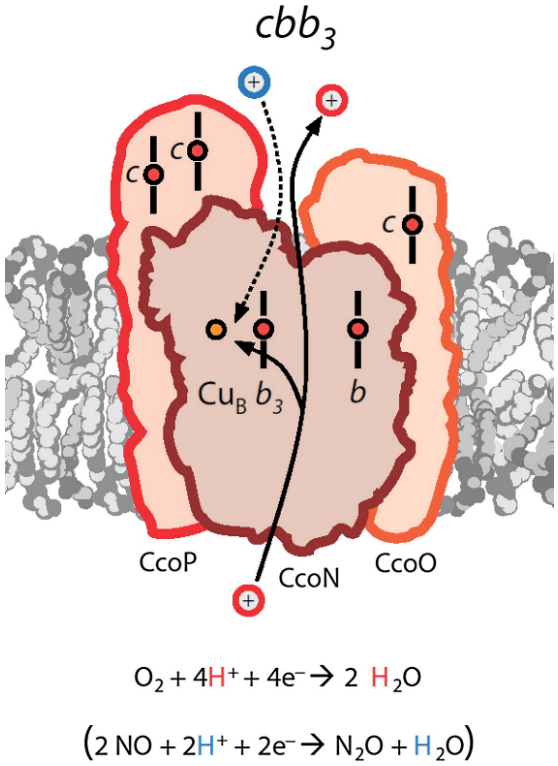

Figure 1.4: **The *cbb*$_3$ oxidase**. This diagram shows the proton input pathway for Oxygen reduction shown in red, and the putative pathway for Nitric Oxide reduction in blue. Also shown are the 3 subunits and their associated heme centres. Adapted from Huang et al.[37].

tidines ligating three cofactors; a high spin heme (one His ligand) and a copper (3 His ligands) in the catalytic site and an additional low-spin heme (two His ligands)"[37]. Sequence alignment has also indicated that bacterial NO-reductase (NOR) might also be a divergent member of the HCO family. A schematic diagram of the *cbb*$_3$ oxidase is shown in Figure 1.4. *cbb*$_3$ is composed of three main subunits with CcoN being the catalytic subunit, which is related to subunit I of *aa*$_3$ oxidases and NorB. This latter relation to NorB explains why *cbb*$_3$ has some Nitric Oxide reduction activity (and conversely why NorB has some Oxygen reduction activity)[37]. CcoN contains the catalytic site – the high-spin heme b_3-Cu_B – and a low spin heme *b*. CcoO is anchored in the inner membrane and contains just one *c-type* heme. CcoP contains two *c*-type hemes and is anchored to the inner membrane. CcoQ, the fourth subunit is small, and helps to stabilise the complex[37].

The mechanism of reduction of O_2 by *cbb*$_3$ oxidases is not fully understood, as the reduction intermediates currently remain unknown[37]. The cytochrome *cbb*$_3$ oxidases have very low K_m values, allowing them to operate even under oxygen limiting conditions. *cbb*$_3$ from *Bradyrhizobium japonicum* has a K_m of 7 nM, much lower than that of the mitochondrial *aa*$_3$ oxidase[38]. This high affinity for oxygen suggests that *N. meningitidis* may have become adapted to surviving in the human host in areas of low oxygen concentration. Since this type of oxidase is also found in other human pathogens it is likely that it is used to allow those pathogens to survive in hypoxic environments in the human host[39].

The catalytic reaction for the *cbb*$_3$ oxidase is:

$$cbb_{3(\text{reduced})} + \tfrac{1}{2}O_2 + 2H^+ \rightarrow cbb_{3(\text{oxidised})} + H_2O \tag{1.1}$$

1.5.2 NorB Nitric Oxide Reductase

Nitric Oxide Reductase is also a Haem Copper Oxidase enzyme which is found in bacteria as an integral membrane protein. There are three types of NOR, the cytochrome *bc* type complex (cNOR), the cytochrome *b* type complex lacking the cytochrome *c* component (qNOR) and a qNOR-type reductase that also includes Cu_A (qCu_ANOR). cNOR-type reductases receive electrons from soluble redox protein donors, whereas qNOR-type reductases receive electrons from quinol[40].

The NOR in *N. meningitidis* is a qNOR-type reductase, and is encoded by the norB gene (NMB1622). It catalyses the reduction of Nitric Oxide to Nitrous Oxide receiving electrons directly from the quinone pool. Under microaerobic conditions this enzyme is important as during dentrification to support growth, Nitric Oxide accumulates as a result of reduction of Nitrite. The build up of Nitric Oxide inhibits aerobic respiration as it binds competitively to the *cbb*$_3$ oxidase. NorB protects the bacteria from the toxicity extracellular NO which is produced by host tissues and macrophages, which produce NO in quantity during infection[28].

The nitric oxide reductase in *Neisseria gonorrhoeae* is predicted to be an 84.3

kDa protein with significant sequence identity to *Ralstonia eutropha* and consists only of the NorB subunit[40]. The NorB protein is highly conserved across all *Neisseria* species as evidenced by sequence analysis[41].

The catalytic reaction for NorB is:

$$\mathrm{NorB_{(reduced)}} + 2\mathrm{NO} + 2\mathrm{H^+} \rightarrow \mathrm{NorB_{(oxidised)}} + \mathrm{N_2O} + \mathrm{H_2O} \qquad (1.2)$$

1.5.3 AniA Nitrite Reductase

AniA nitrite reductase is an anaerobically induced, outer membrane associated protein which uses nitrite as an electron acceptor[42]. It is a copper-containing protein found in many denitrifying proteobacteria.

Nitrite reductases catalyse the reduction of nitrite to nitric oxide with no associated proton translocation. There are two types of nitrite reductase, those that have haem centres, and those which have copper centres. AniA in *N. meningitidis* is a copper-containing and accepts electrons from *c*-type cytochromes (c_5).

In *N. meningitidis* this enzyme is important during oxygen limiting conditions as it allows microaerobic respiration which can supplement growth by denitrification[18].

Interestingly, according to its genome sequence *N. meningitidis* strain 053442 appears to lack the *aniA* gene in its entirety, suggesting that this strain would be unable to perform denitrification and respire anaerobically[41]. 32% of *N. meningitidis* strains sequenced by Barth et al.[41] contain non-functional copies of *aniA* with frameshift mutations. These strains do still possess the *norB* gene for reducing Nitric Oxide however allowing them to prevent its toxic effects. It has been suggested by some that this may actually be evidence that *Neisseria meningitidis* is in the process of evolving away from denitrification to being a Nitric Oxide tolerant aerobe[43].

The catalytic reaction for AniA is:

$$\mathrm{AniA_{(reduced)}} + \mathrm{NO_2^-} + 2\mathrm{H^+} \rightarrow \mathrm{AniA_{(oxidised)}} + \mathrm{NO} + \mathrm{H_2O} \qquad (1.3)$$

1.6 Respiratory Electron Transporters in *N. meningitidis*

1.6.1 NADH Dehydrogenase

NADH (Reduced Nicotinamide Adenine Dinucleotide) Dehydrogenase is an inner membrane bound enzyme that catalyses the transfer of electrons from NADH to the quinone pool in many bacteria. There are three types of NADH dehydrogenase enzymes found in bacteria, NDH-1, NDH-2 and Na^+-NDH. NDH-1 is related to Complex I of the mitochondrial respiratory chain and translocated protons across the inner-membrane whilst reducing the quinone pool[44–46]. NDH-2 does not have any proton pump activity, nor does it have any Fe-S clusters[47]. Na^+-NDH translocates Na^+ ions across the membrane[48]. The NADH dehydrogenase of *N. meningitidis* is of the NDH-1 type[23].

Mitochondrial complex I catalyses the oxidation of NADH and the reduction of ubiquinone whilst translocating 4 protons across the membrane. It does so using the following reaction scheme:

$$\mathrm{NADH} + \mathrm{H^+} + 4\mathrm{H^+_{inner}} + \mathrm{UQ} \rightarrow \mathrm{NAD^+} + 4\mathrm{H^+_{outer}} + \mathrm{UQH_2} \qquad (1.4)$$

1.6.2 Cytochrome bc_1 Complex

The cytochrome bc_1 complex oxidises quinols and reduces metalloprotein electron transporters (usually c-type cytochromes). It is an important part of bacterial respiratory chains, and is also analogous to the mitochondrial complex III[49]. Whilst catalysing the reduction of ubiquinol and the oxidation of c-type cytochromes, the bc_1 complex also translocates protons across the inner membrane from the cytoplasm to the periplasm producing an electrochemical gradient. The bc_1 complex is found in both Gram negative and Gram positive bacteria, however *E. coli* has no bc_1 complex. The homolg the b_6f complex is also used for electron transfer during photosynthesis in higher plants and phototrophic bacteria[50].

In bacteria the bc_1 complex is formed of one cyt *b* subunit which contains two

b-type hemes, one cyt c_1 subunit which contains a single *c*-type heme and an Rieske iron-sulfur protein. These subunits form the two catalytic sites of the bc_1 complex. The reduction of ubiquinol appears to occur in a concerted manner at 1 of these sites, Q_o[50]. Electrons from the quinol are shared between two reaction chains, 1 which transfers electrons to the high-potential iron-sulfur protein and c_1, and another which transfers electrons to the low-potential cytochrome *b*. The other catalytic site Q_i uses the two electrons from the high and low potential chains to reduce quinone, or other metalloprotein electron transporters[51,52]. This modified Q-cycle is shown in Figure 1.5.

The reaction scheme for the bc_1 complex is:

$$QH_2 + 2 \text{ ferricyt } c^{3+} + 2H^+_{\text{Negative}} \Longleftrightarrow Q + 2 \text{ ferrocyt } c^{2+} + 4H^+_{\text{Positive}} \qquad (1.5)$$

1.6.3 Cytochromes c_4, c_x and c_5

Cytochromes c_4, c_x and c_5 are soluble *c*-type cytochromes. These are small heme proteins that are found in the periplasm and are loosely associated with the inner membrane. Along with their presence in proteobacteria, the *c*-type cytochromes also form part of the mitochondrial respiratory apparatus in the form of cytochrome *c*. Bacterial *c*-type cytochromes perform a very similar function to mitochondrial cytochrome *c* in that they transport electrons from the bc_1 complex to the terminal reductases. Cytochromes *c*-552, *c*-553 & *c*-554 from algal chloroplasts and cyanobacteria, c_2 from purple photosynthetic bacteria and c_4 and c_5 from *Azotobacter vinelandii* along with many others all have sequence and structural homology with mitochondrial cytochrome *c*[54]. The mitochondrial and bacterial soluble cytochromes all fall within Ambler's Class I of *c*-type cytochromes[55]. Class I *c*-type cytochromes have their heme-attachment site towards the N-terminus, and the sixth ligand is provided by a methionine residue 40 residues further down the chain towards the C-terminus[55][Re-write this sentence, it is almost plagiarism!]. Cytochrome c_4 is a diheme cytochrome and is the electron donor to cbb_3 transfer-

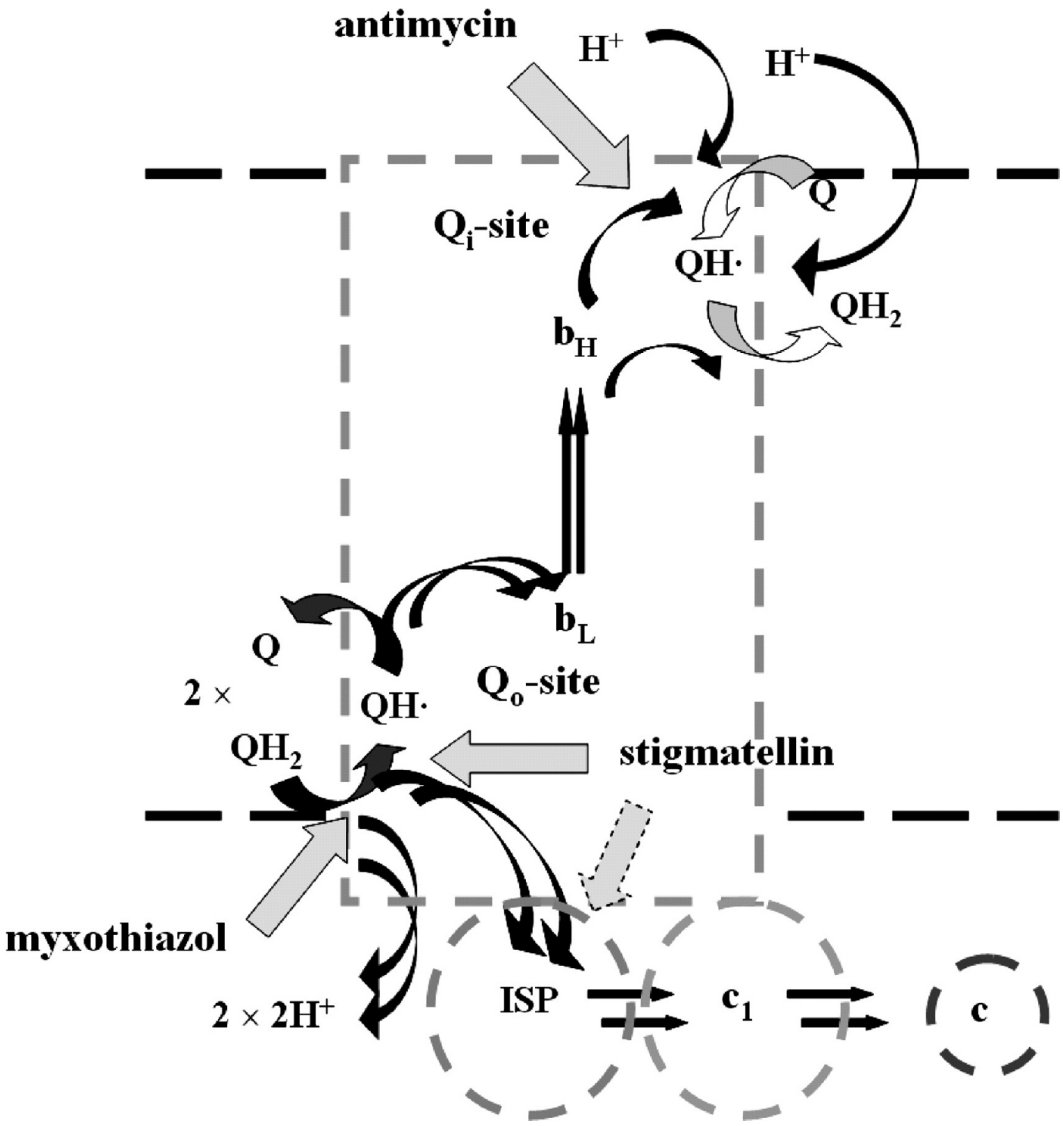

Figure 1.5: **The modified Q-cycle used by the bacterial bc_1 complex.** The cyt *b* subunit is represented by the *dashed gray* outline, and contains the Q_o- and Q_i-sites, connected by hemes b_L and b_H. The ISP and cyt c_1 catalytic domains and cyt *c* are represented by *dashed darker gray circles*. Electron transfer steps are shown by *dark narrow arrows*, proton release and uptake by *lighter arrows*, binding and release of quinone species by *broad curved arrows* (dark gray for Q_o-site, light gray for Q_i-site). Sites of inhibition are indicated by *block arrows* showing sites at which the bound inhibitor displaces quinone species. The *dashed inhibitor arrow* indicates that the reaction of ISPH with cyt c_1 is blocked by the interaction of ISPH with stigmatellin at the Q_o-site. Adapted from Crofts et al.[53].

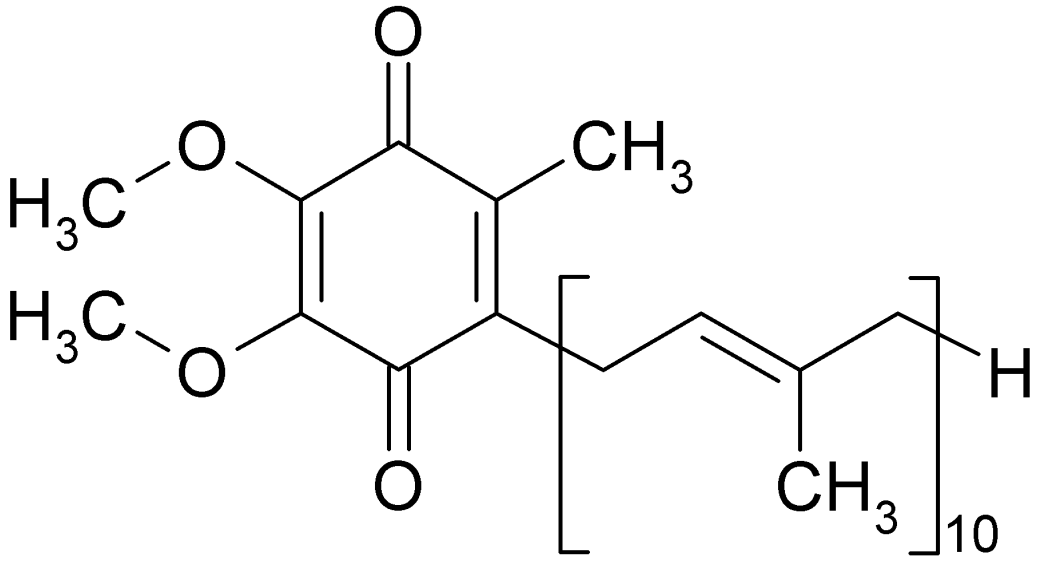

Figure 1.6: **Structure of the ubiquinone molecule.**

ring electrons from the bc_1 complex in *N. meningitidis*[23,29,56].

Cytochrome c_x is a monoheme cytochrome which is also able to transfer electrons from the bc_1 complex to cbb_3[23,29].

Cytochrome c_5 is a diheme cytochrome which appears to be membrane associated. It transfers electrons from the bc_1 complex to AniA during Nitrite reduction[23,29].

1.6.4 Quinone Pool

The quinone source in *N. meningitidis* is predicted to be ubiquinone[23]. Ubiquinone, also known as Coenzyme Q_{10} is found in most eukaryotes. It is a vitamin-like lipid soluble molecule with a long tail made of 10 isoprenyl subunits. This is shown in Figure 1.6.

In its oxidised form it is known as ubiquinone, whereas when reduced it is called ubiquinol. In the *N. meningitidis* respiratory chain, ubiquinone is reduced to ubiquinol by the acceptance of 2 electrons from NADH (amongst others). Ubiquinol then donates electrons either directly to the terminal reductase NorB, or to the bc_1 complex.

1.7 Respiration Regulatory Proteins in *N. meningitidis*

1.7.1 NsrR - Nitrite Sensing Repressor Protein

"NsrR is an NO-sensing Rrf2-type transcriptional repressor"[41]. In *N. meningitidis* (and *N. gonorrhoeae*) it negatively regulates *aniA* and *norB*, and derepression is caused by NO[28,30,31]. Rrf2 proteins have two DNA-binding helix-helix domains[30], with a putative iron-sulfur cluster inbetween. The binding of the iron-sulfur cluster, which is expected to be by NO in NsrR, would perturb the structure of the repressor protein and prevent DNA binding[30].

norB is expressed in a somewhat constitutive manner, in that with no repression *norB* is still expressed to some extent[57]. NsrR represses this expression until NO is present, at which point *norB* can be expressed and the NorB enzyme can start removing the NO that is present.

aniA is positively regulated by FNR, but this seems to be quite insensitive to oxygen in *N. meningitidis*, thus *aniA* would be expressed even at 60 to 80% air saturation with oxygen[30]. *aniA* therefore needs to be corepressed in order to prevent it being expressed excessively in aerobic conditions.

1.7.2 FNR - Fumarate and Nitrate Reductase Regulator

Fumarate Nitrate Reductase is a transcriptional activator which binds to a 4Fe-4S cluster under anaerobic conditions. When oxygen concentrations are low, FNR causes increased expression of proteins that are necessary for anaerobic respiration. "The presence of the 4Fe-4S cluster is correlated with protein dimerization, which enables it to bind promoter DNA"[58]. Four cysteine residues are believed to be ligated to the iron-sulfur cluster and these are required for FNR function. The oxygen sensitivity of FNR is achieved by the iron-sulfur cluster breaking down into 2Fe-2S via 3Fe-4S which is unable to bind DNA. In *N. meningitidis*, *aniA* expression is directly linked to the presence of FNR[18]. When no NsrR is present, *aniA* expression continues even up to 80% oxygen saturation suggesting

that FNR is actually quite insensitive to oxygen, an unusual response compared to FNR from *E. coli*. FNR also becomes less sensitive to oxygen when it is bound to its cognate DNA[58].

1.7.3 NarQ/NarP - Nitrite Response Sensor/Regulator

NarP and NarQ are a two component signal transduction pathway that regulate expression of *aniA* in *Neisseria*. NarQ is the sensor protein located in the inner membrane, while the regulator protein, NarP is found in the cytoplasm. Being a two component system, the sensor protein phosphorylates the regulator allowing it to bind the target DNA (which may consist of multiple sequences) to activate expression of genes.

In *N. gonorrhoeae*, NarP was shown to enhance the expression of *aniA* in response to the presence of nitrite, as a mutant lacking *narP* was significantly slower at growing under denitrifiying conditions[59].

In *N. meningitidis* expression of *aniA* is increased greatly in conditions of high nitrite concentration[18]. This effect is much more pronounced than simply being in oxygen limiting conditions. FNR appears to be required for *aniA* expression even when NarP/NarQ are present[18]. This suggests that the organism is intentionally preventing expression of nitrite reducing components until there is both a high concentration of nitrite *and* a very low concentration of oxygen. This is plausible as even under oxygen limiting conditions oxygen reduction is still favoured over nitrite reduction.

1.8 Organisation of Respiratory Chains in Other Bacteria

The respiratory chain of *N. meningitidis* is shown in a simplified form in Figure 1.7. The components are coloured consistently throughout this section to allow easy comparison between the respiratory chains being discussed. As discussed previously, the respiratory chain of *N. meningitidis* contains an initial electron donor, in this case NADH dehydrogenase. In fact there are a number of other

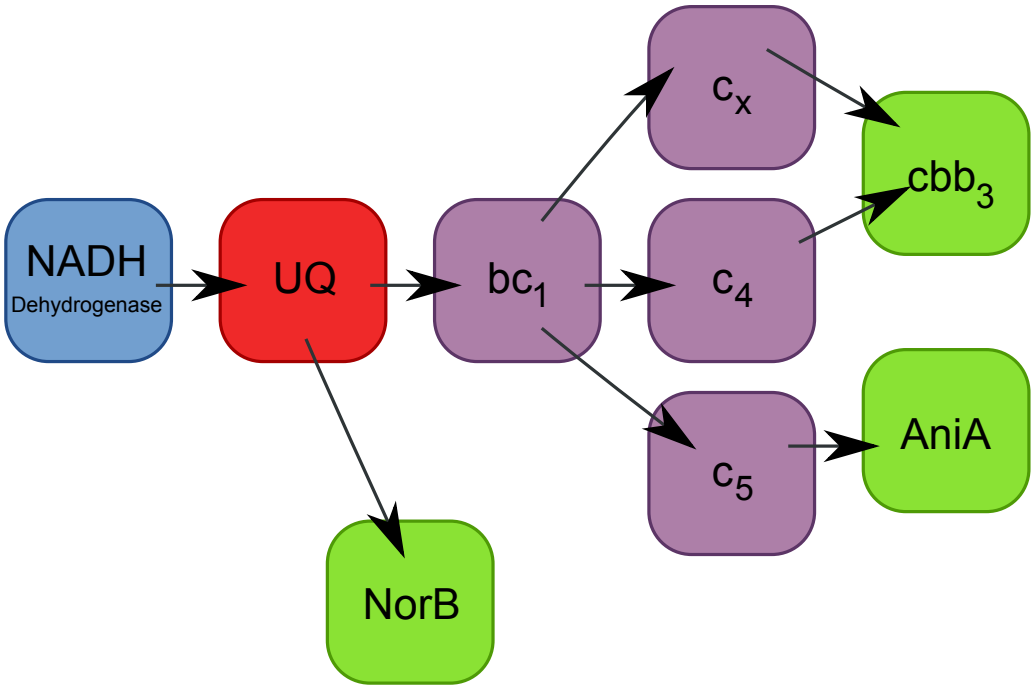

Figure 1.7: **Branched electron transport chains of *N. meningitidis*.** Blue denotes initial electron donor, red denotes quinone pool, purple denotes cytochrome electron transporters and green denotes terminal reductases. UQ = ubiquinone.

electron donors, but they are not discussed here as NADH provides most of the electrons to the respiratory chain. There is also a quinone pool, consisting of ubiquinone/ubiquinol, intermediate *c*-type cytochromes and terminal reductases.

1.8.1 The Respiratory Chain of *Paracoccus denitrificans*

The respiratory chain of *P. denitrificans* is shown in Figure 1.8. It is quite similar to that of *N. meningitidis* with the exception of having a larger number of terminal reductases, and the ability to perform complete denitrification. The chain possesses an initial electron donor, a quinone pool, intermediate cytochrome electron transporters and terminal reductases.

The bc_1 complex of *N. meningitidis* is present as an analogue (Ubiquinol-cyt *c* oxidoreductase), and the chain includes 2 further downstream *c*-type cytochromes. *P. denitrificans* has 3 terminal oxygen reductases, ba_3, which oxidises the quinone pool directly, and cbb_3 and aa_3 which oxidise the *c*-type cytochromes. All three oxygen reductases are HCOs. The branching of the aerobic ETC is quite common

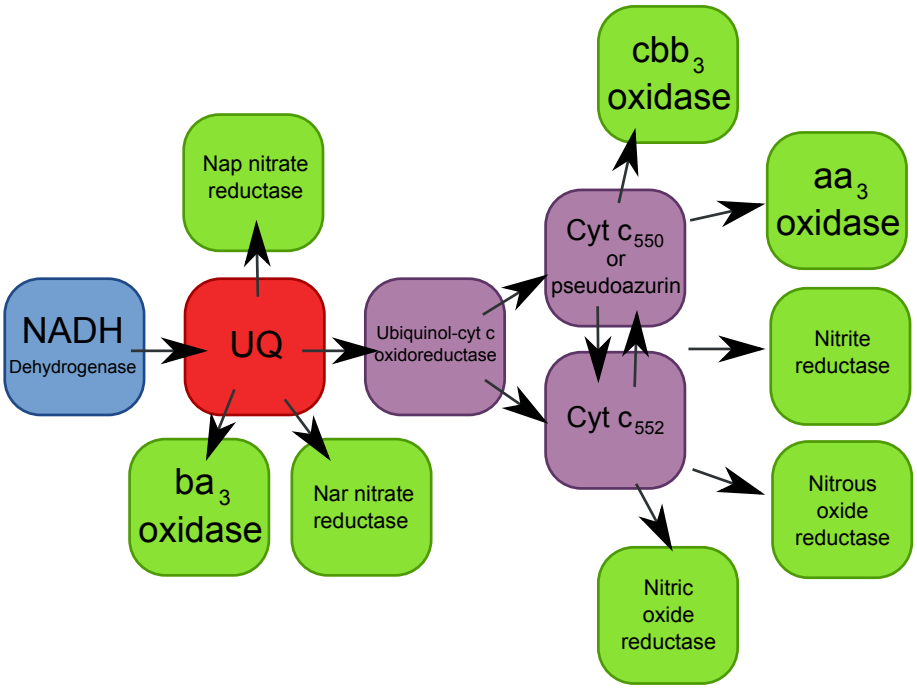

Figure 1.8: **Branched electron transport chains of *Paracoccus* species.** Blue denotes initial electron donor, red denotes quinone pool, purple denotes cytochrome electron transporters and green denotes terminal reductases. UQ = ubiquinone. Electron transfer between cytochromes c_{552} and c_{550} has not been demonstrated experimentally but is possible, given the redox potential of the proteins. Adapted from Baker et al. [60].

among bacteria, but the reason for this is not currently fully understood.

The nitro-reductases found in *P. denitrificans* are capable of complete denitrification as described in Figure 1.1. The nitrate reductases directly oxidise the quinone pool, whereas the nitrite and nitric oxide and nitrous oxide reductases oxidise the *c*-type cytochromes instead.

As with *N. meningitidis* there are a number of potential initial electron donors, but only NADH is shown for simplicity of comparison.

1.8.2 The Respiratory Chain of *Escherichia coli*

The respiratory chain of *E. coli* is shown in Figure 1.9. It can be seen to be quite distinct from other bacteria, and indeed from the mitochondrial respiratory chain. The most obvious difference between *E. coli* and many other bacteria is the lack of *c*-type cytochromes. The terminal reductases are able to be reduced directly by the quinone pool. Additionally, under anaerobic conditions, the quinone pool

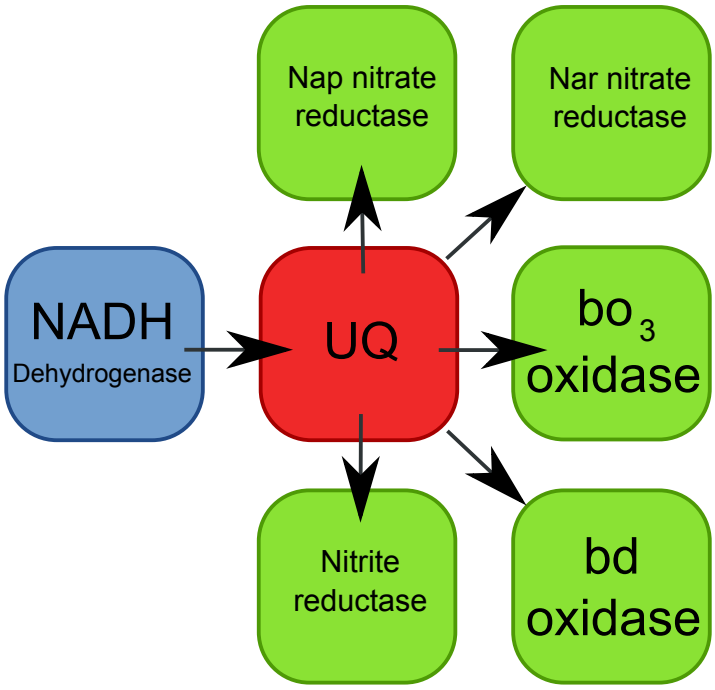

Figure 1.9: **Branched electron transport chains of *E. coli*.** Blue denotes initial electron donor, red denotes quinone pool and green denotes terminal reductases. UQ = ubiquinone. Under anaerobic conditions, ubiquinone is replaced by menaquinone. Adapted from Nicholls and Ferguson [61].

changes from being ubiquinone/ubiquinol to menaquinone/ubiquinol.

E. coli also has a number of different terminal reductases in the form of cyt bo_3 and cyt *bd*. Cyt bo_3 is an HCO and is structurally very similar to cyt aa_3. Cyt *bd* shows no sequence similarity with the HCO superfamily and has no Cu_B site. Cyt *bd* has a much higher affinity for oxygen than cyt bo_3 so is synthesised at low oxygen concentration.

E. coli is also capable of partial denitrification and possesses enzymes to reduce nitrate and nitrite, which are also under the regulatory control of FNR. The reduction of nitrite differs from *N. meningitidis* and *P. denitrificans* as NO_2^- is not reduced to NO, but to NH_4^+ instead.

As with *N. meningitidis* and *P. denitrificans* there are a number of potential initial electron donors, but only NADH is shown for simplicity of comparison.

1.9 Systems Biology

Systems biology is the process of "studying biological systems in their whole [...], reinforced by high throughput [...] molecular tests and considerable sophistication in computational modelling"[62]. Systems biology "combines approaches and methods from systems engineering, computational biology, statistics, genomics, molecular biology, biophysics and other fields"[63].

The aim of Systems biology is to take our detailed understanding of organisms beyond the molecular and cellular level. These are the levels to which the disciplines of molecular and biology and biochemistry (among others) are more suited. It aims to take our understanding to the level of the entire "complex system". Which is to say we gain understanding into the way the organism behaves as a whole, rather than just having knowledge of the individual parts.

The level of complexity in biological systems is far greater than the popular notion of what defines a complex system, however. Biological systems consist of multiple different individual elements each performing specific tasks interacting with each other to create 'coherent' behaviour. This is very different from popular complex systems which are collections of simple, identical components interacting to produce 'complex' behaviour[64].

Gaining understanding such a complex system is difficult, and Kitano suggests that it requires insight into the following properties[65]:

1. **Structure of the system.** This includes the way the system interactions are "laid out" both at a component level and an organismal level.

2. **The dynamics of the system.** This involves understanding how the organism behaves under any given conditions over a particular time period. This may include understanding how the metabolic processes change under these conditions etc.

3. **How the system is controlled.** The control mechanisms can be tailored to suit the desired function or to minimised the chance of malfunction.

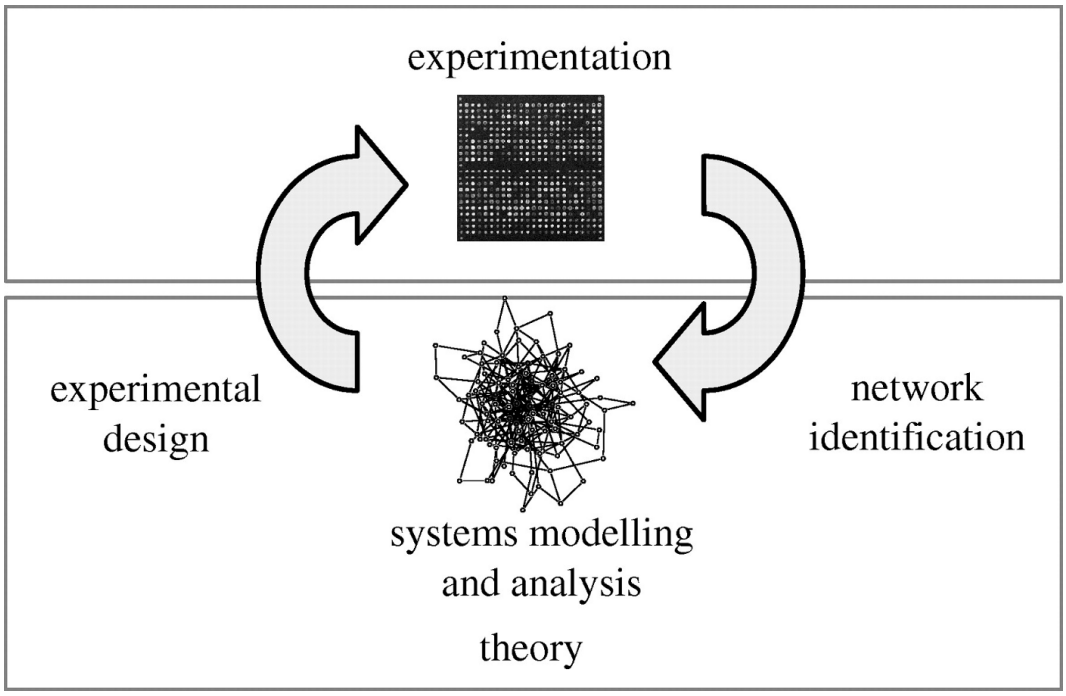

Figure 1.10: **Systems biology cycle.** Interactions between experimental analysis and theoretical approaches, and the main tasks for theory at the interfaces. Doyle and Stelling [63]

4. **How the system is designed.** "Trial and error" experimentation can be done away with, as the system can be designed based on defined properties, backed up by models and simulations.

The level of integration between systems biology approaches and experimentation can be seen in Figure 1.10. This shows the iterative cycles that are necessary to gain understanding in both areas. The experimentation provides data to refine and develop the system model, and data from that model can go on to improve the design of the experiment.

Systems biology extends further into a computational discipline when you consider that if you can create a model of a system, you can potentially run a simulation of the system using the model. Simulations can be developed for multiple stages of the process, from molecular to organismal. Simulations of interactions based on gene regulatory network models are being studied [66], as are complete plant development models [67–69].

Figure 1.11 shows one of the limitations of the current technology "powering"

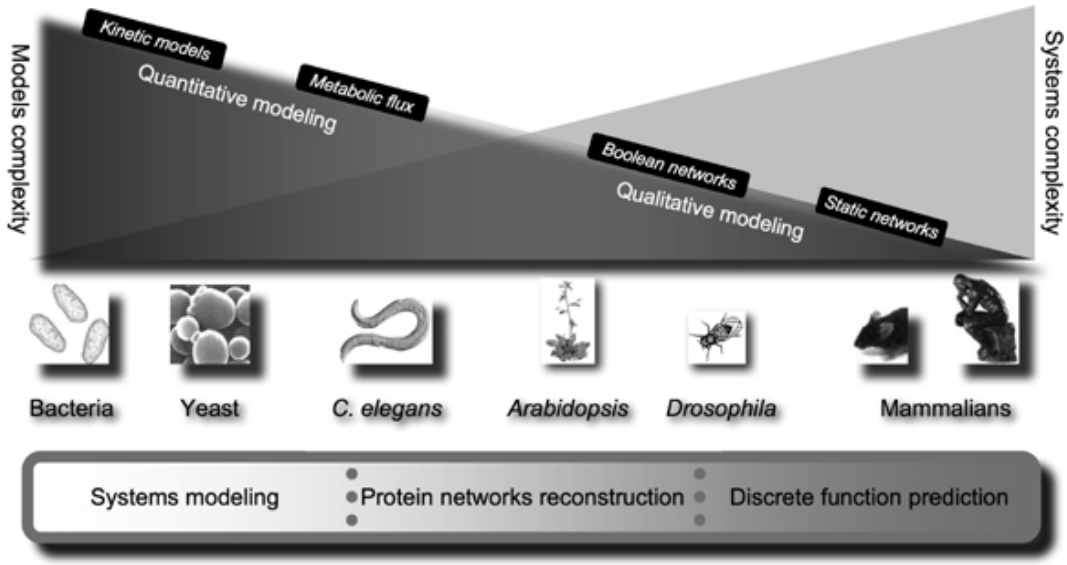

Figure 1.11: **System complexity.** Diagram showing how system complexity varies across organisms, and how the complexity of the models we can produce is currently the inverse of systems complexity. Kahlem and Birney [62]

systems biology. As organisms get more complex, the models we can produce get less complex and less quantitative[62]. This concomitant lack of data in models of complex organisms decreases the likelihood of being able to produce a simulation of the model. We might be able to simulate *aspects* of a complex organism, such as the human heart[70] but we are still a long way from being able to simulate the entire human body.

For simpler systems, like yeast, or *E. coli* an enormous amount of data already exists about individual gene regulation, protein interactions etc. and it is possible to build sophisticated models of the entire gene regulatory network and more[71,72].

A systems biology approach to understanding the mechanism of respiration in *Neisseria meningitidis* is necessary as there are a number of components in the system which are inherently unmeasurable.

1.10 Modelling

1.10.1 Modelling Respiratory Systems

A limited amount of modelling has been carried out on bacterial respiratory chains, these focused on the denitrification pathway and treated the pathway as a simple electrical circuit[73]. An alternative approach involved modelling respiration using "P systems" which are probabilistic models of events. This assigned a probability of each reaction happening, dependant on the state of the system and then iterated through a given set of steps evaluating probabilities and altering values based on the outcome[74]. This approach to modelling was limited in that it was only predicting the quantities of 1 component in each of 2 "compartments"; oxygen in the cell membrane and carbon dioxide in the thylakoid membrane (the model was developed using cyanobacteria).

Some modelling of parts of the respiratory chain in *E. coli* have also been modelled. Peercy et al.[72] created a kinetic model of how cytochrome production is regulated by oxygen using differential equations. They created a set of differential equations to describe the relevant reactions and then populated the model using parameters gathered from the literature.

Since when modelling respiration in a cell, the most important factor is the change in concentration of components over time without any particular spatial constraints, ordinary differential equations (ODEs) are an appropriate technique. In these systems the model does not change with regard to the spatial arrangement of any of the components. If the system requires changes in time *and* space, then partial differential equations (PDEs) would be necessary (and more complicated)[75].

Ordinary differential equations only depend on one variable; the time (t). In this case, the change in concentration over time for each component can be modelled as a single differential equation. For multiple components this leads to multiple differential equations with some that rely on the result of another (if the rate

of one reaction is directly related to the concentration of another component). These ODEs must then be solved in parallel at a suitable time-scale.

Complications arise when using differential equations if the processes are considered to be stochastic, as a differential equation model assumes that every component can have a continuous value, which is not the case as molecules are discrete. However if the system being modelled is sufficiently large, this effect can be ignored. If the reaction component size is small ($<$ 100s of molecules) stochastic simulation algorithms have to be used as described by Gillespie[76]. This method requires far more computation than solving ODEs, as the model will spend most of its time calculating values for reactions involving large molecules even though this is not necessary as the reaction is not stochastic. Additionally, the time interval used between reaction steps is usually very small, meaning the simulation progresses slowly[75].

1.10.2 Modelling Tools

A number of software packages exist that are capable of this type of modelling such as the Systems Biology Workbench[77] and COPASI[78]. These allow you to enter biochemical reactions in a format familiar to biologists, and have pre-defined libraries for types of reactions such as mass-action, or one with Michaelas-Menton kinetics etc. The mathematical equations are then derived automatically from the reactions and can be modified by hand if necessary. Parameters for the mathematical equations must be entered, and these will usually be derived from experimental data, or in some cases educated guesses (at least initially). Once a parameter set has been created, the modelling software can run a time-course using a relevant solver-algorithm. COPASI includes 4 solvers, LSODA (Livermore Solver for Ordinary Differential Equations)[79] for deterministic systems (such as ODEs), Gibson-Bruck[80] for stochastic systems and Runge-Kutta and LSODA for hybrid systems (where portions are not considered to be stochastic).

1.11 Aims

The over-arching aim of this study was to produce a working mathematical model of the respiratory system of *N. meningitidis* which has been refined and parametrised by experimental biological data. This mathematical model should be able to accurately simulate experimental datasets with known outcomes, and also be able to predict the outcome of experiments that have not been performed. This model, will also be able to provide insight into the states of various components throughout the respiratory process, such as enzymatic oxidation states, some of which are very difficult, if not impossible, to obtain in an *in vivo* study.

The layout of *N. meningitidis* respiratory chain, even though it is longer than that of the model organism *Escherichia coli* is more similar to most other bacteria. This, along with its profound medical importance make it an excellent target for the type of mathematical modelling described above.

The individual aims of the study are therefore:

1. **Construct a mathematical model of the *N. meningitidis* respiratory chain.** This will involve the conversion of the kinetic reactions involved in respiration into mathematical equations that can be linked together, and if justified simplifying the chain.

2. **Obtaining experimental data on respiratory rates and enzyme kinetics.** This will involve performing experiments on respiring *N. meningitidis* and recording the concentrations of respiratory substrates under different conditions.

3. **Parametrise the model using experimental data.** To do this a system will need to be developed which can iteratively fit experimental data to specific parts of the mathematical model.

Chapter 2

Materials and Methods

2.1 *Neisseria meningitidis* Strains Used in This Work

Name	Description	Source
MC58	Wild-Type Strain	McGuinness et al. [81]
ΔnorB::spc^r	Wild-Type with insertion of spectinomycin resistance cassette into *norB* gene	Heurlier et al. [28]
ΔnsrR::spc^r	Wild-Type with insertion of spectinomycin resistance cassette into *nsrR* gene	Rock et al. [30]
ΔnorB::spc^r-ΔnsrR::tet^r	Wild-Type with insertion of spectinomycin resistance cassette into *norB* and insertion of tetracycline resistance cassette into *nsrR* genes	Heurlier et al. [28]
ΔaniA::spc^r-ΔnsrR::tet^r	Wild-Type with insertion of spectinomycin resistance cassette into *aniA* and insertion of tetracycline resistance cassette into *nsrR* genes	Heurlier et al. [28]

Table 2.1: Bacterial strains and sources

2.2 Culturing *Neisseria meningitidis*

2.2.1 Growth of *Neisseria meningitidis*

N. meningitidis strains were grown on plates on Columbia Agar Base (CAB) with defibrinated horse blood, and in liquid culture in Müller-Hinton Broth (MHB).

Plates were prepared by adding horse blood to a final concentration of 5% to molten agar, and poured into plastic petri dishes. After streaking with *N. meningitidis* the plates were incubated at 37 °C in a 5% carbon dioxide/air mixture.

Aerobic liquid cultures were grown in 10 ml MHB with 10 mM $NaHCO_3$ in plastic Sterilin tubes, and incubated at 37 °C at 200 rpm. Microaerobic cultures were suspended in 20 ml MHB, 10 mM $NaHCO_3$ in plastic Sterilin tubes, incubated at 37 °C at 100 rpm.

2.2.2 Preparation of Antibiotic Selective Media

Liquid stock solutions of required antibiotics were either added directly to liquid culture, or, if growing on plates, to the molten agar when also adding horse blood. The final concentrations of antibiotics are given in Table 2.2.

Antibiotic	Final concentration (μg/ml)
Spectinomycin	50
Tetracycline	2.5
Chloramphenicol	50

Table 2.2: Final antibiotic concentrations

2.2.3 Preparation of Frozen Bacterial Stocks

Bacteria were grown in liquid culture until late log phase prior to harvesting. Liquid cultures were then centrifuged at 4000 g for 15 minutes, and the pellet was then resuspended in a 25% glycerol, 25% water and 50% MHB, all of which had been autoclaved beforehand. The bacterial stocks were then frozen at -80 °C.

2.2.4 Streaking Plates for OD to CFU Ratio Calculation

Bacterial cultures were grown overnight and then transferred into aerobic liquid culture and samples taken throughout the day to obtain a range of different optical densities. The optical density was recorded at 600 nm on a Jenway 6305 Spectrophotometer (Bibby Scientific Limited, Staffordshire UK), and each sample was serially diluted to the following levels: 10^{-5}, 10^{-6} and 10^{-7}. 100 μl of each of these dilutions was plated on a fresh blood agar plate and left to grow overnight. The following morning the number of colonies on each plate was counted and used to create a simple conversion factor for Optical Density to Colony Forming Units.

2.3 Measuring Oxygen Concentration

Oxygen concentration in respiring cultures was measured using a Clark electrode[82] from Rank Brothers, Cambridge, UK. This electrode has a silver anode and a platinum cathode and uses a saturated potassium chloride solution as electrolyte. The electrode is set at the bottom of a 7 ml reaction chamber separated from its contents by a thin Teflon™ membrane. This apparatus is shown in Figure 2.1. The Teflon™ membrane is permeable to dissolved oxygen, which is reduced by the electrode producing a measurable electrical current. The reaction chamber is maintained at 37 °C by an attached water bath. When performing experiments, 5 ml of culture is added to the reaction chamber, which is stirred by use of a magnetic flea, and the chamber covered with a plastic stopper. The stopper has a number of holes through which the NO probe, or Hamilton syringe can be inserted. Data is collected by attaching the electrode to an external data logger (Pico ADC20, Pico Technology).

2.3.1 Calibration of Oxygen Electrode

Calibration of the oxygen electrode assumes that anaerobic water will not produce any measurable current at the electrode. Oxygen saturated water contains

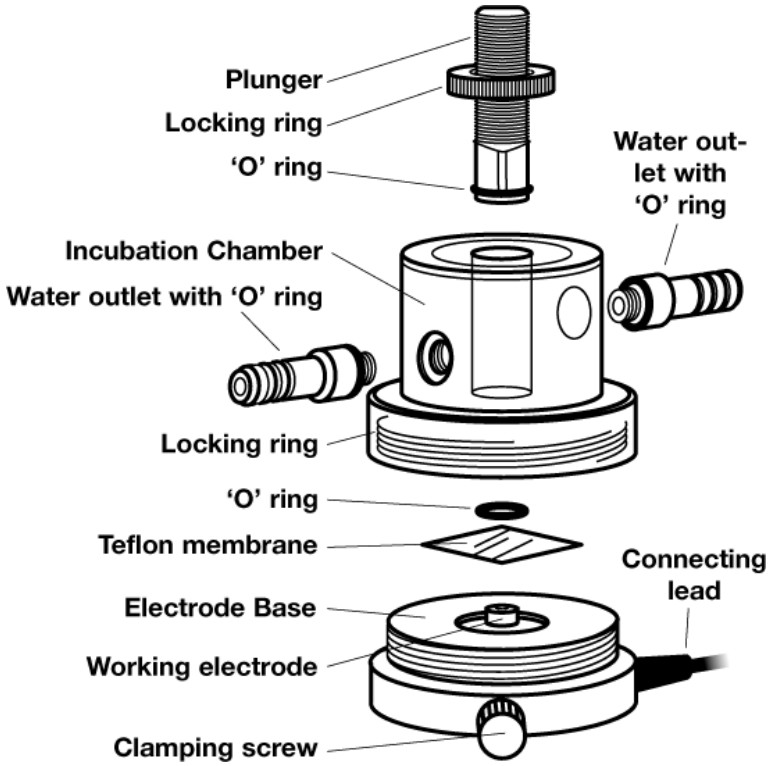

Figure 2.1: **Exploded view of the oxygen electrode.** This assembly sits atop a Rank Brothers Digital Model 10 Controller which acts as a magnetic stirrer and provides the polarising voltage to the electrode (Rank Brothers Ltd [83]).

210 μM Oxygen at 37 °C[84]. 5 ml of ultra pure (18 $M\Omega$) water was added to the electrode chamber, and then aerated to saturation by use of a pasteur pipette. The maximum value recorded by the data logger then corresponds to a concentration of 210 μM Oxygen, with the relationship between mV as recorded against concentration being linear.

2.4 Measuring Nitric Oxide Concentration

Nitric Oxide concentration was measured using a Nitric Oxide probe (ISO-NOP, World Precision Instruments) connected to a Nitric Oxide Meter (ISO-NO mkII, World Precision Instruments). This is also a Clark type electrode, contained within a steel sleeve with a semi-permeable membrane separating the working electrode from the system being measured[85–87]. The NO probe is inserted through one of the holes in the plastic lid of the reaction chamber of the oxygen electrode assembly. The tip of the electrode should be immersed in the culture, with care being

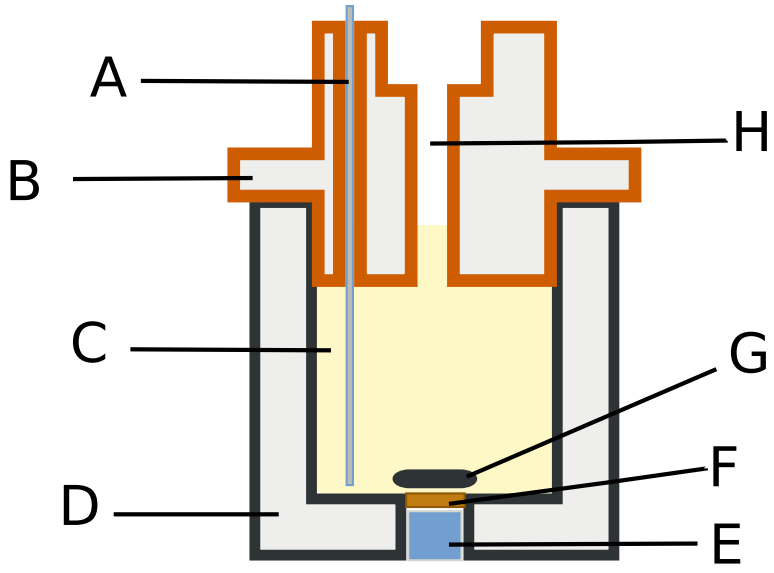

Figure 2.2: **Oxygen electrode chamber with nitric oxide probe inserted.** This shows the set up used to obtain all oxygen and nitric oxide measurements. A - ISO-NOP Nitric Oxide probe. B - Electrode chamber cap. C - Culture media. D - Oxygen electrode chamber. E - Oxygen working electrode. F - Teflon™ membrane. G - Magnetic Flea. H - Air gap.

taken not to trap any air bubbles on the surface of the probe. The sensor is also attached to the same data logger as above. In this way both Oxygen and Nitric Oxide concentrations can be measured in parallel. A diagram of the apparatus when set up is shown in Figure 2.2.

2.4.1 Calibration of Nitric Oxide Electrode

Calibration of the nitric oxide electrode relies on adding known quantities of Nitric Oxide to the electrode chamber. Sodium Nitrite will liberate Nitric Oxide with a 1:1 ratio when added to a solution of excess Potassium Iodide and Sulfuric acid based on the following reaction:

$$2NaNO_2 + 2KI + 2H_2SO_4 \longrightarrow 2NO + I_2 + 2H_2O + 2Na_2SO_4 \qquad (2.1)$$

5 ml of 0.1M Potassium Iodide/Sulfuric Acid was added to the electrode chamber and allowed to stabilise. Then, increasing concentrations of Sodium Nitrite solution were successively added to produce a standard curve of Nitric Oxide concentration to recorded electrode mV. The volume and concentrations of Sodium

$NaNO_2$ Concentration (μM)	Volume (μl)	NO Concentration (nM)
10	50	99
100	25	591
100	50	1561

Table 2.3: Sodium Nitrite concentrations used to calibrate ISO-NOP Nitric Oxide sensor.

Nitrite added to the electrode chamber are detailed in Table 2.3.

2.5 Measuring Nitrite Concentration (Griess Assay)

Nitrite concentration in liquid culture was determined using the colorimetric assay described by Nicholas and Nason[88]. This reaction is based on chemical diazotization which uses sulfanilamide and *N*-1-napthylethylenediamine dihydrochloride (NED) under acidic (hydrochloric acid) conditions. Nitrite is converted to nitrous acid under acidic conditions and this then forms a diazonium salt with the sulfanilamide. The diazonium salt combines with NED and forms a pink azo dye which can be detected using absorbance spectrophotometry at a wavelength of 540 nm. Depending on the expected concentration of nitrite, different sample volumes are used in the assay. The most common sample volume used was 25 μl which allows detection up to around 1 mM nitrite with the following reagent volumes: 875 μl of 1% sulfanilamide in 1 M HCl and 100 μl of 0.02% NED in 1 M HCl. When using different sample volumes, the volume of sulfanilamide was altered such that the volume of sample + sulfanilamide always equalled 900 μl. After adding the sample to the reagents, it was left for 20 minutes for the colour to develop, then the absorbance at 540 nm was measured and compared to a standard curve.

2.6 Nitric Oxide Production

Solutions of Nitric Oxide were prepared using a method derived from one described by Aga and Hughes[89]. The apparatus setup is shown in Figure 2.3. A

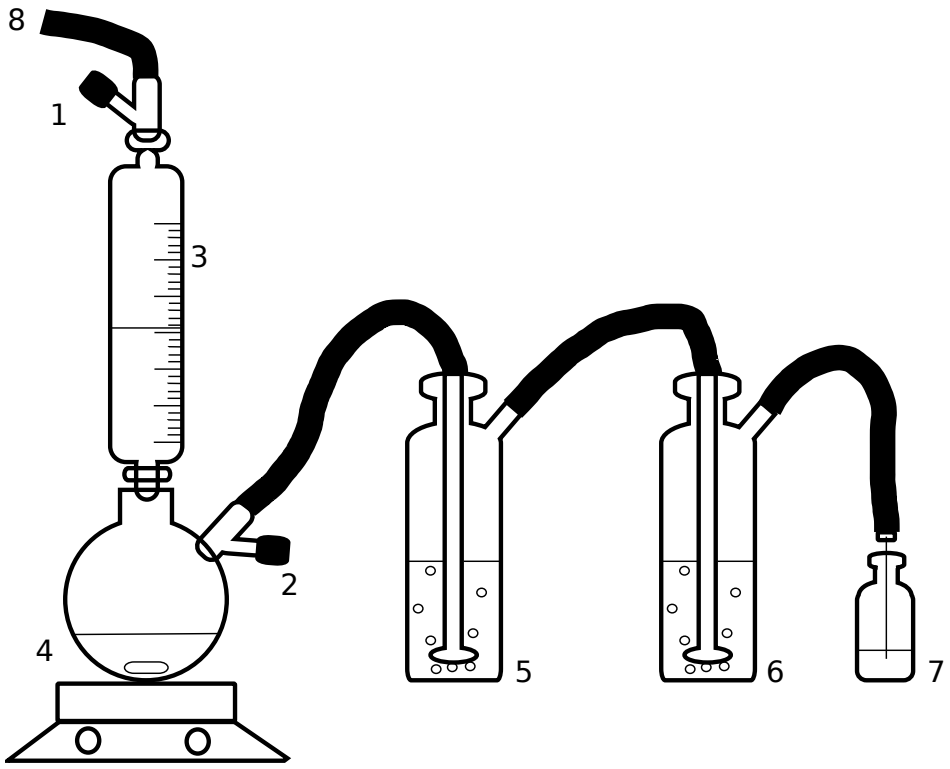

Figure 2.3: **NO making apparatus.** 1 & 2 - N_2 release valves. 3 - Pressure equalizing dropping funnel, containing 50 ml 4 M H_2SO_4. 4 - Stirred, round-bottomed flask, containing 200 ml 2 M $NaNO_2$. 5 - Dreschel bottle with sintered bulb, containing $\approx$ 200 ml 1 M NaOH ($\frac{2}{3}$ full). 6 - Dreschel bottle with sintered bulb, containing $\approx$ 200 ml dH_2O ($\frac{2}{3}$ full). 7 - Small glass bottle with rubber septum and needle entry valve, containing dH_2O $\frac{2}{3}$ full. This bottle either needs to also have a gas exit needle, or at least not be sealed during the process.. 8 - To N_2 gas bottle. Viton rubber tubing is used for all the flexible hoses in this apparatus.

concentrated solution of Sulfuric acid is added from a pressure-equalizing dropping funnel to a concentrated solution of Sodium Nitrite solution in a stirred, round-bottomed flask. This releases NO gas which passes through a solution of Sodium Hydroxide to neutralise any Sulfuric acid present, then through distilled water to remove any Sodium Hydroxide before finally being bubbled into a collection vessel with a sealed rubber septum containing distilled water. The concentrations of the chemicals used in this preparation are shown in Table 2.4. The system should be set up in a fume cupboard as shown in Figure 2.3 and sparged with N_2 gas for 15 minutes (the dropping funnel will allow gas to pass into the round bottomed flask even when the bottom valve is closed). The H_2SO_4 should be sparged separately. Valve 2 should be left open at all times. After sparging close valve 1 and then add the Sulfuric acid dropwise from the drop-

Chemical	Volume (ml)	Concentration (M)
$NaNO_2$	200	2
H_2SO_4	50	4
NaOH	200	1

Table 2.4: Chemicals needed for preparation of Nitric Oxide solution.

ping funnel. Brown gas will start to bubble through to the collection vessel. This apparatus should produce enough NO gas to saturate several small (10 ml) collection vessels which should have the needle removed and be sealed once saturated. Once all the Sulfuric acid has been added leave the reaction to finish which could take 1-2 hours. Before disassembly the apparatus should be sparged with N_2 gas to remove residual NO gas.

The eventual concentration of NO in the solution will vary depending on the temperature, but at 25 °C in ultra pure (18 $M\Omega$) water the concentration will be between 1.88 and 1.96 mM[89,90].

Chapter 3

Model - Construction and Parameters

3.1 Construction

The model was constructed based on existing knowledge of the respiratory chain in *Neisseria meningitidis* from the ETC shown in Figure 1.2 (Chapter 1). I made no *a priori* assumptions about separation of time-scales that would permit the use of Michaelis-Menton kinetics, as the rates of intermediate reaction steps are not known. This approach also permits tracking of the oxidation state of all the intermediates which allows understanding and offers the potential for predictions that may be explored in future *in vivo* studies.

The model was generated as a set of ordinary differential equations which describe the bulk-average concentration of substrates, products, enzymes and their activity within a well-mixed vessel. I have made no assumptions about the bacterial population structure or the variations in concentrations of substrates between the bulk media and within the bacterial cells. Stochastic effects are ignored, but they are unlikely to be of importance. Additionally protein production is largely ignored as the switching mechanism happens on a time-scale that is much shorter than the transcription and translation of new proteins, they are therefore assumed to be expressed constitutively except where stated otherwise.

3.1.1 Converting Biological Reactions into Differential Equations

The rationale for obtaining the form for each of the 9 component equations is described below. Throughout the model the reduced components, i.e. those with available electrons, are denoted as active and have a subscript a. Components lacking a subscript denote the total, constant, amount of a component.

Respiratory Substrates

Oxygen

The change in concentration of oxygen is affected by the following kinetic reactions

$$\emptyset \xrightarrow{\beta} O_2$$

$$O_2 + C_a \xrightarrow{k_1} H_2O + C_i$$

where β is the rate of passive diffusion of O_2 into the electrode chamber. The rate constant k_1 describes the reduction of oxygen and the oxygen reductase cbb_3; this rate depends on the concentration of reduced (i.e. active) cbb_3, C_a and the concentration of O_2. The differential equation that gives the change in oxygen concentration is

$$\frac{d[O_2]}{dt} = \beta(1 - [O_2]/K_O) - k_1[C_a][O_2] \tag{3.1}$$

In isolation the first term gives rise to a simple exponential input of oxygen until the saturation level (K_O) is reached. One small complication encountered was that β is itself affected by the amount of bacteria in the vessel which has implications for fitting.

Nitric Oxide

The change in nitric oxide concentration is affected by the following kinetic reac-

tions

$$NO_2^- + A_a \xrightarrow{m_1} NO + A_i$$

$$NO + B_a \xrightarrow{l_1} N_2O + B_i$$

$$NO + C_a \xrightarrow{k_5} NO\text{-}C_X$$

$$NO\text{-}C_X \xrightarrow{k_6} NO + C_a$$

$$\emptyset \xrightarrow{\gamma} NO$$

The equations above have a number of additional interactions in comparison to O_2. NO is created by the reduction of NO_2^- by AniA, is reduced by its dedicated reductase, NorB, and converted to N_2O which is lost from the cell, interacts with *cbb*$_3$, and is also spontaneously lost from the electrode chamber. I make the assumption that the interaction with *cbb*$_3$ occurs only in a reversible manner, leading to an NO bound and temporarily inactive form C_X. There is evidence that this interaction can also lead to permanent degradation of *cbb*$_3$ via the formation of peroxynitrite at the terminal oxidase. This is not currently considered in this version of the model. These effects are described mathematically in the equation below in the order presented.

$$\frac{d[NO]}{dt} = m_1[NO_2^-][A_a] - l_1[NO][B_a] - k_5[C_a][NO] + k_6[C_X] - \gamma[NO] \qquad (3.2)$$

The rate of synthesis of NO is captured by the first term, with rate constant m_1 and depends on the both the concentration of NO_2^- and reduced AniA (A_a). The reduction of NO is described by the next term with the rate constant l_1 and also depends on the concentration of NO and reduced NorB (B_a). Inhibition of *cbb*$_3$ by NO is modelled by the 3rd component of the equation. k_5 is the rate constant describing the reversible binding of NO to *cbb*$_3$ to form the inactive form of *cbb*$_3$, C_X. k_6 is the rate of recovery of this inhibited *cbb*$_3$. γ is the spontaneous rate of loss of NO from the electrode chamber.

Nitrite

The change in nitrite concentration is affected by the following kinetic reaction

$$NO_2^- + A_a \xrightarrow{m_1} NO + A_i$$

Which can be modelled mathematically by this equation

$$\frac{d[NO_2^-]}{dt} = -m_1[NO_2^-][A_a] \tag{3.3}$$

where m_1 is the rate of reduction of NO_2^- by reduced (active) AniA (A_a).

Electron Transporters

In addition to the rate of change of concentration of the respiratory substrates, the model also contains information about the upstream state of components of the transfer chain, starting from the quinone pool. The ultimate upstream source of electrons into the respiratory chain is from NADH, but I have chosen to subsume all process prior to the quinone pool into a simple single rate. This simplification is made to avoid further complications associated with varying metabolism and to avoid distraction from the stated primary aim of understanding the switching behaviour of the downstream chain. I have chosen the quinone pool as the starting point because it is known that NorB draws electrons directly from this point and therefore this represents the first branch in the chain. I wish understand how competition for electrons at branches effects function and therefore the quinone pool is included in the model.

Quinones

The change in concentration of reduced quinones is affected by the following kinetic reactions

$$Q_i \xrightarrow{g} Q_a$$

$$B_i + Q_a \xrightarrow{l_3} B_a + Q_i$$

$$E_i + Q_a \xrightarrow{f} E + Q_i$$

The differential equation that models these reactions is

$$\frac{d[Q_a]}{dt} = g([Q] - [Q_a]) - l_3[Q_a]([B] - [B_a]) - f[Q_a]([X] - [E]) \tag{3.4}$$

Q_a is the reduced quinone, and Q the total concentration of quinones in the system (Q_i is calculated from these two values). g represents the constant rate of availability of electrons into the quinone pool from NADH. The reduction of NorB by active quinones is parametrised by the rate constant l_3. NorB and reduced NorB are given by B and B_a respectively. As the quinones also reduce the cytochromes, this also needs to be modelled. f is the rate constant parametrising the reduction of cytochromes by the active quinones. Total cytochromes and total reduced cytochromes are given by X and E respectively which are used to calculated E_i in the kinetic reaction.

Cytochromes

I am using a simplified version of cytochromes and therefore X actually represents a pool of different cytochromes, c_x, c_4, c_5 and the bc_1 complex. These are amalgamated into one here to simplify the equations and focus on the simple branching of the chain and competition for electrons. This is a modelling choice and it is further discussed in Chapter 9.

The concentration of active cytochrome pool changes due to both reduction by the upstream quinone pool and oxidation by both of the remaining downstream terminal enzymes as can be seen in the following kinetic reactions

$$C_i + E \xrightarrow{k_3} C_a + E_i$$
$$A_i + E \xrightarrow{m_3} A_a + E_i$$
$$E_i + Q_a \xrightarrow{f} E + Q_i$$

These are modelled with the following differential equation

$$\frac{d[E]}{dt} = -k_3([C] - [C_a] - [C_X])[E] - m_3([A] - [A_a])[E] + f[Q_a]([X] - [E]) \tag{3.5}$$

where k_3 is the rate constant describing the reduction of the available oxidised cytochrome c oxygen reductase (cbb_3) by the quinone pool (via c_x & c_4). C, C_a and C_X represent the overall concentration of cbb_3, reduced (active) cbb_3 and NO inhibited cbb_3 respectively. m_3 is the rate constant describing the reduction of AniA by the cytochrome pool (via c_5). The concentration of active cytochromes thus increases by their reduction by the quinone pool, but this in turn can reduce the flux from the pool because less oxidised cytochrome is available to accept electrons. As stated previously, the relative time scales are unknown so all processes appear explicitly.

Terminal Reductases

Finally the changes in concentration of reduced terminal oxidases, cbb_3, AniA and NorB are described by the following equations. All the terms present in this section have been introduced previously. I could of course equally write these equations for the oxidised form but this can easily be recovered because I am assuming that the total concentration of the oxidases remains constant.

Reduced *cbb*$_3$

The kinetic reactions which affect the concentration of reduced (active) cbb_3 are

$$C_i + E \xrightarrow{k_3} C_a + E_i$$
$$O_2 + C_a \xrightarrow{k_1} H_2O + C_i$$
$$NO + C_a \xrightarrow{k_5} NO\text{-}C_X$$

which is described by

$$\frac{d[C_a]}{dt} = k_3([C] - [C_a] - [C_X])[E] - k_1[C_a][O_2] - k_5[C_a][NO] \tag{3.6}$$

Inhibited *cbb*$_3$

The following kinetic reaction alters the concentrations of reversibly inhibited

cbb_3

$$NO + C_a \xrightarrow{k_5} NO\text{-}C_X \xrightarrow{k_6} NO + C_a$$

which is described by

$$\frac{d[C_X]}{dt} = k_5[C_a][NO] - k_6[C_X] \tag{3.7}$$

Reduced AniA

The concentration of reduced AniA is affected by the following kinetic reactions

$$A_i + E \xrightarrow{m_3} A_a + E_i$$
$$NO_2^- + A_a \xrightarrow{m_1} NO + A_i$$

which can be modelled by

$$\frac{d[A_a]}{dt} = m_3([A] - [A_a])[E] - m_1[NO_2^-][A_a] \tag{3.8}$$

Reduced NorB

Changes in NorB concentration occur via the following kinetic reactions

$$B_i + Q_a \xrightarrow{l_3} Q_i + B_a$$
$$NO + B_a \xrightarrow{l_1} N_2O + B_i$$

and are modelled by this equation

$$\frac{d[B_a]}{dt} = l_3[Q_a]([B] - [B_a]) - l_1[NO][B_a] \tag{3.9}$$

3.1.2 Assumptions and their Justifications

I have made a number of assumptions regarding the kinetics and reactions taking place in the model.

1. **I have assumed that NO inhibits the reduced *cbb$_3$* and not the oxidised form, since I wouldn't expect Nitric oxide to bind to an inactive enzyme.** This is corroborated by Giuffre et al.[91], who show significant levels of inhibition of reduced cytochrome. They do also however observe low levels of inhibition of the oxidised enzyme also. Their experiments used cytochrome c oxidase (aa3) rather than *cbb$_3$*, but I believe this assumption still stands as the enzymes are of the same family.

2. **Bacterial population structure and concentration variation.** The primary substrates of interest are gases which are thought to freely diffuse in and out of the cells.

3. **No backwards reactions.**

4. **No Michaelis-Menton kinetics.** Cannot assume that time-scales are separated as the rates of intermediate reaction steps are not known.

5. **All cytochromes can be modelled as one.**

6. **Laz and c_5 effects on AniA and *cbb$_3$* respectively can be ignored.** They are not the prime electron donors to their terminal reductases and contribute very little overall to the reduction[23].

3.2 Parameters and their Prior Distributions

None of the rate constants or concentrations which were required for this model have previously been determined for *Neisseria meningitidis*, so values from other similar organisms had to be used instead. In some cases there appears to be no data in the literature regarding values of particular components. Table 3.1 lists the values that have been obtained from the literature.

Symbol	Description	Value	Source
k_1	Rate of O_2 reduction by reduced *cbb*$_3$	415 $\mu M^{-1}s^{-1}$	Forte et al.[92] and Hunter[93]
k_3	Rate of *cbb*$_3$ reduction by cytochrome pool	3 $\mu M^{-1}s^{-1}$	Chang et al.[56]
l_1	Rate of NO reduction by reduced NorB	Unknown	N/A
l_3	Rate of NorB reduction by quinone pool	Unknown	N/A
m_1	Rate of NO_2^- reduction by reduced AniA	Unknown	N/A
m_3	Rate of AniA reduction by cytochrome pool	4.8 ± 0.2 $\mu M^{-1}s^{-1}$	Nojiri et al.[94]
k_5	Rate of *cbb*$_3$ inhibition by NO	100 $\mu M^{-1}s^{-1}$	Giuffre et al.[91] and Blackmore et al.[95]
k_6	Rate of recovery of NO inhibited *cbb*$_3$	Unknown	N/A
β	Rate of passive diffusion in of O_2	Unknown	N/A
K_O	Saturation O_2 level	126 μM	This work
g	Rate of electrons in from NADH	Unknown	N/A
f	Rate of reduction of cytochromes by quinones	Unknown	N/A
γ	Spontaneous loss of NO	Unknown	N/A
Q	Concentration of quinones	0.3 μM	Hedrick and White[96]
X	Concentration of cytochromes	$\approx$ 3.97 μM	Deeudom[23]
A	Concentration of AniA	Unknown	N/A
B	Concentration of NorB	Unknown	N/A
C	Concentration of *cbb*$_3$	0.03 μM	Unknown

Table 3.1: Model parameters

Variables

O_2 - Oxygen concentration

This variable is always obtained directly from the experimental dataset as it indicates the starting point for oxygen in the model. It is always set to the first oxygen data point in the dataset and has no prior distribution. It is usually a fixed value, except in cases where the dataset indicates measurement artefacts.

NO - Nitric oxide concentration

As for Oxygen concentration, this variable is simply obtained from the dataset and the same conditions apply.

NO_2^- - Nitrite concentration

Nitrite concentration is also handled in the same way as the oxygen and nitric oxide concentrations.

E - Reduced cytochrome concentration

Unknown at start of simulation. Assume close to zero, and certainly less than total. The best prior to use would be the value after a couple of simulation seconds, however this would no longer be a prior.

A_a - Reduced AniA

Unknown at start of simulation. Assume close to zero, and certainly less than total. The best prior to use would be the value after a couple of simulation seconds, however this would no longer be a prior.

B_a - Reduced NorB

Unknown at start of simulation. Assume close to zero, and certainly less than total. The best prior to use would be the value after a couple of simulation seconds, however this would no longer be a prior.

C_a - Reduced *cbb*$_3$

Unknown at start of simulation. Assume close to zero, and certainly less than total. The best prior to use would be the value after a couple of simulation seconds, however this would no longer be a prior.

C_X - Reversibly NO inhibited *cbb*$_3$

Unknown at start of simulation. Assume close to zero, and certainly less than total. The best prior to use would be the value after a couple of simulation seconds, however this would no longer be a prior.

Q_a - Reduced Quinones

Unknown at start of simulation. Assume close to zero, and certainly less than total. The best prior to use would be the value after a couple of simulation seconds, however this would no longer be a prior.

Parameters

k_1 - Rate of O_2 reduction by reduced *cbb*$_3$

A value for k_1, the rate of O_2 reduction by reduced *cbb*$_3$ was calculated by using the K_{cat} value from *Pseudomonas stutzeri*, and the k_m value from *Neisseria lactamica*, which Forte et al.[92] and Hunter[93] determine are $166s^{-1}$ and $0.4\mu M$ respectively. k_1 can be calculated as $\frac{166s^{-1}}{0.4\mu M} = 415\mu M^{-1}s^{-1}$.

k_3 - Rate of *cbb*$_3$ reduction by cytochrome pool

k_3, the rate of reduction of *cbb*$_3$ by the cytochromes was calculated from values obtained from the maximum reduction rate of *cbb*$_3$ by cytochrome c_4 in *Vibrio cholerae* by Chang et al.[56]. A rate of 300 electrons transported per second was observed with a cytochrome c_4 concentration of $100\mu M$. This concentration was not saturating, but there appears to be a linear relationship between rate and

concentration. We assume that 1 electron equals 1 reduction of cbb_3, thus the rate of reduction of cbb_3 by cytochromes is $\frac{300s^{-1}}{100\mu M} = 3\mu M^{-1}s^{-1}$.

l_1 - Rate of NO reduction by reduced NorB

240 and 256 nanomoles NO reduced per minute per OD600 unit as determined by Barth et al.[41].

This needs fixing. 50% dry weight, rather than 15% wet weight.
Observed rates of NO reduction by Rock et al.[30] give 54 ± 6 nmolmin^{-1}mg^{-1}. This is in whole cells however. ≈ 10 nmols^{-1} in an $OD_{600} = 1$ culture. Converting to molar gives 2 μMs^{-1}.

l_3 - Rate of NorB reduction by quinone pool

Benchmark estimate is somewhere around about 1 $\mu M^{-1}s^{-1}$.

m_1 - Rate of NO_2^- reduction by reduced AniA

m_3 - Rate of AniA reduction by cytochrome pool

The value for m_3, the rate of reduction of AniA by cytochromes, is the observed electron transfer rate between the equivalent cytochrome and nitrite reductase from *Achromobacter xylosoxidans*. A value of $4.8 \pm 0.2\mu M^{-1}s^{-1}$ was observed during stopped-flow experiments by Nojiri et al.[94].

k_5 - Rate of cbb_3 inhibition by NO

Giuffre et al.[91] and Blackmore et al.[95] showed with cytochrome *c* oxidase that NO could bind reversibly and inhibit the activity of the enzyme. The rate they calculated was 10^8 $M^{-1}s^{-1}$. I assume that even though the enzyme is different, its NO binding characteristics would be similar to that of cbb_3 as it is of the same family.

k_6 - Rate of recovery of NO inhibited *cbb*$_3$

Giuffre et al.[91] calculated a half-life of t½≈ 80 min.
K_d from Rock et al.[30] was calculated to be about 500 nM, which tallies with values from k_5 and k_6.

β - Rate of passive diffusion in of O_2

This value is highly dependent on the culture, and is in some way tied to the density of the culture, however the relationship is not known. During early experiments I noticed that oxygen diffusion was slower in high density cultures compared to those of low density, experiments to examine the relationship proved fruitless in determining any relationship. In addition this parameter is a product of the experimental set-up rather than the model itself.

K_O - Saturation O_2 level

This value is dependent on the particular culture being modelled, however it's prior value is usually set to 126 μM as this figure was observed during experiments to determine oxygen diffusion rates into the culture.

g - Rate of electrons in from NADH (or rate of reduction of quinones)

f - Rate of reduction of cytochromes by quinones

Snyder et al.[51] showed by reducing yeast cytochrome bc_1 by using 25 μM menaquinol the rate constants were 7.9 s^{-1} for cytochrome b, and $1.55 - 6.9 \times 10^5$ $M^{-1}s^{-1}$ for cytochrome c_1 (second order). $0.155 - 0.69$ $\mu M^{-1}s^{-1}$.

γ - Spontaneous loss of NO

Q - Concentration of quinones

Q, the concentration of quinones was calculated based on data from Hedrick and White[96]. The protein content of the cells was assumed to be similar to that of

E. coli at 15% of wet weight, where each cell weighed 2pg, and that there were 1μmol of respiratory quinones per g of bacterial protein. A culture of *Neisseria meningitidis* with $OD_{600} = 1$ has 1×10^9cells/ml, therefore there are 1.5nmol of quinones in 5ml culture (5×10^9cells $\times 2 \times 10^{-12}$g $\times$ 15% $\times$ 1μmol/g), converted to molarity is $0.3\mu M$.

X - Concentration of cytochromes

Deeudom[23] suggests total cytochrome concentration (inc. cbb_3) to be about 4000 nM.

A - Concentration of AniA

No idea, probably need to guess based on cell volume (0.6-1.0 μm diameter, no useful ref), 10% of cell volume being membrane, and number of proteins in membrane.

B - Concentration of NorB

No idea, probably need to guess based on cell volume (0.6-1.0 μm diameter, no useful ref), 10% of cell volume being membrane, and number of proteins in membrane.

C - Concentration of cbb_3

No idea, probably need to guess based on cell volume (0.6-1.0 μm diameter, no useful ref), 10% of cell volume being membrane, and number of proteins in membrane.
cbb_3 is probably 0.1-1% of cell protein. 10% of cell is membrane. 15 μg in 5 ml based on numbers from Q above. cbb_3 is approximately 100 kDa in molecular weight. Converting to molarity gives a concentration of approximately 30 nM.

3.3 Implementation of the model

The model contains no implied information about cell density. This means the values for various component concentrations will differ between experiments. Initially the optical density of cultures was used to determine the cell density however experiments proved that this was not a completely reliable proxy for cell density as this also includes dead cells. Using optical density as a cell density proxy should give linear relationships between cell densities and reaction rates, however this proved not to be the case, with rates of oxygen reduction differing between cultures with the same optical density (data not shown). Therefore where possible, any normalisation that was carried out used the initial oxygen reduction rate as a relative indicator of living cells.

3.4 Solving Ordinary Differential Equations

The model equations (given previously) are solved in parallel using the common 6^{th} order Runge-Kutta-Fehlberg algorithm for integrating ordinary differential equations[97]. Adaptive step-sizes were implemented using the Cash-Karp method[98]. The adaptive step size system was required as it prevented the introduction of systemic numerical instabilities.

The parameter estimation system and ODE solver were a bespoke implementation written in Java. The Runge-Kutta algorithm was modified from that found in Numerical Recipes in C[99]. I decided to write a custom implementation rather than using off the shelf systems for solving ODEs and parameter estimation as I wanted the greatest flexibility in how I integrated the two techniques, and it allowed me to quickly and easily tailor the code to my needs. Initially I tried using COPASI[78], however at that time it had limitations that I could not overcome, such as an inability to allow bulk addition of components at arbitrary time-points.

The implementation of the model has no constraints on respiratory substrate concentration, thus allows the altering of these concentrations whilst solving the

equations, however changes to substrate concentration have to be made programmatically to inform the model of the change (`if (t == 50) then NO_conc += 20;`). This ability means that the switch between aerobic and anaerobic respiration can be examined synthetically, and the model is also capable of simulating how the respiratory system responds to the sudden addition of substrates such as Nitric Oxide. More complicated methods are possible, but given the high diffusion of the substrates concerned as well as the deliberate injection of the relevant substrate this method was a simpler and reasonable mimic for my empirical method. This ability was an absolute requirement, as in order to fully parametrise the model it was necessary to isolate sections of the model, which required adding aliquots of respiratory substrate during respiration.

3.5 Parameter Estimation

Estimating the parameter values for the components in the mathematical model involved comparing the biological results with those produced by solving the ODEs and adjusting the parameter values to minimise the difference between the two results. The different methods for parameter estimation that I investigated are detailed in Chapter 4 [Parameter Estimation Methodologies].

Chapter 4

Parameter Estimation Methodologies

Below are the various different methods for parameter estimation that I investigated during the course of this work. All of these methods involve a sampling system that attempts to select parameter values which minimise the difference between the simulation result and the experimental data by calculating a *fitness value*. The aim of the parameter estimation methodology was to get this *fitness value* as close to zero (perfect fit/no difference) as possible. Two different calculations were used to create the *fitness value*. One was the sum of the Least Squares Differences between the measured components in the experimental data and the simulation result. This was used in early parameter estimation runs.

$$f = \sum_{j=1}^{n} \left(\sqrt{\sum_{i=1}^{m} (\Delta x_{ij})^2} \right) \tag{4.1}$$

The second method for calculating the *fitness value* was a lognormal correlation which allowed greater tuning, as the standard deviation of the distribution could be set to adjust how much fitter the simulation result needed to be to be accepted.

$$f = \sum_{j=1}^{n} \left(\sum_{i=1}^{m} \left(\ln \left(\frac{1}{2\pi\sigma_j^2} e^{-\frac{(0-0)^2}{2\sigma_j^2}} \right) - \ln \left(\frac{1}{2\pi\sigma_j^2} e^{-\frac{(x_{ijFIT} - x_{ijDATA})^2}{2\sigma_j^2}} \right) \right) \right) \tag{4.2}$$

In most cases the components used for calculating the *fitness value* are Oxygen and Nitric Oxide, as these were the primary measured chemicals.

The main difference between the parameter estimation methodologies laid out below are the ways in which they generate new parameter values, either from a probability distribution or based on the previous value, and the way this is applied and tested against the experimental data.

Monte Carlo Methods

I include a brief section here to describe Monte Carlo Methods, as the techniques I used for parameter estimation all use this method as their estimator in some form. "Monte Carlo Methods" is a generalised term to describe a stochastic technique that makes use of random numbers to examine a problem in conjunction with probability statistics. Monte Carlo Methods allow us to model complex systems without having to exhaustively search every possible outcome. Large systems are sampled in random configurations and that data applied in such a way that it can be used to describe the system as a whole. "Monte Carlo techniques are often the only practical way to evaluate difficult integrals or to sample random variables governed by complicated probability density functions"[100].

4.1 Simulated Annealing

This technique was described independently by Kirkpatrick et al.[101] and Černý[102]. The name comes from the metallurgical annealing process whereby large crystals are formed while a material is slowly cooled. The slow cooling increases the probability of individual crystals obtaining lower energy states than the ini-

```
c1 <- c0;
c2 <- mutate(c1);
i <- 0;
while i < i_max
  if fitness(c1) > fitness(c2)
    c2 <- mutate(c1)
  else
    c1 <- mutate(c2)
  i <- i + 1
if fitness(c1) > fitness(c2)
  return c1
else
  return c2
```

Figure 4.1: **Pseudo-code showing how the simplest annealing algorithm works.**

tial. As the material cools the "distance" each crystal can move along the energy landscape decreases. Simulated annealing "consists of a discrete-time inhomogeneous Markov chain"[103] whereby the previous state is modified with a perturbation kernel (the neighbouring states) and then accepted or rejected using a transition probability which depends on the current temperature and the energies of the previous and current states. The advantage of this scheme is that areas of local minima have a lesser effect on the outcome of the Markov chain as the high initial temperature allows for the chain to "jump" out of this minima.

Figure 4.1 contains some simple pseudo-code which shows how the basic algorithm works (without the annealing temperature). This will provide a "best" parameter set, but there is no information about the possible spread of values in the parameter set. Given that it is unlikely that a single point-value parameter-set solution exists that will accurately describe the system it is necessary to produce a spread of results that will adequately describe the system instead. To this end I used a modified version of simulated annealing integrated with aspects of a simple genetic algorithm. In the genetic algorithm paradigm a synthetic "chromosome" is created containing which contains "genes" representing the parameters in the simulation. These include the rate constants, concentrations of various components and initial concentrations of substrates and products. This chromosome is then copied and perturbed several times (depending on the eventual

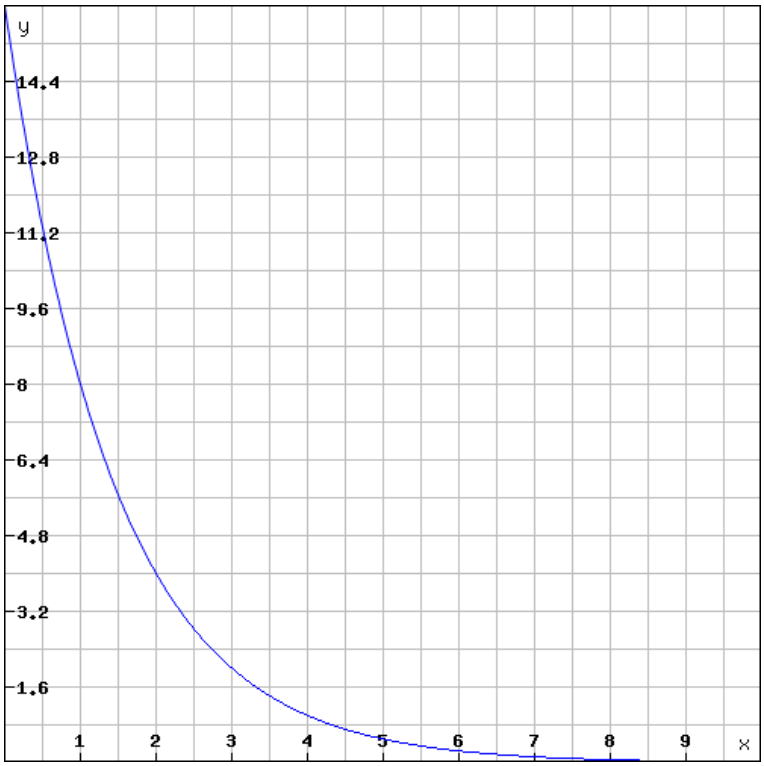

Figure 4.2: **Example simulated annealing temperature schedule.** This represents how the annealing temperature changes as the annealing process progresses. Temperature is denoted by the y-axis value, and simulation progress by the x-axis value. This is a heavily compressed time-frame, as in reality the system would normally process 10,000 sets of parameters at each annealing temperature.

population size required), with the size of the perturbation being dependent on the current annealing temperature. For instance the highest temperature could indicate that the individual parameters can be perturbed by up to $\pm 10\%$, and as the temperature decreases the perturbation percentage has a concommitant decrease. An example annealing temperature schedule is shown in Figure 4.2. The annealing temperature is programmed to decrease after a defined number of iterations such that the magnitude of individual mutations becomes smaller as the simulation progresses. This should have the effect of honing in on a set of parameters with high fitness. Once the chromosome population has been created, 2 are selected at random and their fitnesses evaluated, in this case by the Least Squares Difference method. The chromosome with the higher *fitness value* is discarded and the other is cloned and perturbed. The two chromosomes are then added back to the chromosome population. The genetic algorithm is used to

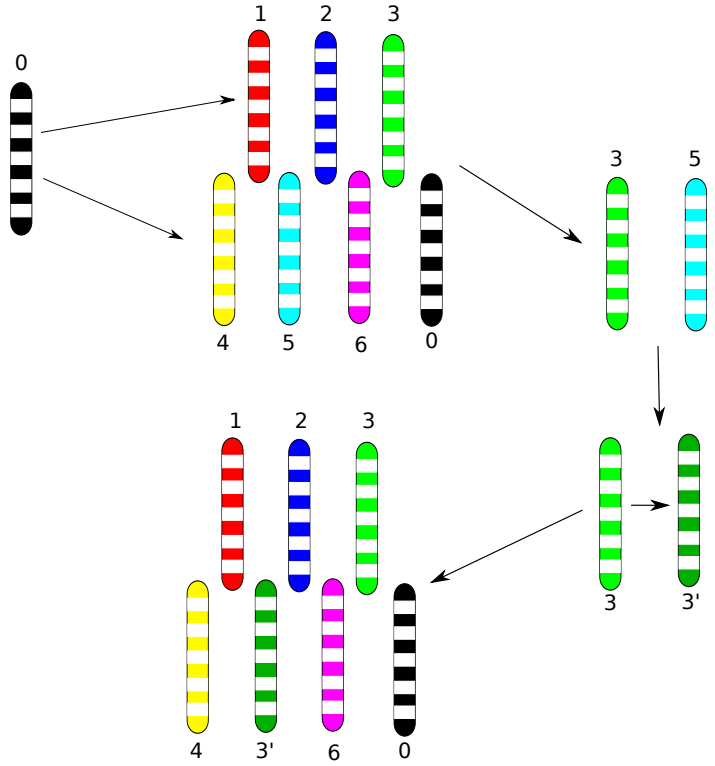

Figure 4.3: **Schematic diagram showing the technique used to generate a spread of parameters using a synthetic chromosome.** The parameters are loaded as genes on the chromosome which are then perturbed, 2 chosen and the fittest kept and perturbed. Each time a chromosome is perturbed it is reintroduced into the chromosome pool, and the next 2 chromosomes are chosen at random.

improve the parameters sets by perturbing genes (individual parameters) from fit chromosomes (complete parameter sets), re-running the simulation and discarding unfit parameter sets. An unfit parameter set is defined as one with an *fitness value* lower than the best so far. This technique involves having two chromosomes selected at any one time. The parameters from each chromosome are simulated and the least fit one is discarded. At this point the contents from the fitter chromosome are cloned and perturbed, and the cycle is repeated. Figure 4.3 shows this diagrammatically. After many cycles (upwards of 1000) the chromosome pool should only contain the best fitting parameter sets to the experimental data. The spread of the parameters can be used to infer the sensitivity of the simulation to changes in parameter values in a similar way to that described by Toni et al.[104].

Advantages

- Easy to implement.
- Can avoid local energy minima by jumping when the temperature is high.
- Energy need only be calculated for 2 samples at any one time.
- High optimisation performance on some problems.

Disadvantages

- Slow performance on certain problems.
- Cannot produce probability distributions.

Reason(s) for rejection

- Seemed to be incapable during testing of settling on solutions to Nitric Oxide reduction datasets.
- No probability distributions which were eventually required to incorporate data from previous datasets.

4.2 Approximate Bayesian Computation by Sequential Monte Carlo

"Approximate Bayesian Computation methods have been conceived with the aim of inferring posterior distributions where likelihood functions are computationally intractable or too costly to evaluate. They exploit the computational efficiency of modern simulation techniques by replacing calculation of the likelihood with a comparison between the observed data and simulated data"[104].

To incrementally improve the parameter sets, a version of Bayesian inference is used in conjunction with a standard Monte Carlo method in a system called Approximate Bayesian Computation by Sequential Monte Carlo (ABCSMC) as described by Toni et al.[104]. An implementation of algorithm (S) was used from that paper.

Bayesian Inference - This a statistical method for inferring the probability of a hypothesis based on available evidence. As more evidence is accumulated, the

inference is updated and the probability of the hypothesis being true is changed. Given enough evidence, the probability of the hypothesis being true should either be very high or very low causing you to either accept or reject the hypothesis. Bayesian inference relies on having a prior probability (or probability distribution) for the hypothesis, and this can inevitably introduce a level of bias into the inference. Bayesian inference can be described thus:

$$P(H \mid E) = \frac{P(E \mid H)}{P(E)} \cdot P(H) \tag{4.3}$$

- $P(H \mid E)$ is the posterior distribution of H given E.
- $P(H)$ is the prior distribution
- $\frac{P(E \mid H)}{P(E)}$ is the impact of E on the degree of belief in H.

A simplistic example of using Bayesian inference to alter a hypothesis could happen in the case of having two jars of sweets. Jar 1 has 15 strawberry sweets and 25 raspberry sweets. Jar 2 has 20 of each. Supposing a third party selects 1 sweet at random from 1 of the jars. They select a strawberry sweet, what is the probability that it came from Jar 1? From the point of view of our third party both jars are identical, therefore $P(H_1) = P(H_2)$ and the total probability must equal 1, so the prior probability of each jar is 0.5. The observation, E is of a strawberry sweet, which we can then use to calculate the likelihood of it being from each jar individually by $P(E \mid H_1) = 15/40 = 0.375$ and $P(E \mid H_2) = 20/40 = 0.5$. Bayes formula can then be used to work out the probability of the strawberry sweet being from jar 1, that is $P(H_1 \mid E)$.

$$P(H_1 \mid E) = \frac{P(E \mid H_1)P(H_1)}{P(E \mid H_1)P(H_1) + P(E \mid H_2)P(H_2)}$$

$$= \frac{0.375 \times 0.5}{0.375 \times 0.5 + 0.5 \times 0.5}$$

$$= 0.429 \tag{4.4}$$

Before the observation of the sweet, the probability of the third party taking from jar 1 was the prior probability of 0.5. After the observation this probability must be revised to 0.429.

Bayesian inference is widely used in computational analysis for artificial intelligence and email spam identification. It is also used in the field of population genetics and phylogenetics[105].

Approximate Bayesian Computation - This is an adaptation of Bayesian inference which allows approximately the same inferences to be made, with considerably less computation. It operates on representations of the datasets rather than the datasets themselves. Common examples are population mean and variance. This is useful for large complex datasets where the probability of a simulation of the dataset matching the original is very small (unacceptably so), in this case a representation of the datasets can be used, and the difference calculated. If the difference is less than a pre-defined acceptance threshold, then the simulated dataset is accepted. ABC originally came from the fields of population and evolutionary genetics[106], but are now being applied to complex and stochastic dynamical systems[104,107,108].

ABC differs from standard Bayesian inference shown in Equation 4.3 in that the likelihood term does not need to be calculated. Instead the difference between the summary statistics of the observed data and the simulated data is used. The simulated data is considered a true sample from the posterior distribution if the

difference in summary statistics is less than a predefined acceptance threshold. The most basic ABC methods takes the following form:
θ is a parameter vector to be estimated, $\pi(\theta)$ is the prior probability distribution, and x is the observed data. The posterior distribution is $\pi(\theta \mid x) \propto f(x \mid \theta) \cdot \pi(\theta)$.

1. Create a candidate parameter vector θ^* from the prior distribution $\pi(\theta)$.

2. Simulate dataset x^* using the model and parameter vector θ^*.

3. Compare x^* with x using a distance function d and an acceptance criteria ϵ. If $d(x, x^*) \leq \epsilon$, accept θ.

Given a low enough value for ϵ, the output distribution should approximate the true posterior distribution if sampled a large enough number of times.

Sequential Monte Carlo - This is a method of particle filtering whereby a large set of samples (N) are drawn from the prior distribution, and for each sample, the probability is calculated. Weights for each particle are assigned based on the probabilities, and these affect how likely a particle is to be selected in subsequent rounds of selection. At the end of each round, the posterior distribution, that of the N particles becomes the prior distribution for the next round.

Approximate Bayesian Computation by Sequential Monte Carlo - This combines the previous two methods by drawing a large number of particles from the prior distribution using Bayesian inference. The prior distribution is discrete in the scheme used here, so a perturbation kernel based on a laplacian or gaussian distribution is used on each sample to provide small deviations to better approximate a continuous prior distribution. Each sample is simulated and only accepted if it exceeds the acceptance threshold. This is calculated based on the least-squares difference (LSD) between the simulated data and the original dataset. If a sample is rejected, a new one is drawn from the prior distribution and SMC then continues as described above. The weights of the accepted samples are calculated based on the probabilities of being selected from the prior and the samples go on to form the posterior distribution. For each subsequent round,

the mean LSD of the posterior distribution from the previous round is used as the acceptance threshold. This ensures that each round results in better fitting parameter sets. The cycle is then repeated until a pre-defined cycle limit is reached [104].

A significant advantage of this technique is that it is readily parallelisable, as each particle in the SMC process is independent, thus can be simulated in parallel. A parallel version of this algorithm was implemented in the JAVA programming language which resulted in significant speed-ups when multiple processing threads can be used. The threading manager means that the algorithm is theoretically most efficient (in terms of computational time) when the number of particles is an exact multiple of the number of processing threads. In practice however this is negated by the fact that some particles require multiple samples due to them not meeting the acceptance criteria.

Advantages

- Paralellisable. Leading to improved performance on multiprocessor systems.

Disadvantages

- Requires a suitable distance function or summary statistic.

Reason(s) for rejection

- Seemed incapable of settling on sensible posterior distributions with some datasets. I suspect the distance function used was causing a conflict which meant the algorithm was accepting bad parameter sets and rejecting good ones.

4.3 Metropolis Hastings Monte Carlo

The Metropolis-Hastings algorithm is Markov Chain Monte Carlo method to retrieve sequences of random samples from a probability distribution which cannot be sampled directly (or would be very difficult) such as when no probability distribution function exists. The algorithm was originally developed by Metropolis

et al.[109] for generating samples from the Boltzmann distribution. It was later extended to a more general form for any distribution by Hastings[110].

MHMC allows each individual parameter to follow a biased random walk until it reaches a point of maximum "fitness." The typical output of this algorithm is a set of parameter trajectories which begin with a "burn in" period, followed by a parameter distribution. The "burn in" period contains data that is discarded, as it does not form part of the target distribution. The length of this burn in period often varies depending on how far the starting samples are from the target distribution. The parameter distribution can be calculated from the data that is left after the burn in period. This is done by a simple statistical analysis of the resulting data points. Since the distributions cannot easily be described as functions, the data are transformed into histograms with a set bin width. These histograms can be read and used a priors for subsequent runs of the MHMC algorithm.

The MHMC algorithm has been validated initially by using a much simpler ODE system than is required by the respiration model. A Lotka-Volterra system was used as this can be solved much more quickly by virtue of having far fewer parameters (4 as opposed to >20). The Lotka-Volterra system describes a simple predator-prey relationship and only requires two first-order, non-linear differential equations, which are shown in equation 4.5.

$$\begin{aligned} \frac{dx}{dt} &= x(\alpha - \beta y) \\ \frac{dy}{dt} &= -y(\gamma - \delta x) \end{aligned} \tag{4.5}$$

Validation of using this system required a simulated dataset with known parameter values to be produced. This dataset then forms the input for the MHMC algorithm which will try and obtain those same parameter values. Given the simplicity of this system, a particularly bad set of initial parameter estimates was

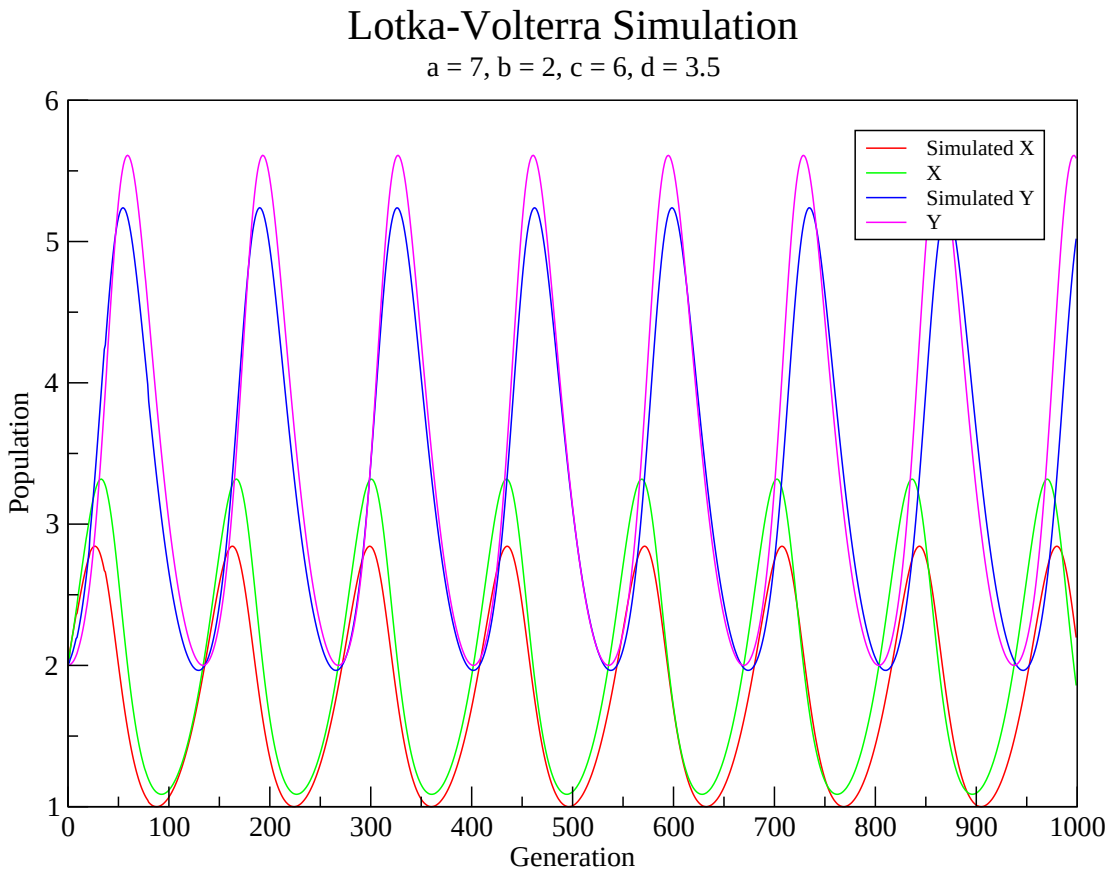

Figure 4.4: **Simulation results of the Lotka-Volterra validation run.**

given to exaggerate the burn in period, and to show that given a long enough time the simulation will eventually settle on "correct" values. This validation step also informs the likely values for two tuning variables in the algorithm; the *acceptance* - how stringent the algorithm is on accepting new parameter sets, and the *sigma* value - this describes the magnitude of parameter perturbation at each iteration. The graphical results of the Lotka-Volterra validation are shown in figures 4.4 and 4.5.

4.4 Implementation

The initial parameters used to solve the equations were a set of priors based on preliminary experimental results. These parameters only provide a starting point as the second stage of computation involves modifying the parameters in order to provide a better fit against experimental data. To incrementally improve the parameter sets, a version of Bayesian inference is used in conjunction with a stan-

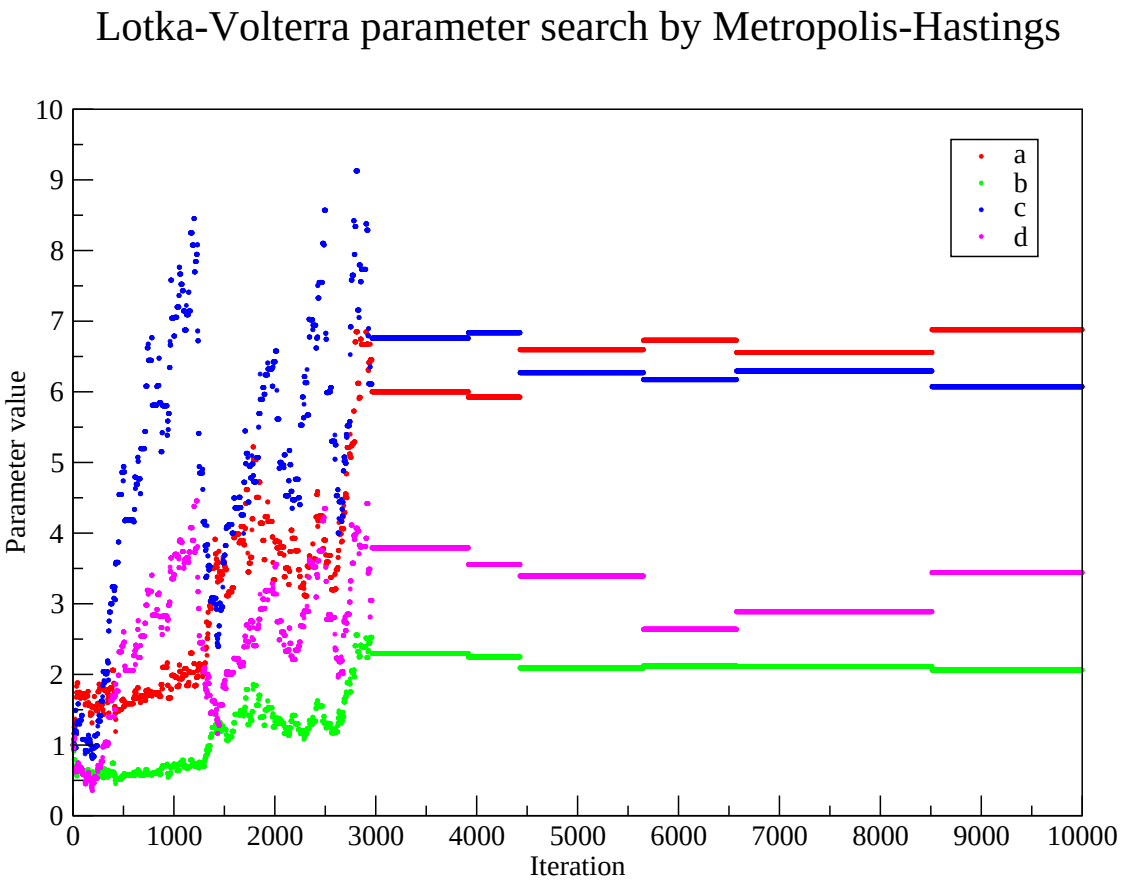

Figure 4.5: **MHMC results of the Lotka-Volterra validation run.** Note the initial burn-in period followed by the distribution trajectory.

dard Metropolis-Hastings Monte-Carlo method.

I used Bayesian inference to inform the simulation parameters for a particular dataset based on prior probability distributions. These distributions were obtained as output from a previous dataset. I integrated this with a Metropolis-Hastings algorithm for sampling the prior probability distributions. Each parameter was sampled, and the parameter set was used to solve the ODE model. Based on the fitness output of the solved model, the Metropolis-Hastings algorithm allows parameters to be modified in a biased random walk which ultimately leads them to their most fit state, calculated using Log Normal probability.

Advantages

-

Disadvantages

-

4.5 Integrative Scheme

Currently copied verbatim from paper

In order for us to iteratively generate a parameter set we needed to separate the model into simpler units whereby we can obtain data about a specific set of variables. We did this so that the simplest part of the model was parametrised first. In this case it was oxygen respiration, which only requires one enzyme (although it does still require the ETC). This section of the model also has the simplest experimental dataset. After parametrisation, a new section of the model was introduced, with its associated experimental dataset.

Experimental data was gathered for the first dataset, and this is used as a training set, with almost flat priors based on preliminary experimental data. The data was pre-processed and normalised if necessary and then presented to the Bayesian Parameter Estimation system. The MHMC algorithm samples from the prior distribution and then uses those samples as parameters to solve the model. It aims to improve the calculated fitness value and is ordinarily run for at least 100,000 iterations to give the system time to settle on the fittest parameters. The system is run on the same dataset 10 times to generate statistically significant results. The eventual output of the MHMC runs are posterior probability distributions for each of the parameters in the model. In accordance with Bayesian inference these are then used as prior distributions.

At this point the next section of the model to be parametrised is decided, the appropriate experimental data identified and obtained, and the process is repeated until the entire model has been populated. The final result should be a set of reasonably narrow probability distributions for each of the parameters which describe the system accurately enough to correctly predict the behaviour of the system *in vivo*.

Chapter 5

Oxygen Reduction in *N. meningitidis*

5.1 Aerobic Reduction of Oxygen

5.1.1 Introduction

The first dataset I used in my iterative approach to parameter estimation was of a simple oxygen reduction experiment carried out in aerobic conditions. This dataset is the simplest biologically as under aerobic conditions and without the presence of any microaerobic substrates (nitrite or nitric oxide) the only respiratory pathway that is active is the oxygen reducing one. Additionally, the other parts of a respiratory chain influence the oxygen reducing pathway either by competing for electrons, or chemically inhibiting it. The relevant portions of the ETC are shown graphically in Figure 5.1.

The equations that describe this portion of the ETC are:

$$\begin{aligned}
\frac{d[O_2]}{dt} &= \beta(1 - [O_2]/K_O) - k_1[C_a][O_2] \\
\frac{d[Q_a]}{dt} &= g([Q] - [Q_a]) - l_3[Q_a]([B] - [B_a]) - f[Q_a]([X] - [E]) \\
\frac{d[E]}{dt} &= -k_3([C] - [C_a] - [C_X])[E] - m_3([A] - [A_a])[E] + f[Q_a]([X] - [E]) \\
\frac{d[C_a]}{dt} &= k_3([C] - [C_a] - [C_X])[E] - k_1[C_a][O_2] - k_5[C_a][NO]
\end{aligned}$$

These equations describe the change in concentration of oxygen over time, which

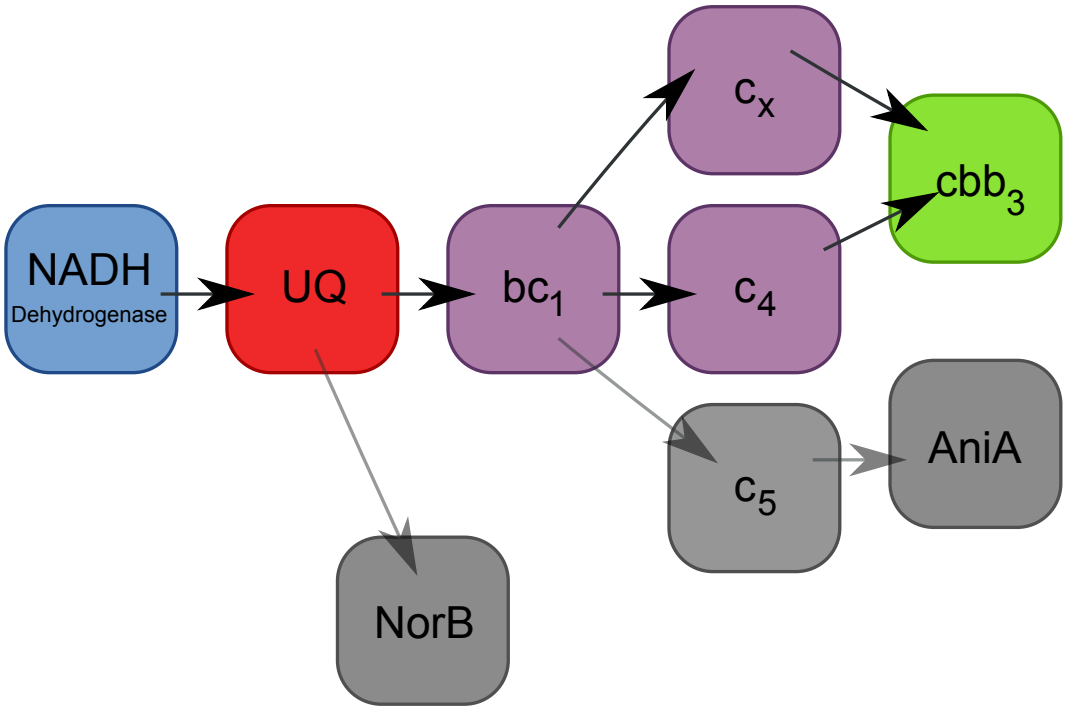

Figure 5.1: **Oxygen reducing electron transport chain of *N. meningitidis*.** This shows the complete electron transport chain of *Neisseria meningitidis* with the components irrelevant to oxygen reduction greyed out. In the mathematical model all of the purple elements (cytochromes) are amalgamated into one entity.

is the experimentally observable value, the reduction state of the quinone pool and the reduction state of the cytochrome "pool". This portion of the model involved 13 parameters and variables which I tried to estimate (the model actually contains 17 such parameters and variables, but under these conditions the remaining 4 are set to 0 as they are related to nitrite reduction effects).

5.1.2 Experimental Results

Generation of oxygen reduction datasets required the growth of MC58 (wild-type *Neisseria meningitidis*) in aerobic conditions until mid log-phase growth had been achieved. This corresponds to an OD_{600} of 0.3-0.9 and usually required an incubation period of roughly 3 hours. Once the required cell density had been obtained, I transferred the culture to the oxygen electrode chamber and recorded the oxygen concentration as the culture respired. At this point the cells are only using whatever amount of oxygen is presently dissolved in the culture medium in addition to that diffusing in through the cap (negligible). Once the culture had used

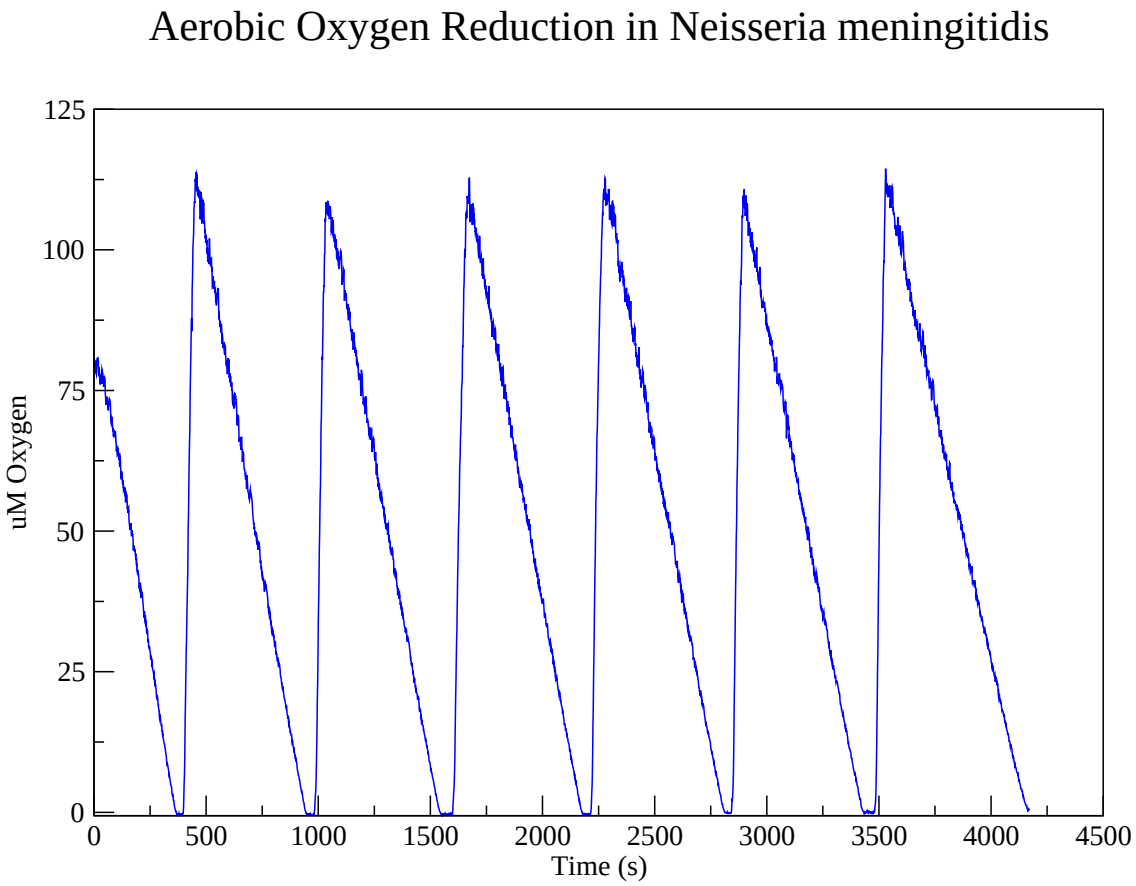

Figure 5.2: **Highly repeatable oxygen reduction.** This shows an oxygen reducing culture being repeatedly aerated after oxygen depletion with very similar rates of subsequent oxygen reduction

up all its dissolved oxygen, I removed the electrode chamber cap and aerated the culture media using a Pastuer pipette. This restores oxygen levels throughout the culture and allows the bacteria to continue respiring in aerobic conditions. In many cases if the culture is allowed to become completely anaerobic for a prolonged period of time, the bacteria will die, evidenced by a subsequent lack of oxygen reduction, however this is not always the case as shown in Figure 5.3. It is therefore advisable to aerate the culture before the oxygen level reaches zero. A typical oxygen reduction plot is shown in Figure 5.2. This is split into individual reduction sections, which can then be used as input data for parameter estimation.

The experiments used to generate data for oxygen reduction are highly repeatable and consistently generate the same basic result of a linear reduction of oxygen with time.

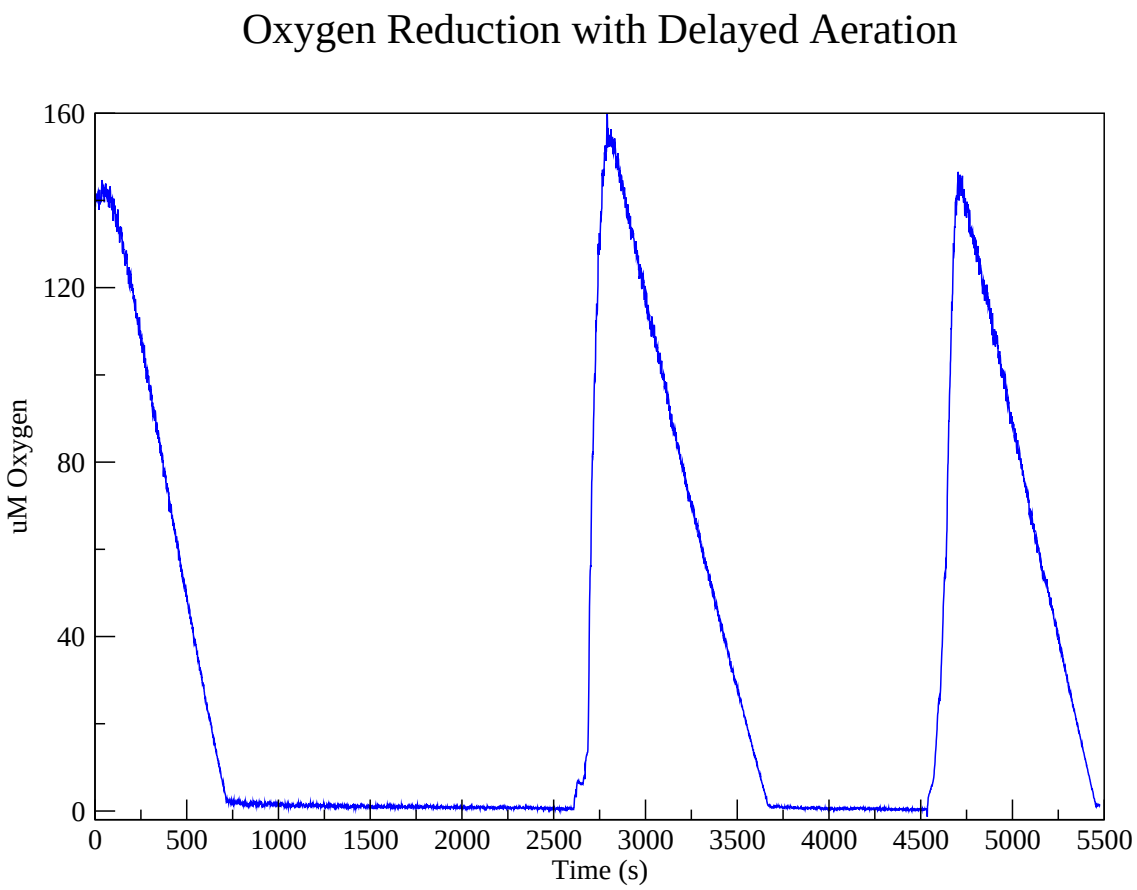

Figure 5.3: **Aerating oxygen reducing cultures with significant delay.** The oxygen reducing ability of *N. meningitidis* can be robust as evidenced by the 1000s delays between aeration with no change in subsequent respiration rate. Also of note is that nitric oxide concentration is not changing, suggesting that reduction of nitrite is not occurring either.

Generation of Prior Probability Distributions

In accordance with the integrative scheme I introduced in Chapter 4, I attempted to estimate the distributions of the parameters involved in modelling these data. In order to do this I needed to create probability distributions to act as priors to feed into the estimation system as this is required for a Bayesian approach. These probability distributions were generated from data obtained in the published literature, which is described in Chapter 3, and preliminary experimental data. I assumed that all the prior probabilities would be normally distributed, therefore the distributions I used were created under the following scheme:

- Where the literature value had bounds associated with it (i.e. published with $\pm$ values), I assumed that the bounds covered 3σ of the normal distri-

bution. This essentially assumes that 99.7% of the distribution falls within the given bounds.

- Where the literature value has no bounds associated with it (i.e. published as a single figure), I assumed that a range of $\pm 10\%$ was covered by 3σ of the normal distribution. This means that 99.7% of the distribution falls within $\pm 10\%$ of the given value.

- Where there are no literature values available, the value was estimated based on preliminary experimental data and no bounds were associated. In this case the prior was free to be perturbed giving it an effective range of $0 < x < \infty$.

With reference to the above, the initial probability distributions used to start the Monte-Carlo run are shown in Figure 5.4. As can be seen, very little information is readily available in the literature to populate the model.

Parameter Estimation Results

The parameter estimation process produces a large amount of output data which can be processed. Included in these data are the best simulation results from each run. Best is defined here as the simulation with the lowest fitness value, i.e. the one with the closest match to the experimental data. For the oxygen reduction training datasets, of which there are 3, each was run 20 times for 20,000 iterations. This lower iteration count was chosen as a compromise between execution time and statistical accuracy. In fact given that the burn-in time for these runs was relatively short, 20,000 iterations still provides plenty of data. A representative example of the simulated data is shown in Figure 5.5. This figure was generated from the set of parameters that produced the most fit output compared to the input dataset.

Initially the simulation results are not particularly good fits compared to the experimental data and as such have high "fitness values". As the parameter esti-

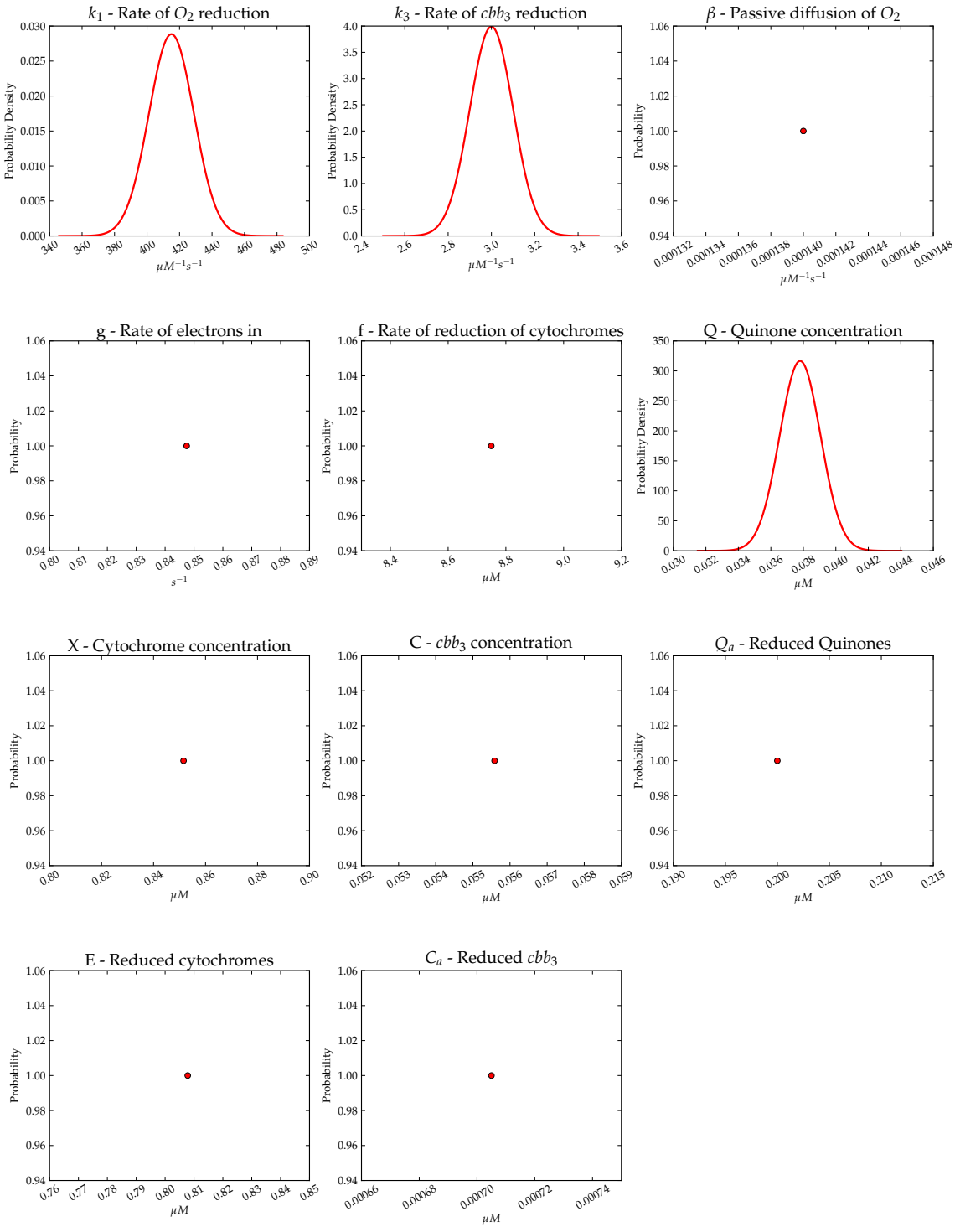

Figure 5.4: **Prior probability distributions for oxygen reduction**. These are the probability distributions used as priors by the parameter estimation algorithm. Where no values were available in the literature, the probability distribution represents a flat prior from 0 to ∞ with the initial value being determined by preliminary experiment.

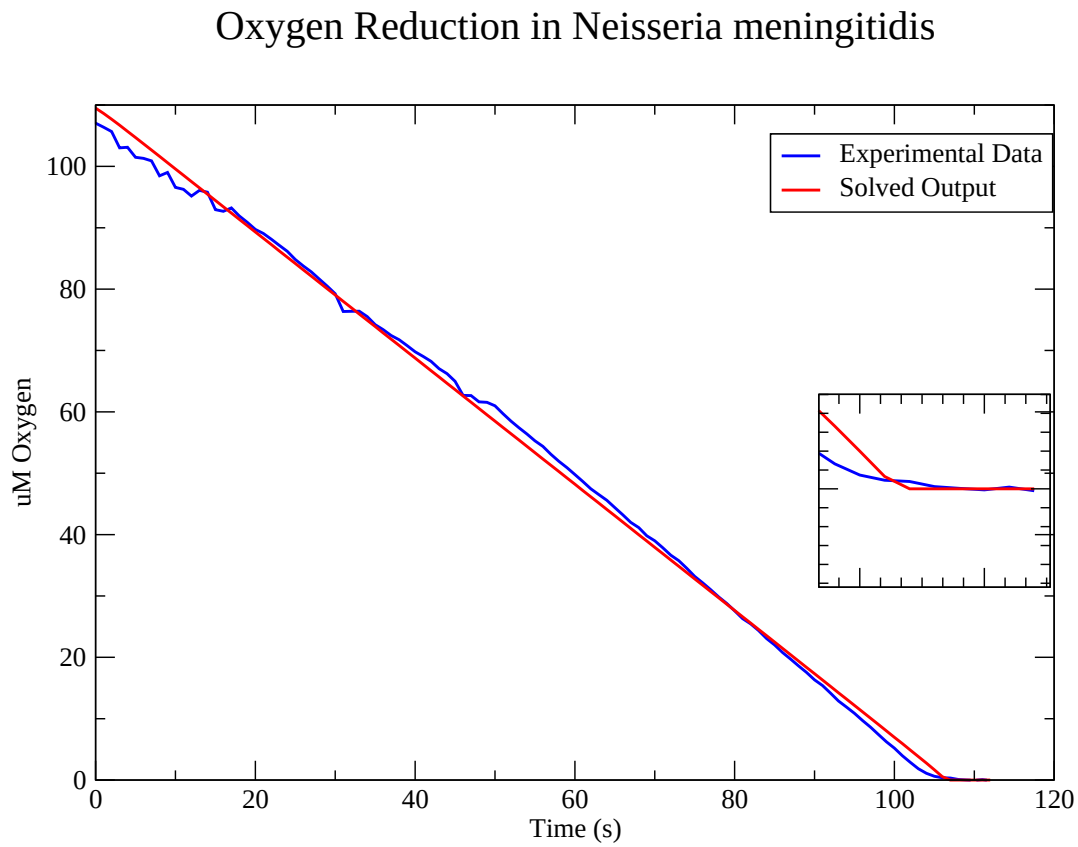

Figure 5.5: **Oxygen Reduction in *Neisseria meningitidis*.** This dataset shows the simple linear reduction of Oxygen in aerobic conditions. The high affinity of cbb_3 for oxygen is evidenced by very little non-linearity at low oxygen concentrations. The solved output is a representative result of the parameter estimation system.

mation progresses the "fitness value" reduces as the simulated result gets closer and closer to the experimental data. Quite often this does not take many iterations and a representative plot showing how the simulation's "fitness value" decreases is shown in Figure 5.6. The initial period where the "fitness value" is high up until the point it settles at a lower value is classed as "burn-in" and is discarded when generating posterior distributions.

Each of the parameters that are to be estimated produces a trajectory of values for each run of the estimation algorithm. These trajectories are used to generate the posterior probability distributions required for Bayesian inference in subsequent steps. During the "burn in" period the parameter values can be observed to change rapidly from one iteration to the next as they approach their optimum values. Once the "burn in" has completed the values settle and produce largely

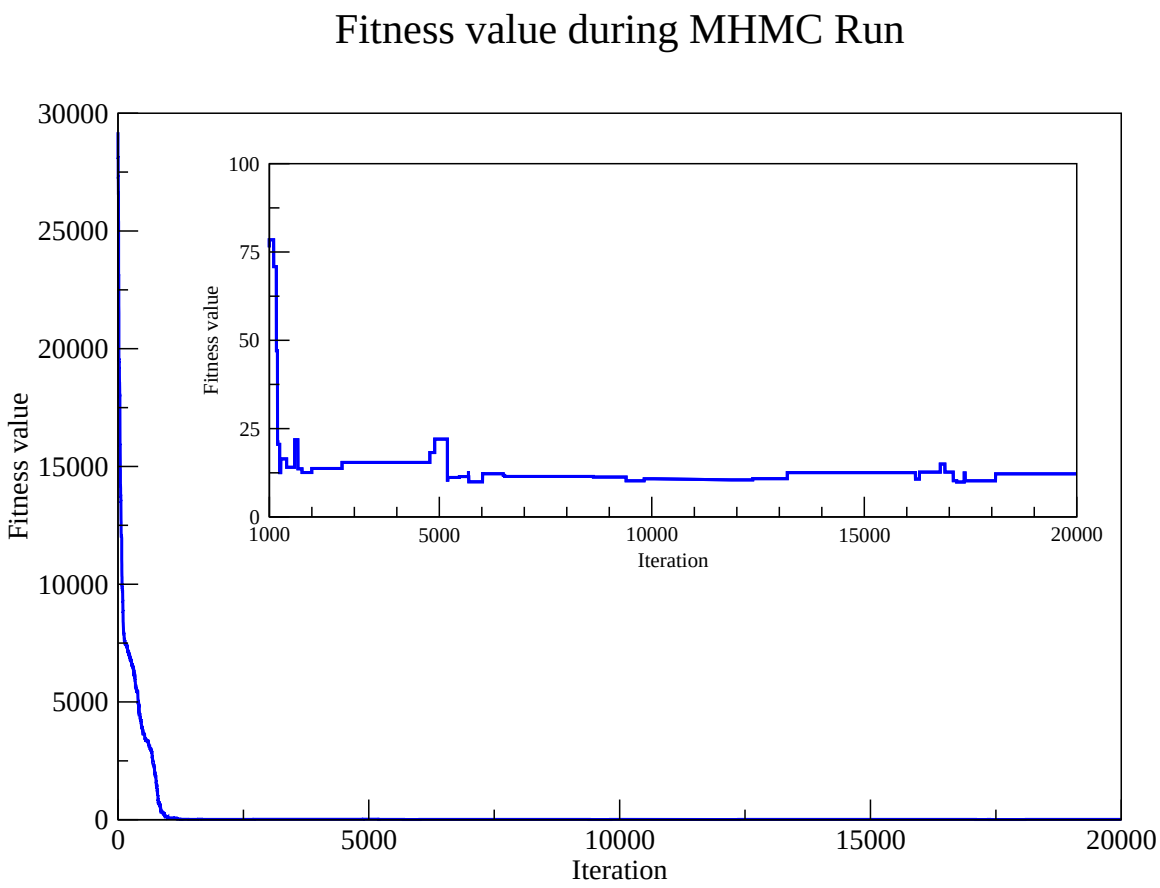

Figure 5.6: **Simulation fitness value improves as parameter estimation progresses.** This is a representative figure constructed from a single run on one dataset. Initially the fitness value is high showing that the simulated result does not match the experimental dataset. As the parameter estimation algorithm progresses, the fitness value decreases as the simulated result approaches the experimental dataset. The inset shows a zoomed in view of the fitness value after the "burn-in" process has finished.

flat trajectories with minor deviations around the optimum value. This settled region is used as the source for generating the posterior probability distributions. Figure 5.7 shows the the trajectories from each simulation run on a single dataset for the k_3 parameter. In this case the trajectory has been truncated to around 17000 iterations.

Not all parameters in this stage of the model will produce trajectories like the one shown, as if there is a great deal of freedom as to what value a particular value can take without drastically increasing the "fitness value" it will be accepted by the parameter estimation algorithm. In this case the trajectories will not converge, and will ultimately produce a wide probability distribution. This is not necessarily indicative of a problem however, as this output still contains

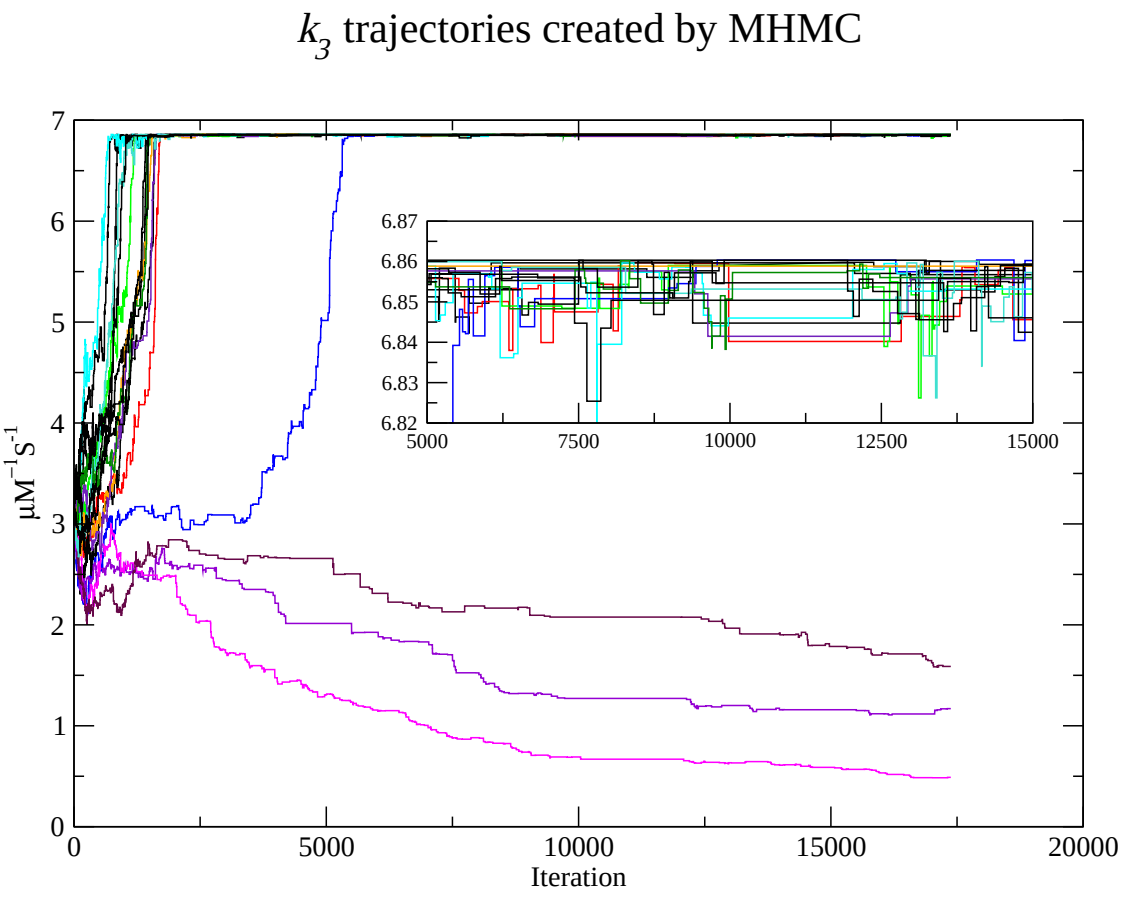

Figure 5.7: **Individual parameter trajectories for multiple runs on the same experimental dataset.** This figure shows the trajectories for the same parameter, in this case k_3 - the rate of cbb_3 reduction, from 20 individual runs of parameter estimation upon the same input data. The inset shows a zoomed in view of the trajectories that hit high values after "burn-in".

information that can be used in the next stage of parameter estimation with new datasets.

The trajectories above are processed to produce probability distributions given as histograms. The "burn in" is discarded and the settled data is then binned and counted. For the datasets used, the burn-in period differed and was filtered based on a pre-determined "fitness value" threshold. Datasets 1 & 2 were had a threshold of $fv < 50.0$ and dataset 3 had a threshold of $fv < 90.0$. The reason for this difference is that dataset 3 never achieves a "fitness value" lower than about 80 due to noise in the experimental data. It is possible to assign these histogram probabilities as the posterior distributions and in turn use them directly as prior probability distributions for new datasets, however it was decided that given that the distribution around a particular value is likely to be normal, the

histograms should be transformed into normal distribution probability density functions. This also has the advantage of allowing me to directly overlay the posterior probability distributions over the priors shown in Figure 5.4.

The posterior probability distributions generated from the three experimental datasets, each started with 20 runs are shown in Figure 5.8. In the case of parameters which represent concentrations, such as X and C, the concentrations of cytochromes and cbb_3 respectively, the parameter distribution shown is the lower portion of the obtained distribution. As the initial oxygen reduction rates differed between these datasets (dataset 2 had a reduction rate about 5x higher than that of datasets 1 and 3) due to cell density differences (as reflected by experimental OD_{600} measurements), the probability distributions were bimodal showing two distinct peaks one at roughly 5x the value of the other. Therefore the lower of the two peaks is shown, representing the oxygen reduction rate of datasets 1 and 3.

Additionally k_1, the rate of reduction of Oxygen by cbb_3 showed bimodality (not shown currently) *and* a very broad range. The bimodal nature of this distribution was not matched in any of the other parameters. This parameter is the last rate in the ETC of oxygen reduction, so it is quite possible that the rate limiting steps are in the previous stages of the ETC and thus in the parameter estimation system k_1 essentially becomes "free".

Some of the posterior probability distributions appear to have expanded outside their prior bounds. I am fairly certain that this is not an error and that samples *are* being taken from the prior distributions, but rather that the prior distributions were sufficiently incorrect that the penalty for selecting a parameter value from the prior distribution which is very unlikely is outweighed by the large decrease in "fitness value" that this affords.

Analysis of Convergence

It is possible to calculate the degree of convergence of the parameters from the Monte Carlo trajectories using the R statistic introduced by Gelman and Rubin [111].

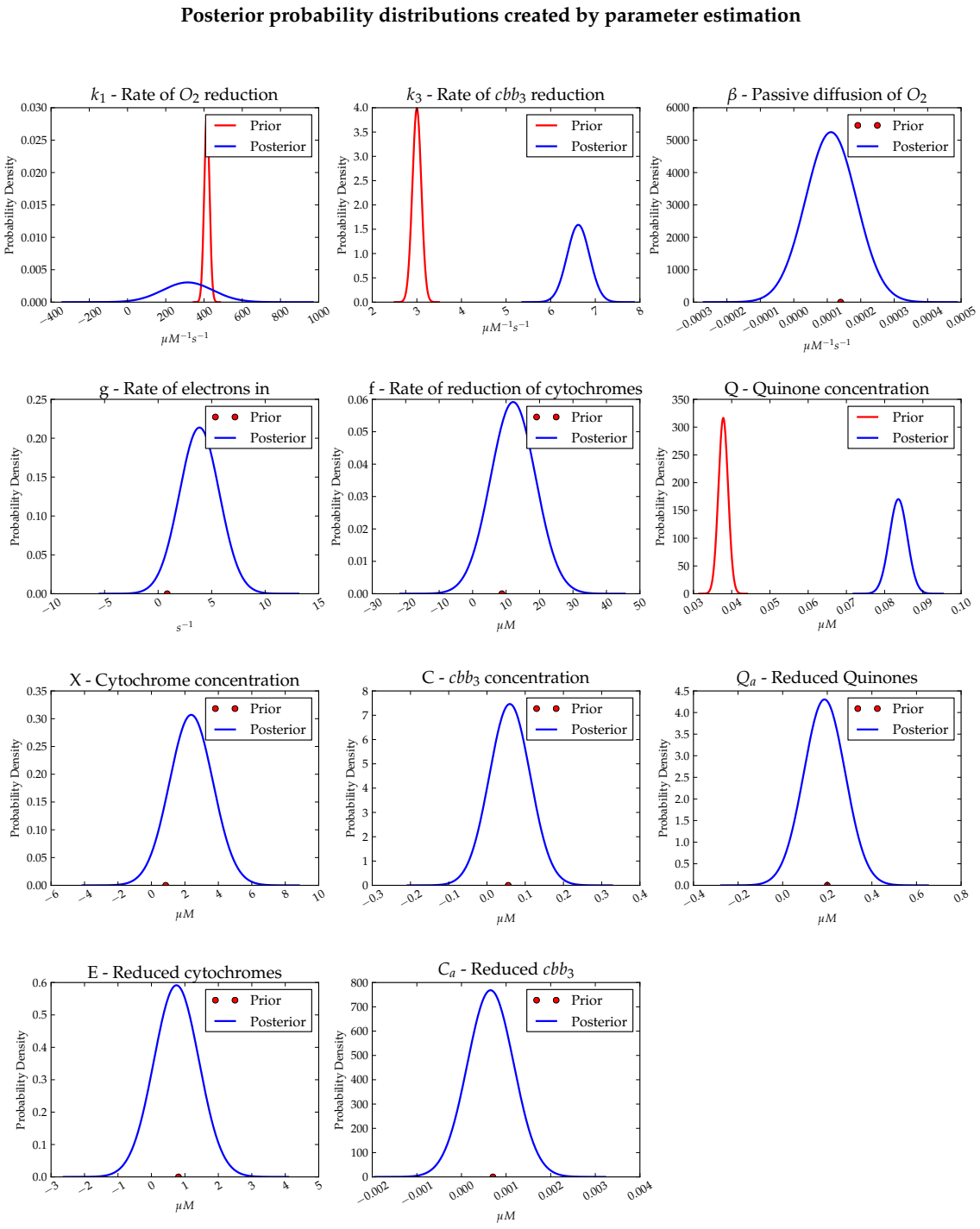

Figure 5.8: **Posterior probability distributions for oxygen reduction**. These are the probability distributions generated by parameter estimation on 3 oxygen reduction datasets. These have been overlayed onto the prior probability distributions used by the parameter estimation algorithm, also shown in Figure 5.4.

This statistic produces in a single figure what could interpreted from the posterior probability distributions as it is essentially a measure of how close the trajectories have become towards the end of said trajectory. This statistic is calculated on the trajectories from multiple runs *for each parameter individually*. The R statistic was calculated using the *Bolstad2*[112] library for R[113].

Analysis of Correlation

Given the large number of parameters, and the simple form of the experimental data it is quite likely that a number of the parameters will be correlated with one another. This effect should also be exacerbated at this stage due to the limited constraints (by virtue of wide prior probabilities) on the ranges of values that parameters can take. In order to investigate this I constructed a correlation matrix by calculating the Pearson's Product-Moment Correlation Coefficient for each of the parameters. This value provides the direction of correlation as indicated by the sign, and the degree of linearity as indicated by the magnitude. A positive correlation indicates that as the value of one parameter increases, the other increases also. A negative correlation indicates that as the value of one parameter increases, the other decreases.

The upper-triangle correlation matrix is shown in Figure 5.1 and was constructed by concatenating all the trajectories created by the parameter estimation system (discarding the burn-in) together and the Pearson's Product-Moment Correlation Coefficient calculated for each combination. The matrix is upper-triangle only as the lower triangle is a duplicate of the same data. The diagonal is shown in grey as it is not useful data since the correlation of X against X is always 1.

The correlation matrix shows that the majority of the parameters are not correlated with each other, giving very low R^2 values. A number of the parameters showed moderate correlation, which is to be expected. Parameters such as k_1 - the rate of reduction of oxygen - and k_3 - the rate of reduction of cbb_3 - broadly speaking would increase as g - the rate of electrons in - increased. This was expected as

more electrons means higher observable rates are possible. Strong positive correlations exist between the concentrations of cytochromes (X), cbb_3(C) and the rate of electrons in (g). This makes sense if the system wants to increase throughput of electrons but cannot do it by increasing the size of the quinone pool. Large numbers of electrons can be reduced by the cytochromes to eventually reduce oxygen.

Interestingly there were no negative correlations observed. This is somewhat odd as it might be expected that as the reduction rates of enzymes goes down, the concentration of the enzyme increases to maintain the same overall electron throughput. It appears however that the system is always trying to maximise oxygen throughput.

	k_1	k_3	β	g	f	Q	X	C	Q_a	E	C_a
k_1	1	0.28599	0.013212	0.420123	0.154821	0.009968	0.369637	0.367247	0.00344	0.000229	0.046062
k_3		1	0.008486	0.586606	0.351956	0.002927	0.617929	0.681098	0.000559	0.001062	0.012978
β			1	0.009472	0.07071	6.58×10^{-5}	0.001034	0.019449	0.006711	0.055052	0.002166
g				1	0.426205	0.008692	0.86507	0.811637	0.009455	0.003244	0.076195
f					1	0.00461	0.329468	0.432466	0.106478	0.012951	0.001404
Q						1	0.008756	0.006046	0.00024	7.86×10^{-6}	0.003555
X							1	0.803124	1.47×10^{-5}	3.43×10^{-5}	0.064213
C								1	0.018731	7.27×10^{-5}	0.046421
Q_a									1	0.108255	0.00897
E										1	0.003167
C_a											1

Table 5.1: **Regression Analysis of Oxygen Reduction Parameters.** This table shows the R^2 values from linear regression analysis on the combined parameter trajectories for Oxygen reduction. Parameters with high correlation have been coloured green ($R^2 > 0.8$) and those with moderation correlation have been coloured orange ($0.8 > R^2 > 0.3$).

5.1.3 Rate of oxygen diffusion

During the course of this experimental stage I noticed that on occasions where the respiring cultures died, either through being left in essentially anaerobic conditions for too long, or intentionally killed with Chloramphenicol, the oxygen levels in the culture media would begin to rise slowly. This did not occur in every case, and after some further experimentation I concluded that it probably occurs when an air bubble gets trapped underneath the lid of the oxygen electrode chamber. The average rates of oxygen diffusion were very small, and on the experimental time-scales are probably negligible, but I thought it necessary to include in the model for completeness.

The equation used to fit raw data for oxygen diffusion is a 3 parameter exponential:

$$f(x) = c - ae^{-bx}$$

In the differential equation this collapses to two parameters, the oxygen saturation level, and the rate of oxygen recovery thus:

$$\frac{d[O_2]}{dt} = \beta(1 - O_2/K_O)$$

Integrating and separating this equation gives:

$$\begin{aligned} -\beta\frac{t}{K_O} + C &= ln([O_2] - K_O) \\ \Rightarrow [O_2] - K_O &= Ae^{\left(-\beta\frac{t}{K_O}\right)} \\ \Rightarrow [O_2] &= K_O + Ae^{\left(-\beta\frac{t}{K_O}\right)} \end{aligned}$$

5.1.4 Discussion

The experimental dataset shows that oxygen reduction in *Neisseria meningitidis* is a simple linear system with the reductase having a high affinity for oxygen

demonstrated by the almost complete lack of non-linearity as oxygen concentration approaches zero. This apparent simple linearity could be modelled with a high degree of accuracy with just 2 parameters in a simple $y = -mx + c$ system. However this does mean that the posterior distributions generated are very wide and therefore allows much greater freedom for the next dataset to explore the parameter space.

Given our knowledge of the underlying transport chain and the affinity of cbb_3 for oxygen, we expect a linear reduction of oxygen with high affinity over nearly two orders of magnitude. It is however remarkable that we can model this behaviour with so few components in the model, as it requires significant changes in the reduction state of the enzymes to achieve this.

Chapter 6

Nitric Oxide Reduction in *N. meningitidis*

Modelling nitric oxide reduction involves adding nitric oxide whilst cultures are respiring aerobically. The conditions are the same as for oxygen reduction, except that nitric oxide solution is added to a concentration of ≈ 5 μM and the culture then left to respire nitric oxide.

In the model, Equations (2, 7 & 9) are now involved, as the nitric oxide reductase NorB is being used in addition to the requirement to model the chemical inhibition of cbb_3 by nitric oxide. The parameter posterior probability distributions generated from the Monte-Carlo runs from the oxygen reduction dataset were used as prior probability distributions for this next dataset. The unknown parameters (those not included in the previous dataset) were set to sensible non-zero values which would allow them to burn-in and generate subsequent posterior distributions. The datasets used for this section of the model describe the effect on oxygen reduction as nitric oxide is introduced to a system that is only partially primed for microaerobic respiration. There will be a small amount of NorB (the nitric oxide reductase) present to remove and nitric oxide that is present. The $nsrR^{-}$ mutant, which expresses NorB in an essentially constitutive manner was not effective in generating a usable dataset as it removed any NO almost instan-

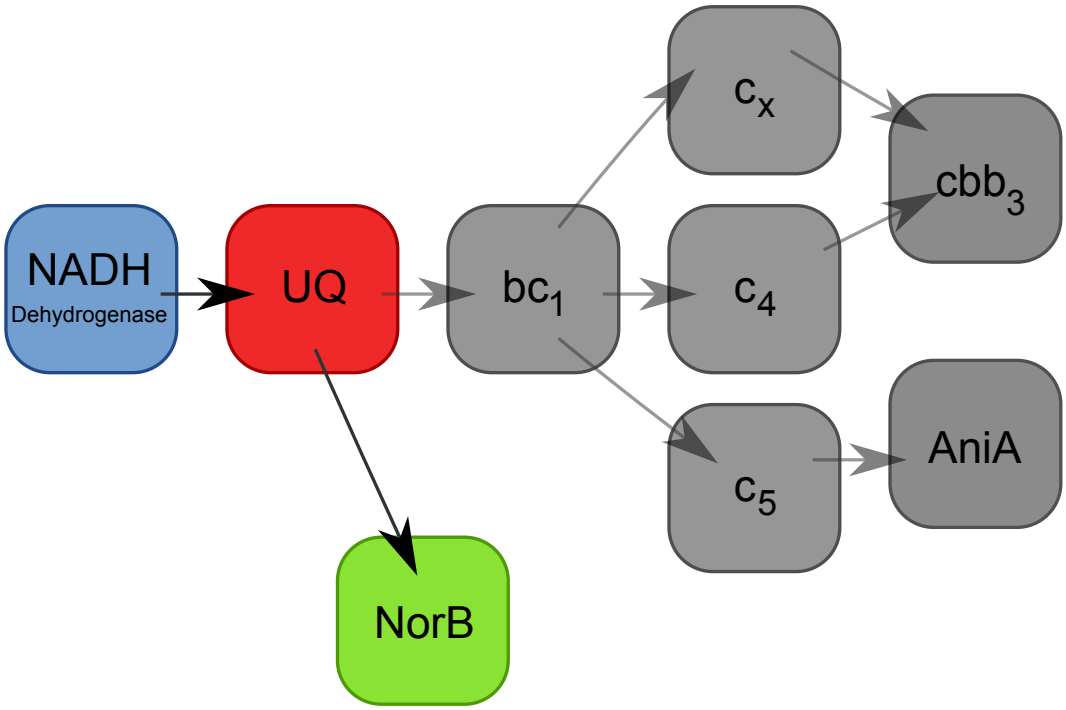

Figure 6.1: **Nitric oxide reducing electron transport chain of *N. meningitidis*.** This shows the complete electron transport chain of *Neisseria meningitidis* with the components irrelevant to nitric oxide reduction greyed out.

taneously resulting in an almost featureless dataset (data not shown).

The dataset and final solved output from the Monte-Carlo run are show in figure 6.2. This is a more complex dataset than for oxygen respiration. Initially the oxygen reduction is carried out in exactly the same manner as the previous dataset, which is able to be modelled with the parameters selected from the prior distributions. Upon addition of nitric oxide, oxygen respiration slows and almost stops as a result of competition for electrons between cbb_3 and NorB, and the direct chemical inhibition of cbb_3 by NO. Nitric oxide starts being removed as a combination of simple diffusion (although this rate will be low) and reduction via NorB. Once the NO has been removed from the system oxygen reduction resumes at almost the same rate as before and still has the same high affinity feature as the previous dataset. The closeness of fit of the solved parameter set to the experimental data shows that the model has been able to accommodate a parameter set from the prior distributions that is able to accommodate all these features, and will still be able to model simple oxygen reduction.

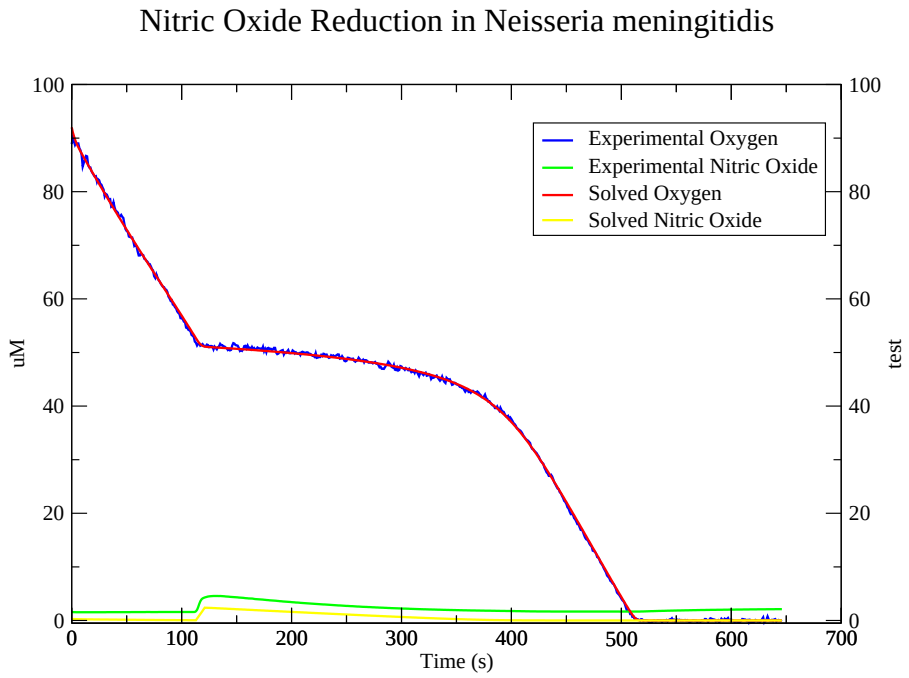

Figure 6.2: **Nitric Oxide Reduction in *Neisseria meningitidis*.** This dataset shows the effect on rate of oxygen reduction as nitric oxide is introduced to the system. The solved output, using prior probabilities from the oxygen reduction dataset show an almost perfect match to the features of the experimental dataset. The solved oxygen concentrations match the experimental dataset so closely as to be almost invisible.

6.1 Aerobic Nitric Oxide Reduction

6.1.1 Introduction

6.1.2 Results

6.1.3 Discussion

6.2 Microaerobic Nitric Oxide Reduction

6.2.1 Introduction

6.2.2 Results

6.2.3 Discussion

6.3 Aerobic Nitric Oxide Reduction in *nsrR*$^{-}$ mutant

6.3.1 Introduction

6.3.2 Results

6.3.3 Discussion

Chapter 7

Nitrite Reduction in *N. meningitidis*

Modelling nitrite reduction involves growing NsrR deficient cultures in aerobic conditions. This mutant expresses AniA and NorB in a constitutive manner, removing the necessity for growing the cultures in microaerobic conditions. The cultures are grown for 3-4 hours after which the culture is added to the electrode chamber and Sodium Nitrite added to a concentration of 1 mM.

In the model, Equations (3.3 & 3.8) are now also involved, allowing parametrisation of kinetic rates of AniA. This experimental dataset does not unfortunately describe how the concentration of NO changes while Nitrite is being reduced. The prior probability distributions used for this dataset were the posteriors generated from the Nitric Oxide Reduction dataset described above, in accordance with Bayesian inference. The unknown parameters were given non-zero values with flat priors, allowed to burn-in and were then used to generate posterior probability distributions.

A representative dataset and solved output is shown in figure 7.2.

This is a simpler dataset than for Nitric oxide reduction as it only describes nitrite reduction, along with a small change in oxygen concentration. In combination with prior probability distributions from the afore mentioned dataset it means that the possible values for the kinetic rates involved are automatically going to be limited to those that work alongside the given priors. Without the prior probability distributions the posterior distributions would have a similar

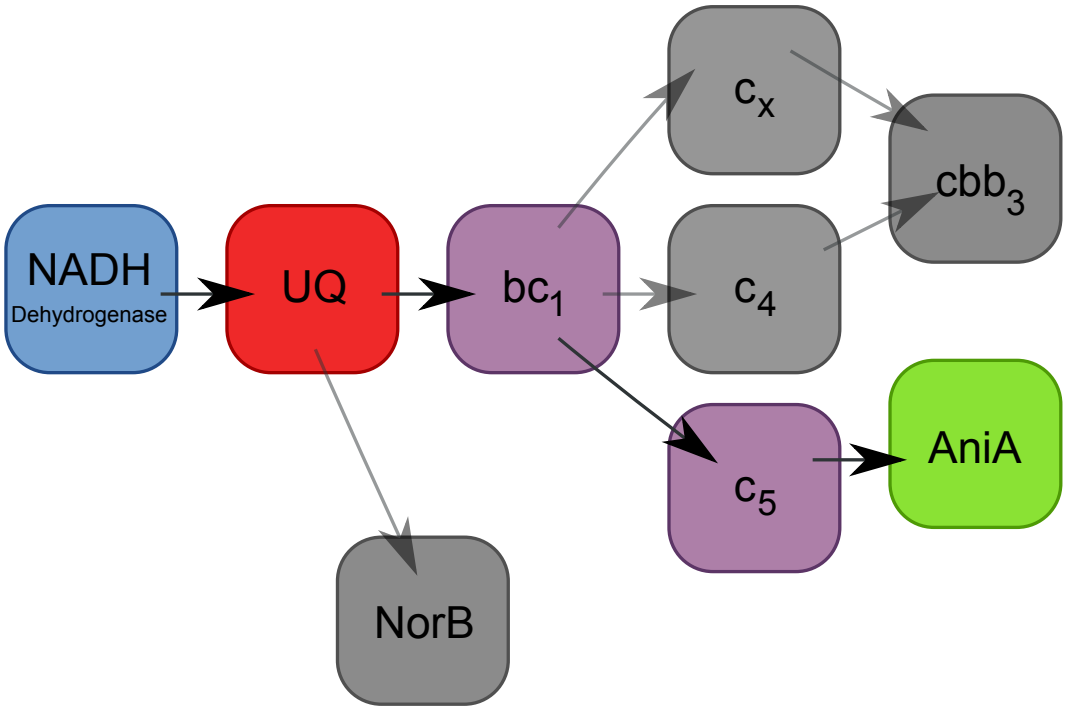

Figure 7.1: **Nitrite reducing electron transport chain of *N. meningitidis*.** This shows the complete electron transport chain of *Neisseria meningitidis* with the components irrelevant to nitrite reduction greyed out. In the mathematical model all of the purple elements (cytochromes) are amalgamated into one entity.

outcome to that of the first dataset used, where simple oxygen reduction was modelled, i.e. very wide distributions.

Figure 7.2: **Nitrite Reduction in *Neisseria meningitidis*.** This dataset shows the rate of nitrite reduction when cultures have been grown in microaerobic conditions. The concentrations of nitrite were measured off-line leading to discontinuous data, however the solved output closely matches the experimental data for nitrite.

7.1 Microerobic Nitrite Reduction

7.1.1 Introduction

7.1.2 Results

7.1.3 Discussion

7.2 Microaerobic Nitrite Reduction in *norB*$^-$ mutant

7.2.1 Introduction

7.2.2 Results

7.2.3 Discussion

7.3 Aerobic Nitrite Reduction in *nsrR*$^-$ mutant

7.3.1 Introduction

7.3.2 Results

7.3.3 Discussion

7.4 Aerobic Nitrite Reduction in *nsrR*$^-$-*norB*$^-$ mutanterobic Nitrite Reduction in nsrR- - norB- mutant

7.4.1 Introduction

7.4.2 Results

7.4.3 Discussion

Chapter 8

AniA and NorB Expression in *N. meningitidis*

8.1 Aerobic and Microaerobic Expression

8.1.1 Introduction

8.1.2 Results

8.1.3 Discussion

Chapter 9

The Completed Model

9.1 Amalgamation of cytochromes

Appendix A

Appendix

$$
\begin{aligned}
\frac{d[O_2]}{dt} &= \beta\left(1-\frac{[O_2]}{K_O}\right)-k_1[C_a][O_2] \\
\frac{d[NO]}{dt} &= m_1[NO_2^-][A_a]-l_1[NO][B_a]-k_5[C_a][NO]+k_6[C_X]-\gamma[NO] \\
\frac{d[NO_2^-]}{dt} &= -m_1[NO_2^-][A_a] \\
\frac{d[Q_a]}{dt} &= g([Q]-[Q_a])-l_3[Q_a]([B]-[B_a])-f[Q_a]([X]-[E]) \\
\frac{d[E]}{dt} &= -k_3([C]-[C_a]-[C_X])[E]-m_3([A]-[A_a])[E]+f[Q_a]([X]-[E]) \\
\frac{d[A_a]}{dt} &= m_3([A]-[A_a])[E]-m_1[NO_2^-][A_a] \\
\frac{d[B_a]}{dt} &= l_3[Q_a]([B]-[B_a])-l_1[NO][B_a] \\
\frac{d[C_a]}{dt} &= k_3([C]-[C_a]-[C_X])[E]-k_1[C_a][O_2]-k_5[C_a][NO] \\
\frac{d[C_X]}{dt} &= k_5[C_a][NO]-k_6[C_X] \\
\frac{d[A]}{dt} &= \left(R\left(1-\frac{[O_2]+k_{10}[NO]}{[O_2]+k_{10}[NO]+k_{11}}\right)-S\left(1-\frac{[NO]}{[NO]+k_{13}}\right)\right)-k_8[A] \\
\frac{d[B]}{dt} &= T\left(\frac{[NO]}{[NO]+k_{15}}\right)-k_{16}[B]
\end{aligned}
\tag{A.1}
$$

Symbol	Description
O_2	Oxygen concentration
NO	Nitric oxide concentration
NO_2^-	Nitrite concentration
E	Reduced cytochrome concentration
A_a	Reduced AniA
B_a	Reduced NorB
C_a	Reduced cbb_3
C_X	Reversibly inhibited cbb_3
Q_a	Reduced Quinones

Table A.1: Model Variables

Symbol	Description
k_1	Rate of O_2 reduction by reduced cbb_3
k_3	Rate of cbb_3 reduction by cytochrome pool
l_1	Rate of NO reduction by reduced NorB
l_3	Rate of NorB reduction by quinone pool
m_1	Rate of NO_2^- reduction by reduced AniA
m_3	Rate of AniA reduction by cytochrome pool
k_5	Rate of cbb_3 inhibition by NO
k_6	Rate of recovery of NO inhibited cbb_3
β	Rate of passive diffusion in of O_2
K_O	Saturation O_2 level
g	Rate of electrons in from NADH
f	Rate of reduction of cytochromes by quinones
γ	Spontaneous loss of NO
Q	Concentration of quinones
X	Concentration of cytochromes
A	Concentration of AniA
B	Concentration of NorB
C	Concentration of cbb_3

Table A.2: Model Parameters

List of Abbreviations

ABC	Approximate Bayesian computation
ABCSMC	Approximate Bayesian Computation by Sequential Monte Carlo
AniA	Anaerobically inducible protein A from *Neisseria* sp.
ATP	Adenosine triphosphate
CAB	Columbia Agar Base
CFU	Colony Forming Units
CSF	Cerebrospinal Fluid
DNA	Deoxyribonucleic Acid
ETC	Electron Transport Chain
FNR	Fumarate and Nitrite reduction Regulator
HCO	Haem Copper Oxidase
LSD	Least-Squares Difference
LSODA	Livermore Solver for Ordinary Differential Equations
MHB	Müller-Hinton Broth
MHMC	Metropolis-Hastings Monte Carlo
NADH	Nicotinamide adenine dinucleotide
NarP	Nitrate/Nitrite Response Regulator
NarQ	Nitrate/Nitrite Response Sensor
NED	*N*-1-napthylethylenediamine dihydrochloride
NOR	Nitric Oxide Reductase
NorB	Nitric Oxide Reductase B from *Neisseria* sp.
NsrR	Nitrite sensing repressor protein
OD	Optical Density
ODE	Ordinary Differential Equation

PDE	Partial Differential Equation
rpm	Revolutions Per Minute
SMC	Sequential Monte Carlo
spc^r	Spectinomycin resistance
tet^r	tetracycline resistance

References

1. van Deuren M, Brandtzaeg P, van der Meer JWM (2000) Update on Meningococcal Disease with Emphasis on Pathogenesis and Clinical Management. Clin Microbiol Rev 13: 144–166.

2. Stephens DS (2009) Biology and Pathogenesis of the Evolutionarily Successful, Obligate Human Bacterium *Neisseria meningitidis*. Vaccine 27: B71–B77.

3. Rosenstein NE, Perkins BA, Stephens DS, Popovic T, Hughes JM (2001) Meningococcal Disease. N Engl J Med 344: 1378–1388.

4. DeVoe IW (1982) The Meningococcus and Mechanisms of Pathogenicity. Microbiol Mol Biol Rev 46: 162–190.

5. Aas JA, Paster BJ, Stokes LN, Olsen I, Dewhirst FE (2005) Defining the Normal Bacterial Flora of the Oral Cavity. J Clin Microbiol 43: 5721–5732.

6. Madigan M, Martinko J, editors (2005) Brock Biology of Microorganisms. 11th ed., Prentice Hall.

7. Carbonnelle E, Hill DJ, Morand P, Griffiths NJ, Bourdoulous S, et al. (2009) Meningococcal Interactions with the Host. Vaccine 27: B78–B89.

8. Stephens DS, Greenwood B, Brandtzaeg P (2007) Epidemic meningitis, meningococcaemia, and Neisseria meningitidis. Lancet 369: 2196–2210.

9. Larson JA, Higashi DL, Stojiljkovic I, So M (2002) Replication of Neisseria neningitidis Within Epithelial Cells Requires TonB-Dependent Acquisition of Host Cell Iron. Infect Immun 70: 1461–1467.

10. Archibald FS, DeVoe IW (1978) Iron in *Neisseria meningitidis*: Minimum Requirements, Effects of Limitation, and Characteristics of Uptake. J Bacteriol 136: 35–48.

11. Perkins-Balding D, Ratliff-Griffin M, Stojiljkovic I (2004) Iron Transport Systems in *Neisseria meningitidis*. Microbiol Mol Biol Rev 68: 154–171.

12. Yazdankhah SP, Caugant DA (2004) *Neisseria meningitidis*: An Overview of the Carriage State. J Med Microbiol 53: 821–832.

13. Beddek AJ, Li MS, Kroll JS, Jordan TW, Martin DR (2009) Evidence for Capsule Switching between Carried and Disease-Causing *Neisseria meningitidis* Strains. Infect Immun 77: 2989–2994.

14. Moxon ER, Rainey PB, Nowak MA, Lenski RE (1994) Adaptive Evolution of Highly Mutable Loci in Pathogenic Bacteria. Current Biology 4: 24–33.

15. Pathan N, Faust SN, Levin M (2003) Pathophysiology of Meningococcal Meningitis and Septicaemia. Arch Dis Child 88: 601–607.

16. Exley RM, Shaw J, Mowe E, Sun YH, West NP, et al. (2005) Available Carbon Source Influences the Resistance of *Neisseria meningitidis* Against Complement. J Exp Med 201: 1637–1645.

17. Beno DW, Devine LF, Larson GL (1968) Identification of *Neisseria meningitidis* Carbohydrate Fermentation Patterns in Mueller-Hinton Broth. J Bacteriol 96: 563.

18. Rock JD, Mahnane MR, Anjum MF, Shaw JG, Read RC, et al. (2005) The Pathogen *Neisseria meningitidis* Requires Oxygen, but Supplements

Growth by Denitrification. Nitrite, Nitric Oxide and Oxygen Control Respiratory Flux at Genetic and Metabolic Levels. Mol Microbiol 58: 800–9.

19. Rock JD, Moir JWB (2005) Microaerobic Denitrification in *Neisseria meningitidis*. Biochem Soc Trans 33: 134–6.

20. Tuttle DM, Scherp HW (1952) Studies On The Carbon Dioxide Requirement Of *Neisseria meningitidis*. J Bacteriol 64: 171–182.

21. Lundberg JO, Weitzberg E, Cole JA, Benjamin N (2004) Nitrate, Bacteria and Human Health. Nat Rev Micro 2: 593–602.

22. Deeudom M, Rock J, Moir J (2006) Organization of the Respiratory Chain of *Neisseria meningitidis*. Biochem Soc Trans 34: 139–42.

23. Deeudom M (2007) The Electron Transport Chains of *Neisseria meningitidis*. Ph.D. thesis, University of York.

24. Preisig O, Zufferey R, Thony-Meyer L, Appleby C, Hennecke H (1996) A High-affinity cbb3-Type Cytochrome Oxidase Terminates the Symbiosis-Specific Respiratory Chain of *Bradyrhizobium japonicum*. J Bacteriol 178: 1532–1538.

25. Brown GC, Cooper C (1994) Nanomolar Concentrations of Nitric Oxide Reversibly Inhibit Synaptosomal Respiration by Competing with Oxygen at Cytochrome Oxidase. FEBS Letters 356: 295–298.

26. Sharpe MA, Cooper CE (1998) Interaction of Peroxynitrite with Mitochondrial Cytochrome Oxidase. J Biol Chem 273: 30961–30972.

27. Anjum MF, Stevanin TM, Read RC, Moir JWB (2002) Nitric Oxide Metabolism in *Neisseria meningitidis*. J Bacteriol 184: 2987–2993.

28. Heurlier K, Thomson MJ, Aziz N, Moir JWB (2008) The Nitric Oxide (NO)-Sensing Repressor NsrR of *Neisseria meningitidis* has a Compact Regulon

of Genes Involved in NO Synthesis and Detoxification. J Bacteriol 190: 2488–95.

29. Deeudom M, Koomey M, Moir JWB (2008) Roles of C-type Cytochromes in Respiration in *Neisseria meningitidis*. Microbiology 154: 2857–64.

30. Rock JD, Thomson MJ, Read RC, Moir JWB (2007) Regulation of Denitrification Genes in *Neisseria meningitidis* by Nitric Oxide and the Repressor NsrR. J Bacteriol 189: 1138–44.

31. Isabella V, Wright LF, Barth K, Spence JM, Grogan S, et al. (2008) Cis- and Trans-Acting Elements Involved in Regulation if NorB (NorZ), The Gene Encoding Nitric Oxide Reductase in *Neisseria gonorrhoeae*. Microbiology 154: 226–239.

32. Pitcher RS, Watmough NJ (2004) The Bacterial Cytochrome cbb3 Oxidases. Biochimica et Biophysica Acta (BBA) - Bioenergetics 1655: 388 – 399.

33. Puustinen A, Verkhovsky MI, Morgan JE, Belevich NP, Wikstrom M (1996) Reaction of the *Escherichia coli* Quinol Oxidase Cytochrome bo3 with Dioxygen: The Role of a Bound Ubiquinone Molecule. Proc Natl Acad Sci U S A 93: 1545–1548.

34. van der Oost J, de Boer AP, de Gier JW, Zumft WG, Stouthamer AH, et al. (1994) The Heme-Copper Oxidase Family Consists of Three Distinct Types of Terminal Oxidases and is Related to Nitric Oxide Reductase. FEMS Microbiol Lett 121: 1–9.

35. García-Horsman JA, Barquera B, Rumbley J, Ma J, Gennis RB (1994) The Superfamily of Heme-Copper Respiratory Oxidases. J Bacteriol 176: 5587–5600.

36. Keilin D, Hartree EF (1939) Cytochrome and Cytochrome Oxidase. Proceedings of the Royal Society of London Series B, Biological Sciences 127: pp. 167–191.

37. Huang Y, Reimann J, Singh LMR, Adelroth P (2010) Substrate Binding and the Catalytic Reactions in Cbb3-type Oxidases: The Lipid Membrane Modulates Ligand Binding. Biochim Biophys Acta 1797: 724–731.

38. Zufferey R, Preisig O, Hennecke H, ThÃűny-Meyer L (1996) Assembly and Function of the Cytochrome cbb3 Oxidase Subunits in *Bradyrhizobium japonicum*. J Biol Chem 271: 9114–9119.

39. Preisig O, Zufferey R, Hennecke H (1996) The *Bradyrhizobium japonicum* fixGHIS Genes are Required for the Formation of the High-Affinity cbb3-type Cytochrome Oxidase. Arch Microbiol 165: 297–305.

40. Householder TC, Fozo EM, Cardinale JA, Clark VL (2000) Gonococcal Nitric Oxide Reductase is Encoded by a Single Gene, NorB, Which is Required for Anaerobic Growth and is Induced by Nitric Oxide. Infect Immun 68: 5241–5246.

41. Barth KR, Isabella VM, Clark VL (2009) Biochemical and Genomic Analysis of the Denitrification Pathway within the Genus Neisseria. Microbiology 155: 4093–4103.

42. Clark VL, Campbell LA, Palermo DA, Evans TM, Klimpel KW (1987) Induction and Repression of Outer Membrane Proteins by Anaerobic Growth of *Neisseria gonorrhoeae*. Infect Immun 55: 1359–1364.

43. Moir JW (2011) A Snapshot of a Pathogenic Bacterium Mid-evolution: *Neisseria meningitidis* is Becoming a Nitric Oxide-Tolerant Aerobe. Biochem Soc Trans 39: 1890–1894.

44. Weiss H, Friedrich T, Hofhaus G, Preis D (1991) The Respiratory-Chain NADH Dehydrogenase (Complex I) of Mitochondria. Eur J Biochem 197: 563–576.

45. Carroll J, Fearnley IM, Shannon RJ, Hirst J, Walker JE (2003) Analysis of the Subunit Composition of Complex I from Bovine Heart Mitochondria. Mol Cell Proteomics 2: 117–126.

46. Friedrich T, Böttcher B (2004) The Gross Structure of the Respiratory Complex I: a Lego System. Biochim Biophys Acta 1608: 1–9.

47. Yagi T (1991) Bacterial NADH-Quinone Oxidoreductases. J Bioenerg Biomembr 23: 211–225.

48. Gemperli AC, Dimroth P, Steuber J (2002) The Respiratory Complex I (NDH I) from *Klebsiella pneumoniae*, a Sodium Pump. J Biol Chem 277: 33811–33817.

49. Thöny-Meyer L (1997) Biogenesis of Respiratory Cytochromes in Bacteria. Microbiology and Molecular Biology Reviews 61: 337–76.

50. Darrouzet E, Valkova-Valchanova M, Ohnishi T, Daldal F (1999) Structure and Function of the Bacterial bc1 Complex: Domain Movement, Subunit Interactions, and Emerging Rationale Engineering Attempts. J Bioenerg Biomembr 31: 275–288.

51. Snyder CH, Gutierrez-Cirlos EB, Trumpower BL (2000) Evidence for a Concerted Mechanism of Ubiquinol Oxidation by the Cytochrome bc 1 Complex. Journal of Biological Chemistry 275: 13535–13541.

52. Berry EA, Huang LS (2011) Conformationally Linked Interaction in the Cytochrome bc(1) Complex Between Inhibitors of the Q(o) Site and the Rieske Iron-Sulfur Protein. Biochim Biophys Acta 1807: 1349–1363.

53. Crofts AR, Shinkarev VP, Kolling DRJ, Hong S (2003) The Modified Q-Cycle Explains the Apparent Mismatch Between the Kinetics of Reduction of Cytochromes c1 and bh in the bc1 Complex. J Biol Chem 278: 36191–36201.

54. Wood PM (1983) Why do c-type Cytochromes Exist? FEBS Lett 164: 223–226.

55. Ambler RP (1991) Sequence Variability in Bacterial Cytochromes c. Biochim Biophys Acta 1058: 42–47.

56. Chang HY, Ahn Y, Pace LA, Lin MT, Lin YH, et al. (2010) The Diheme Cytochrome C(4) from *Vibrio cholerae* is a Natural Electron Donor to the Respiratory cbb(3) Oxygen Reductase. Biochemistry 49: 7494–7503.

57. Clark VI, Isabella VM, Barth K, Overton TW (2010) Regulation and Function of the Neisserial Denitrification Pathway: Life with Limited Oxygen. In: Genco CA, Wetzler L, editors, Neisseria: Molecular Mechanisms of Pathogenesis, chap. 2, pp. 19–39, Caister Academic Press.

58. Edwards J, Cole LJ, Green JB, Thomson MJ, Wood AJ, et al. (2010) Binding to DNA Protects *Neisseria meningitidis* Fumarate and Nitrate Reductase Regulator (FNR) from Oxygen. Journal of Biological Chemistry 285: 1105–1112.

59. Overton TW, Whitehead R, Li Y, Snyder LAS, Saunders NJ, et al. (2006) Coordinated Regulation of the *Neisseria gonorrhoeae*-Truncated Denitrification Pathway by the Nitric Oxide-Sensitive Repressor, NsrR, and Nitrite-Insensitive NarQ-NarP. J Biol Chem 281: 33115–33126.

60. Baker SC, Ferguson SJ, Ludwig B, Page MD, Richter OM, et al. (1998) Molecular Genetics of the Genus Paracoccus: Metabolically Versatile Bacteria with Bioenergetic Flexibility. Microbiol Mol Biol Rev 62: 1046–1078.

61. Nicholls DG, Ferguson SJ (1992) Bioenergetics 3. 2nd ed., Academic Press.

62. Kahlem P, Birney E (2006) Dry Work in a Wet World: Computation in Systems Biology. Mol Syst Biol 2: 40.

63. Doyle FJr, Stelling J (2006) Systems Interface Biology. J R Soc Interface 3: 603–16.

64. Kitano H (2002) Computational Systems Biology. Nature 420: 206–10.

65. Kitano H (2002) Systems Biology: A Brief Overview. Science 295: 1662–4.

66. Valencia A, Pazos F (2002) Computational Methods for the Prediction of Protein Interactions. Curr Opin Struct Biol 12: 368–73.

67. Mündermann L, Erasmus Y, Lane B, Coen E, Prusinkiewicz P (2005) Quantitative Modeling of Arabidopsis Development. Plant Physiol 139: 960–8.

68. Prusinkiewicz P (2004) Modeling Plant Growth And Development. Curr Opin Plant Biol 7: 79–83.

69. Prusinkiewicz P, Rolland-Lagan AG (2006) Modeling Plant Morphogenesis. Curr Opin Plant Biol 9: 83–8.

70. Crampin EJ, Halstead M, Hunter P, Nielsen P, Noble D, et al. (2004) Computational Physiology and the Physiome Project. Exp Physiol 89: 1–26.

71. Barabási AL, Oltvai ZN (2004) Network Biology: Understanding the Cell's Functional Organization. Nat Rev Genet 5: 101–13.

72. Peercy BE, Cox SJ, Shalel-Levanon S, San KY, Bennett G (2006) A Kinetic Model of Oxygen Regulation of Cytochrome Production in *Escherichia coli*. J Theor Biol 242: 547–563.

73. Almeida JS, Reis MAM, Carrondo MJT (1997) A Unifying Kinetic Model of Denitrification. Journal of Theoretical Biology 186: 241–249.

74. Cavaliere M, Ardelean II (2006) Applications of Membrane Computing, chap. Modeling Respiration in Bacteria and Respiration/Photosynthesis

Interaction in Cyanobacteria Using a P System Simulator, pp. 129–158. Springer.

75. Klipp E, Herwig R, Kowald A, Wierling C, Lehrach H (2005) Systems Biology in Practice. Concepts, Implementation and Application. WILEY-VCH Verlag GmbH & Co. KGaA, Weinheim.

76. Gillespie DT (1977) Exact Stochastic Simulation of Coupled Chemical Reactions. The Journal of Physical Chemistry 81: 2340–2361.

77. Sauro HM, Hucka M, Finney A, Wellock C, Bolouri H, et al. (2003) Next Generation Simulation Tools: The Systems Biology Workbench and BioSPICE Integration. OMICS: A Journal of Integrative Biology 7: 355–372.

78. Hoops S, Sahle S, Gauges R, Lee C, Pahle J, et al. (2006) COPASI–a COmplex PAthway SImulator. Bioinformatics 22: 3067–3074.

79. Radhakrishnan K, Hindmarsh AC (1993) Description and Use of LSODE, the Livermore Solver for Ordinary Differential Equations. Tech. rep., NASA.

80. Gibson MA, Bruck J (2000) Efficient Exact Stochastic Simulation of Chemical Systems with Many Species and Many Channels. The Journal of Physical Chemistry A 104: 1876–1889.

81. McGuinness B, Barlow AK, Clarke IN, Farley JE, Anilionis A, et al. (1990) Deduced Amino Acid Sequences of Class 1 Protein (Pora) from Three Strains of *Neisseria meningitidis*. Synthetic Peptides Define the Epitopes Responsible for Serosubtype Specificity. J Exp Med 171: 1871–1882.

82. Clark LC, Wolf R, Granger D, Taylor Z (1953) Continuous Recording of Blood Oxygen Tensions by Polarography. Journal of Applied Physiology 6: 189–193.

83. Rank Brothers Ltd (2012) Oxygen Electrode Exploded Views. http://www.rankbrothers.co.uk/prod1exp.htm.

84. YSI Incorporated (2012) Oxygen Solubility Table. http://www.ysi.com/media/pdfs/DO-Oxygen-Solubility-Table.pdf.

85. Liu X, Liu Q, Gupta E, Zorko N, Brownlee E, et al. (2005) Quantitative Measurements of No Reaction Kinetics with a Clark-Type Electrode. Nitric Oxide 13: 68 – 77.

86. Bedioui F, Villeneuve N (2003) Electrochemical Nitric Oxide Sensors for Biological Samples: Principle, Selected Examples and Applications. Electroanalysis 15: 5–18.

87. Serpe MJ, Zhang X (2007) The Principles, Development and Application of Microelectrodes for the In Vivo Determination of Nitric Oxide. In: Michael AC, Borland LM, editors, Electrochemical Methods for Neuroscience, chap. 21, CRC Press.

88. Nicholas DJ, Nason A (1957) Determination of Nitrate and Nitrite. In: Methods in Enzymology, vol. 3, pp. 981–984, Academic Press.

89. Aga RG, Hughes MN (2008) The Preparation and Purification of NO Gas and the Use of NO Releasers: The Application of NO Donors and Other Agents of Nitrosative Stress in Biological Systems. In: Poole RK, editor, Globins and Other Nitric Oxide-Reactive Proteins, Part A, vol. 436 of Methods in Enzymology, pp. 35 – 48, Academic Press.

90. Cole LJ, Huston WM, Moir JWB (2008) Delivery of Nitric Oxide for Analysis of the Function of Cytochrome C'. In: Poole RK, editor, Globins and Other Nitric Oxide-Reactive Proteins, Part A, vol. 436 of Methods in Enzymology, pp. 21 – 33, Academic Press.

91. Giuffre A, Barone MC, Mastronicola D, D'Itri E, Sarti P, et al. (2000) Reaction of Nitric Oxide with the Turnover Intermediates of Cytochrome c Ox-

idase: Reaction Pathway and Functional Effects. Biochemistry 39: 15446–15453.

92. Forte E, Urbani A, Saraste M, Sarti P, Brunori M, et al. (2001) The Cytochrome cbb3 from *Pseudomonas stutzeri* Displays Nitric Oxide Reductase Activity. Eur J Biochem 268: 6486–6491.

93. Hunter H (2007) Characterisation of the Oxidase Activity in *Neisseria lactamica*, University of York BSc Honours Project Report.

94. Nojiri M, Koteishi H, Nakagami T, Kobayashi K, Inoue T, et al. (2009) Structural Basis of Inter-Protein Electron Transfer for Nitrite Reduction in Denitrification. Nature 462: 117–120.

95. Blackmore RS, Greenwood C, Gibson QH (1991) Studies of the Primary Oxygen Intermediate in the Reaction of Fully Reduced Cytochrome Oxidase. Journal of Biological Chemistry 266: 19245–9.

96. Hedrick DB, White DC (1986) Microbial Respiratory Quinones in the Environment: I. A Sensitive Liquid Chromatographic Method. Journal of Microbiological Methods 5: 243 – 254.

97. Butcher JC (2003) Numerical Methods for Ordinary Differential Equations. John Wiley and Sons.

98. Cash JR, Karp AH (1990) A Variable Order Runge-Kutta Method for Initial Value Problems with Rapidly Varying Right-hand Sides. ACM Trans Math Softw 16: 201–222.

99. Press WH, Teukolsky SA, Vetterling WT, Flannery BP (1992) Numerical Recipes in C. 2nd ed., Cambridge University Press.

100. Nakamura (Particle Data Group) K (2010) Review of Particle Physics. Journal of Physics G: Nuclear and Particle Physics 37: 075021 and 2011 partial update for the 2012 edition.

101. Kirkpatrick S, Gelatt CD, Vecchi MP (1983) Optimization by Simulated Annealing. Science 220: pp. 671–680.

102. Černý V (1985) Thermodynamical Approach to the Traveling Salesman Problem: An Efficient Simulation Algorithm. Journal of Optimization Theory and Applications 45: 41–51.

103. Bertsimas D, Tsitsiklis J (1993) Simulated Annealing. Statistical Science 8: pp. 10–15.

104. Toni T, Welch D, Strelkowa N, Ipsen A, Stumpf MPH (2009) Approximate Bayesian Computation Scheme for Parameter Inference and Model Selection in Dynamical Systems. Journal of The Royal Society Interface 6: 187.

105. Ronquist F, Teslenko M, van der Mark P, Ayres D, Darling A, et al. (2011) MrBayes 3.2: Efficient Bayesian Phylogenetic Inference and Model Choice Across a Large Model Space. Systematic Biology in press: 0–0.

106. Beaumont MA, Zhang W, Balding DJ (2002) Approximate Bayesian computation in population genetics. Genetics 162: 2025–2035.

107. Sisson SA, Fan Y, Tanaka MM (2007) Sequential Monte Carlo without likelihoods. Proc Natl Acad Sci U S A 104: 1760–1765.

108. Beaumont MA (2010) Approximate Bayesian Computation in Evolution and Ecology. Annual Review of Ecology, Evolution, and Systematics 41: pp. 379–406.

109. Metropolis N, Rosenbluth AW, Rosenbluth MN, Teller AH, Teller E (1953) Equation of State Calculations by Fast Computing Machines. The Journal of Chemical Physics 21: 1087–1092.

110. Hastings WK (1970) Monte Carlo Sampling Methods Using Markov Chains and Their Applications. Biometrika 57: 97–109.

111. Gelman A, Rubin DB (1992) Inference from Iterative Simulation Using Multiple Sequences. Statistical Science 7: pp. 457–472.

112. Curran J (2011) Bolstad2: Bolstad functions.

113. R Development Core Team (2010) R: A Language and Environment for Statistical Computing. R Foundation for Statistical Computing, Vienna, Austria.